ARTICLE IN PRESS

Physics Reports ▮ (▮▮▮▮) ▮▮▮–▮▮▮

Contents lists available at SciVerse ScienceDirect

Physics Reports

journal homepage: www.elsevier.com/locate/physrep

Dispersion-managed solitons in fibre systems and lasers

Sergei K. Turitsyn[a,*], Brandon G. Bale[a,b], Mikhail P. Fedoruk[c,d]

[a] *Aston Institute of Photonic Technologies, Aston University, Birmingham, B4 7ET, UK*

[b] *MIT Lincoln Laboratory, 244 Wood Street, Lexington, MA 02421, USA*

[c] *Novosibirsk State University, Novosibirsk, 630090, Russia*

[d] *Institute of Computational Technologies, SB Russian Academy of Science, Novosibirsk, 630090, Russia*

ARTICLE INFO

Article history:
Accepted 21 July 2012
Available online xxxx
editor: D.K. Campbell

Keywords:
Solitons
Dispersion management
Fibre lasers
Nonlinear systems

ABSTRACT

Nonlinear systems with periodic variations of nonlinearity and/or dispersion occur in a variety of physical problems and engineering applications. The mathematical concept of dispersion managed solitons already has made an impact on the development of fibre communications, optical signal processing and laser science. We overview here the field of the dispersion managed solitons starting from mathematical theories of Hamiltonian and dissipative systems and then discuss recent advances in practical implementation of this concept in fibre-optics and lasers.

Contents

* Corresponding author. Tel.: +44 121 204 3538.
E-mail address: s.k.turitsyn@aston.ac.uk (S.K. Turitsyn).

0370-1573/$ – see front matter
doi:10.1016/j.physrep.2012.09.004

Please cite this article in press as: S.K. Turitsyn, et al., Dispersion-managed solitons in fibre systems and lasers, Physics Reports (2012), doi:10.1016/j.physrep.2012.09.004

1. Optical solitons: terminology, brief history and basics

The concept of soliton (this term with roots in Latin *solitarius* – solitary was created from "solitary wave" by Norman Zabusky and Martin Kruskal in 1965 [1]) – that a stable, localized, particle-like object can be formed by nonlinear interactions of field(s) (distributed waves) is one of the fundamental unifying ideas in modern theoretical physics and mathematics [2–21]. Localization of the distributed field energy in time or space by nonlinearity is a very general phenomenon observed in many areas of science. Ramifications of the soliton concept in a broad range from pure theory and mathematics to technologies already implemented in practical devices is the best indication of the importance and generality of this paradigm. The soliton theory has been applied to numerous practical and fundamental problems in areas as diverse as hydrodynamics, plasma, nonlinear optics, molecular biology, field theory, and astrophysics. There are two key general classes of solitons: dynamical and topological solitons. Dynamical solitons occur as a balance between linear effects (which would spread a localized wave packet of small amplitude) and nonlinear effects. Topological solitons occur in systems with topologically nontrivial ground states. Examples of topological solitons include vortices, kinks, domain walls, 2π optical pulses and other structures [22–24]. Although solitons typically occur in certain nonlinear regimes and linear wave theory is not adequate to describe the dynamics of such localized lumps of energy, their stability and robustness allows for a convenient and adequate language to describe many complex nonlinear phenomena. In the mathematical literature this term is often associated with particle-like solutions of a particular class of models—the so-called integrable nonlinear equations, that interact elastically and regain their forms after collisions. In particular, in the inverse spectral transform theory multi-soliton solutions of integrable nonlinear partial differential equations correspond to reflectionless potentials for the associated scattering problems [3,4,12–14]. In terms of the scattering data corresponding to a solution of a Cauchy problem there is a natural and well defined decomposition into a discrete set of eigenvalues which correspond to solitons and continuous spectrum data (reflection coefficients) which correspond to non-soliton radiation. It can be shown that the radiative part of the energy is dispersing and vanishing with propagation distance [3,12,25]. Under certain resonance conditions multiple solitons may form bound states (soliton fusion) or decay into more elementary solitons [26,27]. Solitons also interact elastically with radiation which corresponds to non-diagonal elements of the scattering matrix [25,28,29]. There has been attempts made in some part of the mathematical community to keep the term soliton only for solutions of integrable equations using the term "solitary wave" for non-integrable models. This attempt largely failed because the detailed mathematical differences between solutions of integrable and non-integrable models to physicists and engineers seem to be less important compared to the key soliton properties, such as, localization, coherence and stability that are observed for both integrable and non-integrable nonlinear models. Many characteristics of solitons that are important for applications are not related to its strict mathematical definition and integrability. Therefore, typically in physics and engineering applications integrability is not the primary concern (and hence with any mathematical definitions of the soliton) of the mathematical models involved. Indeed, in most real-world applications a more careful consideration of practical perturbations or realistic boundary conditions leads to non-integrable modifications of the models. In general, in such non-integrable models solitons interact inelastically, may exchange energy, momentum, or charges, and they may create bound states or even annihilate. In this review we use the term soliton in a broad sense considering non-integrable nonlinear models that possess solutions that describe spatially or temporally coherent, localized structures. Stable particle-like long term behaviour is the key feature in such a physical definition of the soliton. Though the mathematical models and techniques that we will discuss are of very general use, we will focus in this review on the optical manifestations and applications of soliton theory. Specifically we will build our review of nonlinear methods in fibre-optic and laser applications around general soliton theory. We will mostly use here the term soliton for a robust localized (in time) electromagnetic wave that can propagate without significant distortion of its shape even in the presence of substantial nonlinear response of the medium.

The generality of the soliton concept and a broad variety of applications of soliton theory in physics, biology, engineering and other fields reflects the generic nature of the underlying mathematical models. Soliton prevalence is largely due to a relatively small number of versatile nonlinear equations governing a wide range of physical and biological systems. Nonlinear models governing rather different and otherwise unconnected physical phenomena engaging nonlinearity can be quite similar or even exactly the same mathematically. Therefore, the analysis of such generic nonlinear models is of great importance in a range of physical contexts. Optical soliton history can be linked to an introduction of the two master models of optical solitons—the Ginzburg–Landau equation (GLE) and the nonlinear Schrödinger equation (NLSE). They provide a platform for describing a large variety of physical phenomena. The Ginzburg–Landau equation arises in physics, in particular, as a first-approximation "envelope" (or "amplitude") equation that governs the non-equilibrium dynamics of nonlinear systems in the presence of gain/loss and other effects such as linear and nonlinear dispersion or gain/loss saturation, depending on the specifics of the physical problem. It was first proposed, as one can guess, by Ginzburg and Landau in the context of phase transitions and superconductivity [30]. Since it has been used to describe a vast variety of physical phenomena, including convection [31,32], the theory of mode-locking laser systems [33] as well as generic nonlinear optics models [34], and in a number of other physical problems (see e.g. [10,35,36] and references therein).

A precursor to the nonlinear Schrödinger equation was the approach used as early as 1947 in the context of a microscopic theory of superfluidity (as a model of weakly interacting Bose gas) to describe the spectrum of a condensate [37]. Interestingly, a possibility of instability (which eventually became known as modulation instability) was also mentioned in this study. In the 1960s the classical nonlinear Schrödinger equation was introduced in the studies of atomic Boson systems and is also known in that field as the Gross–Pitaevskii equation [38,39]. Following this work, the NLSE was used for the analysis of powerful optical beams [40–43] as well as in the context of describing hydrodynamical surface wave instability [44]. Although these applications were quite different, it was interesting that the same general mathematical model, the NLSE, was used to describe each of them. An important milestone was achieved by Zakharov in [44] when he derived the nonlinear Schrödinger for an arbitrary Hamiltonian system under very general assumptions, thus, effectively predicting its very generic nature. Indeed, the broad impact of the NLSE was fully confirmed in the following years in many other physical applications [45]. In a seminal paper, Zakharov and Shabat demonstrated the integrability of the NLSE, which inspired much research into the rich mathematical properties of this model [46]. Mathematically, the NLSE can be treated as a conservative (energy preserving) limit of the general complex Ginzburg–Landau equation. Indeed, the versatile nature of the NLSE reflects very general and simple assumptions made in its derivation [44]. It governs high-frequency nonlinear wave propagation in a medium with Kerr-type nonlinearity when gain/loss effects do not make essential contributions to the nonlinear wave dynamics, or when their overall effect is averaged out leading to the pure NLSE.

The proposal of the NLSE in fibre-optics originated from a rather brave (taking into account the level of fibre loss at the time) theoretical prediction of optical solitons in fibre by Hasegawa and Tappert [47]. In optical fibre the Kerr nonlinearity counterbalances the effect of dispersive broadening and the optical pulse becomes self-trapped in its own effective potential. Such a balance between nonlinearity and dispersion is very robust and the soliton pulse preserves its shape during propagation over very long distances even in the presence of numerous perturbations. Experimental demonstrations of optical solitons in [48] and soliton-based transmission [49–51] have established optical solitons as a routine optical engineering technique that can be used in a range of applications (see e.g. [5] and references therein). The NLSE is one of the very important underlying mathematical models in optics and has important applications in all-optical signal processing, transmission, pulse compression, pulse shaping, optical data regeneration, frequency conversion, and the design and operation of a number of nonlinear photonic devices. Many of these applications are based on the existence of a robustly stable solution of the NLSE—the fundamental soliton. These solutions can be implemented in very different physical systems ranging from rather different physical platforms such as optical fibre, silicon devices, as well as many potentially unforeseen applications (surely the "soliton story" is far from being over!). Since an optical soliton is a stable pulse and can represent an elementary "bit", it has many features that make it attractive for transmission, storage and processing of digital information. Indeed, practical applications of solitons take advantage of their "particle-like" nature. An important consequence of this feature is that solitons are robust in the presence of various perturbations (that could be of different physical nature, e.g. loss, filtering, non-perfect launch conditions an so on) and the perturbed pulses will eventually regenerate into stable solitons. Linear optical communication and signal processing technologies are essentially based on the same principles as radio frequency systems. Soliton-based (or general *nonlinear*) fibre systems are fundamentally different, because they utilize the inherent nonlinearity of the optical fibre. In what follows we will use terminology of fibre-optics, however, we would like to reiterate that the generic nature of the basic mathematical models allows for the presented results to be directly (or with minor modifications) applied to a very broad range of other physical problems.

Please cite this article in press as: S.K. Turitsyn, et al., Dispersion-managed solitons in fibre systems and lasers, Physics Reports (2012), doi:10.1016/j.physrep.2012.09.004

In general, pulse propagation in optical fibre systems may be affected by a combined action of dissipation, amplification, dispersion and nonlinearity and cannot be described in a simple way. The governing equation to describe the main effects of such a system is the perturbed NLSE or a version of the GLE

$$iU_Z - \frac{1}{2}\beta_2 U_{TT} + \gamma |U|^2 U = i\,G(Z, |U|^2, \ldots) \times U, \tag{1}$$

where U represents the slowly varying electromagnetic field envelope, T represents retarded time in the rest frame of the pulse, and Z is the propagation distance along the fibre. Here β_2 is the second order group velocity dispersion coefficient (in units of [Time]^2 $\times$ [Length]$^{-1}$) and $\gamma = 2\pi n_2/(\lambda_0 A_{\rm eff})$ is the nonlinear coefficient (in units of [Power]$^{-1}$ $\times$ [Length]$^{-1}$) where n_2 is the nonlinear refractive index, λ_0 is the carrier wavelength, and $A_{\rm eff}$ is the effective fibre area. The right hand side of Eq. (1) introduces dissipation to the pure NLSE with some arbitrary function G, which depends on the physical application. From the mathematical point of view there are two key possibilities for solutions to Eq. (1). When the average dissipative effects can be separated out, the system is effectively conservative (Hamiltonian) and described by the NLSE. However, when the dissipative effects cannot be separated or averaged out and solitons are formed as a result of interplay and balance between dissipative and conservative processes, the dynamics is described by the GLE. The later solitons are often called *dissipative solitons* or *autosolitons* to stress that their parameters are uniquely determined by the system, in contrast to conservative solitons that often present a family of solutions with free parameters. Indeed, these two types of soliton solutions occur in similar systems for optical pulse propagation in fibre based transmission and laser systems.

A key component in classifying the different limits and potential solutions can be based on the length scales in Eq. (1). A typical system can be normalized by scales that are natural to the pulse, such as the typical pulse width T_0 and peak power P_0. The local dispersion length $L_D = T_0^2/|\beta_2|$ in an optical fibre is defined as the distance in which linear dispersion causes the pulse to broaden to twice its initial value. Another important length that is particularly important in dispersion managed systems is the so-called residual dispersion length $L_{\langle D\rangle} = T_0^2/|\langle\beta_2\rangle|$, where $\langle\beta_2\rangle$ is the average dispersion of the system. Yet another important length scale is the so-called nonlinear length $L_{NL} = 1/(\gamma P_0)$, and is the distance in which a pulse achieves a nonlinear phase rotation of π at the maximum of the pulse. Finally, in a system where dissipative elements exist, there are intrinsic amplification distances such as the amplification period L_A in transmission systems or the round trip cavity length $L_R = cT_R$, where T_R is the round trip time in the laser resonator. Taking into consideration all the mentioned length scales, one can classify all possible solutions. Indeed, in this review we try to emphasis the length scales as they give a natural description to the overall pulse dynamics for solutions that arise. To highlight the scaling of the physical model, it is typical to introduce the non-dimensional parameters $t = T/T_0$, $|u|^2 = |U|^2/P_0$ and $z = Z/L$, where T_0, P_0 and L is the characteristic time, power and propagation length of the system, respectively. Using these definitions we obtain

$$iu_z + \frac{s}{2} d u_{tt} + \epsilon |u|^2 u = i\,g(z, |u|^2, \ldots) \times u, \tag{2}$$

where $s = -\mathrm{sign}(\beta_2) = \pm 1$ for the so-called anomalous ($s = +1$) and normal ($s = -1$) dispersion, $d = L/L_D$, $\epsilon = L/L_{NL}$ and $g = LG$. In the following we describe certain solutions that occur for particular limits of Eq. (2).

1.1. Key analytical solutions of the conservative NLSE

When the characteristic length is equal to both the dispersion and nonlinear lengths ($L = L_D = L_{NL} \to \epsilon = d = 1$), special symmetries occur in the conservative NLSE (Eq. (2) with $g = 0$) and lead to a wide variety of analytical solutions. Here we review some of the different types of solutions for this particular case. First, following a comprehensive analysis by Kuznetsov and Spector in [52], we overview standing-wave solutions that propagate along the z-direction without changing their shape. The most general mathematical form (that also provides a systematic description of all particular solutions) can be presented through the Weierstrass functions $\wp$, ζ and σ

$$u(z,t) = F(t)\,e^{-iskz/2}, \quad F(t) = \sqrt{s}\,\frac{\sigma(t + i\omega' + a)}{\sigma(t + i\omega')\sigma(a)}\,e^{-\zeta(a)t - a\zeta(\omega')}, \tag{3}$$

where the functions σ and ζ are related to the Weierstrass function $\wp(x)$ as

$$\wp(x|\omega,\omega') = \frac{1}{x^2} + \sum_{\substack{m,n \\ m^2+n^2\neq 0}} \left[\frac{1}{(x - 2m\omega - 2n\omega')^2} - \frac{1}{(2m\omega + 2n\omega')^2}\right] = -\frac{d\zeta(x)}{dx}, \quad \zeta(x) = \frac{d\log\sigma(x)}{dx}. \tag{4}$$

Although this presentation seems to be quite complicated mathematically, it can be efficiently used in numerical simulations and for the construction of a number of particular solutions exploiting known properties of elliptic functions [53]. The double periodic Weierstrass function $\wp(x)$ defined in the complex plane x has two periods: 2ω is the period along the real axis (the period of $|F(t)|^2 = -s[\wp(t + i\omega') - \wp(a)]$) and $2\omega'$ is the period along the imaginary axis. The solution depends on the parameter a that is defined through $\wp(a) = -\frac{k}{3}$. The restrictions on the parameter a are imposed by the requirement of real k and are different for different signs of s. The symmetry properties of $\wp(x) = \wp^*(x^*) = \wp(-x)$ and periodicity of $\wp(x)$ define two intervals $(0, i\omega')$ and $(\omega, \omega + i\omega')$ (and all periodic continuations) where $\wp(x)$ takes real values. The most general solution given by Eq. (3) is quasi-periodic (in t) and presents a nonlinear Bloch-wave function with the quasi-momentum $q = i[\zeta(a) - a\,\frac{\zeta(\omega)}{\omega}]$:

$$F(t) = U_q(t)\, e^{iqt}, \tag{5}$$

where $U_q(t)$ is a periodic function with the period 2ω. The following limiting cases lead to purely periodic (in t) solutions:

(1) $s = 1, a = \omega, F(t) = \nu\, dn(\nu t)$;
(2) $s = 1, a = \omega + i\omega', F(t) = s\,\nu\, cn(\nu t)$;
(3) $s = -1, a = i\omega', F(t) = s\,\nu\, sn(\nu t)$.

Here dn, cn and sn are the Jacobi elliptical functions, $\nu^2 = e_1 - e_3$, $s^2 = \frac{e_2-e_3}{e_1-e_3}$, $s'^2 = \frac{e_1-e_2}{e_1-e_3}$. The parameters $e_1 > e_2 > e_3$ are defined as: $e_1 = \wp(\omega)$, $e_2 = \wp(\omega + i\omega')$, $e_3 = \wp(i\omega')$. Another important limit of the general solution is when $\omega' \to \infty$, giving a plane wave solution: $u = \lambda \exp(i\lambda^2 z)$. Further, the general solution Eq. (3) presents a lattice of solitons [54] since:

$$|F(t)|^2 = -\frac{sk}{3} + \frac{\zeta(i\pi/\lambda)}{i\pi/\lambda} + \sum_{-\infty}^{+\infty} \frac{2\lambda^2}{\cosh^2 \lambda(t - 2n\omega)}. \tag{6}$$

In the limit of a large lattice period $\omega \gg \omega'$, Eq. (6) gives single soliton solutions that are different for normal ($s = -1$) and anomalous ($s = 1$) dispersions. In the case of anomalous dispersion, the general solution in this limit is given by the fundamental soliton: $u(z, t) = \lambda \exp(i\lambda^2 z/2)/\cosh(\lambda t)$ (see Fig. 1(a)). In the case of normal dispersion the general solution in this limit is given by a grey-soliton: $u(z, t) = \lambda(\sqrt{1-\mu^2} + i\mu \tanh[\mu\lambda(t - \lambda\sqrt{1-\mu^2} z)])\, \exp(i\lambda^2 z)$, corresponding to the power dependence: $|u(z, t)|^2 = \lambda^2(1 - \mu^2/\cosh^2[\mu\lambda(t - \lambda\sqrt{1-\mu^2} z)])$. Note that in the limit $\mu = 1$ this solution diverges into the so-called dark soliton solution $u(z, t) = \lambda \tanh[\lambda t] \exp(i\lambda^2 z)$ [55–57]. It is possible to obtain more complex solutions by transformations of these basic solutions using both conventional symmetries of the conservative NLSE and very specific symmetries linked to its integrability [58–61].

In addition to stationary solutions to the conservative NLSE, there also exist more complex solutions with nontrivial dynamics of power (intensity) along the z-direction. This is directly relevant to the main topic of this review—management of the field evolution (along the z) in nonlinear systems. Indeed, periodicity in z can be observed even without any periodic management of the system parameters. Knowledge of such internal resonances might be used for efficient excitation of specific nonlinear modes of the system. There are a variety of analytical non-stationary (in z) solutions of the NLS equation that can be found by a various methods. Indeed, this vastness of solutions is a direct result of the integrability of the NLS equation [46]. A popular and relatively compact periodic (breathing) 2-soliton solution was presented in [62] for $s = 1$

$$u_2(z, t) = \frac{4[\cosh(3t) + 3\cosh(t)\exp(i4z)]}{\cosh(4t) + 4\cosh(2t) + 3\cos(4z)}\, e^{iz/2}, \tag{7}$$

As seen in Fig. 1(b), this solution is a periodic breather with period $\pi/2$. The power (intensity) of a general periodic (in z) N-soliton solution can be presented in the following compact form:

$$|u_N(z, t)|^2 = 2\frac{\partial^2}{\partial t^2}[\log\det(I + CC^*)], \tag{8}$$

where $C = [c_{ij}]$ is an $N \times N$ matrix defined using $c_i = e^{2i\lambda_i^2 z + \nu_i}$ as follows: $c_{ij} = \frac{\sqrt{c_i c_j^*}}{\lambda_i - \lambda_j^*} e^{i(\lambda_i - \lambda_j^*)t}$, where the λ_i and ν_i are arbitrary complex numbers that satisfy the obvious constraints that prevent singularities in the above expression. Applications for practical devices which use such periodic solutions with breathing dynamics are as of yet not well explored apart from the use of the N-soliton solution in optical signal compression. Under certain conditions in specially designed media the N-soliton solution might play an important role in super-continuum generation [63,64] where nonlinearity dominates dispersion creating a natural pre-condition for multi-soliton generation.

In comparison to previously described solutions to the conservative NLSE, there exist even more exotic solutions with non-zero boundary conditions e.g. $|u|^2 \to \lambda^2$. One of the most important examples are periodic (in z) solutions ($s = 1$)

$$u(z, t) = \lambda\left[1 - 2\nu \frac{\nu\cos(\Omega z) + i\sqrt{1+\nu^2}\sin(\Omega z)}{\sqrt{1+\nu^2}\cosh(2\lambda\nu t) - \cos(\Omega z)}\right] \exp(i\lambda^2 z), \tag{9}$$

where $\Omega = 2\nu\sqrt{1+\nu^2}$ determines the period of oscillation (in z) of the localized bump (dip) in the temporal distribution of the power. We will call these solutions "Kuznetsov breathers", to pay credit to E. A. Kuznetsov who first discovered such non-stationary solutions of the NLS equation [65] (see also later publications [66,67]). Interesting solutions with nontrivial dynamics in z can be derived from the Kuznetsov breathers. For example, letting $\nu = i\mu$ gives the so-called Akhmediev breather solution [68,69]

$$u(z, t) = \lambda\left[\frac{(2\mu^2 - 1)\cosh(bz) + ib\sinh(bz) + \sqrt{1-\mu^2}\cos(2\lambda\mu t)}{\sqrt{1-\mu^2}\cos(2\lambda\mu t) - \cosh(bz)}\right] \exp(i\lambda^2 z), \tag{10}$$

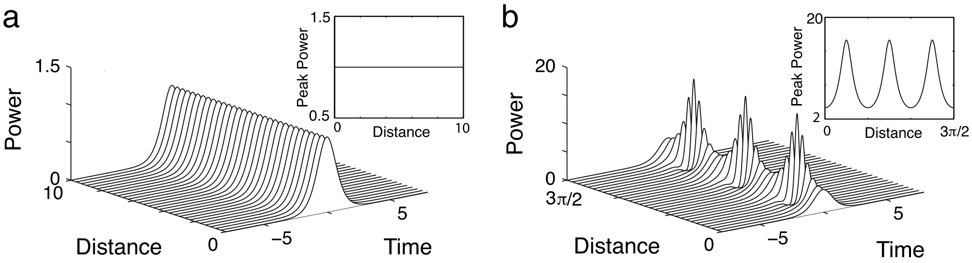

Fig. 1. (a) Fundamental soliton solution and (b) 2-soliton solution for the conservative NLSE (2) with $g = 0$ and $s = d = 1$. Note that (a) represents a stationary solution and (b) represents a periodic breathing solution. This is highlighted in the insets which show the evolution of the peak power.

where $b = 2\mu\sqrt{1-\mu^2}$. Although these solutions are called breathers, it is a bit misleading as these solutions oscillate in time t, not in propagation distance z. It is difficult to change nomenclature when it is already accepted by some part of a community, but here we would like to provide a natural name for such solutions since they are closely associated with the so-called "instanton" [22,70–72], rather than a breather. Another interesting limit of the Kuznetsov breather (9) occurs when $\nu \to 0$ giving the so-called Peregrine soliton [73]

$$u(z,t) = \lambda\left[1 - \frac{4+8iz}{1+4t^2\lambda^2+4z^2}\right]\exp(i\lambda^2 z). \tag{11}$$

Like the Akhmediev breather (instanton), this solution is localized in z and it would be more appropriate to call it an instanton. This solution, as well as other breather and instanton solutions has recently received a lot of attention in the theory of freak wave (rare waves of high amplitudes) formation in physical systems that can be modelled by the NLSE with $s = 1$ [74–76]. An initial perturbation (lump) into the uniform field (continuous wave) may develop into a breather or instanton when an effective area over the perturbation exceeds some critical value [75]. The Peregrine instanton can be treated as a temporally localized nonlinear structure with only one oscillation in z (a one-time-breather), thus capturing the key feature of freak waves in that they appear out of nowhere and a disappear without a trace. It was recently demonstrated that the development of a freak wave pattern in the NLSE is most probably linked with the Peregrine instanton with the peak amplitude close to three times the background level [75]. Further, it has been experimentally demonstrated that in a nonlinear optical fibre system the generation of femtosecond pulses with strong temporal and spatial localization might be linked to the Peregrine instanton [76].

Here we have presented a wide range of exact solutions for the particular limit of the conservative NLSE when $d = \epsilon = 1$. Indeed, in this limit more general solutions as well as solutions resulting from the interaction between basic solutions exist. This wide range of exact analytical solutions and their behaviours represents the deep symmetries and integrability of the conservative NLSE in this limit. In addition to exact solutions, there are also important approximate solutions to the NLSE. Of particular interest is in wave-breaking free high-intensity parabolic pulses ($s = -1$) [77]. By neglecting a linear dispersive term, it was shown that the pulse form remains parabolic with the addition of a quadratic phase profile. Although the pulse temporal profile remains parabolic, its amplitude decays monotonically while the pulse duration increases monotonically with propagation. Thus the pulse is not a breather, but both nonlinearity and dispersion are acting in such a way as to preserve its overall temporal profile.

1.2. The path average (guiding-centre) solitons in the presence of periodic gain and loss

Fundamental optical solitons in conservative systems experience effects from both anomalous chromatic dispersion as well as nonlinearity. The dispersive broadening of the pulse propagating in the anomalous dispersion region can be exactly compensated by the nonlinear phase shift, leading to stable and robust solutions. Indeed, the potential for solitons as optical bits for optical fibre transmission systems was recognized immediately. However, in such transmission systems the signal power is attenuated in passive fibre due to inherent fibre loss (see Fig. 2, a), and needs to be compensated using optical fibre amplifiers. The recovery, though, is not complete because amplified spontaneous emission noise from the amplifier is added to the signal, degrading the signal-to-noise ratio. Optical amplification can be implemented in a number of ways using Erbium-doped fibre amplifiers (EDFA), semiconductor optical amplifiers (SOA) or distributed Raman amplification (DRA) [78–81]. Of fundamental importance to such transmission systems is the stability of the fundamental soliton in the presence of periodic gain and loss. For moderate pulse durations and peak powers, when the amplifier spacing L_A is considerably shorter than the characteristic dispersion and nonlinear lengths (L_D, L_{NL}) a natural separation of scales highlights that at leading order the pulse evolution between two consecutive amplifiers is governed only by the gain and loss dynamics (see Fig. 2). These factors cause a change in the peak power, however the profile of the pulse remains approximately unchanged. It is only at the next order, and for long-scale propagation where dispersion and nonlinearity effect the pulse.

Mathematically such a system can be described by Eq. (2) where the gain only depends on propagation distance $g = g(z)$. Here we describe the slow (average) dynamics of a field u on the propagation scale larger than L_A, the so-called path-averaged

Please cite this article in press as: S.K. Turitsyn, et al., Dispersion-managed solitons in fibre systems and lasers, Physics Reports (2012), doi:10.1016/j.physrep.2012.09.004

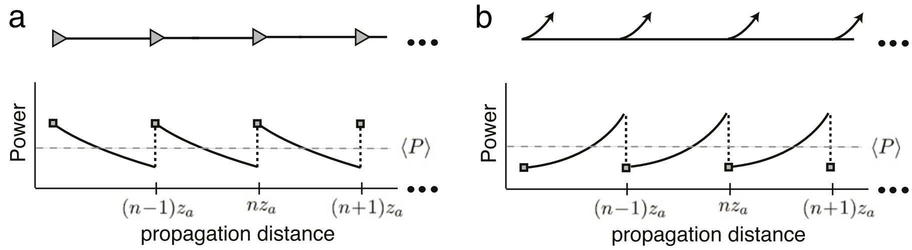

Fig. 2. Typical optical systems where dissipative elements are included along with dispersion compensation. The top panel shows schematically: (a) consecutive fibre spans and amplifiers (grey triangles); and (b) three round trips with periodic power out-coupling (out facing arrows) from a laser cavity. The value $\langle P\rangle$ is the average power, and z_n is the length of the nth segment or round trip. (a) Example of a telecommunications system where the power is attenuated by fibre loss and regenerated by amplification. (b) Example of a laser application where the power is amplified by an active fibre and part of the signal is output at discrete points.

(guiding-centre) model [50,82,83]. Consider a physically realistic example where the amplifiers are equidistantly spaced by an interval L_A. If treated as a point-like action (e.g. EDFA or SOA), the form of the amplification to compensate the fibre loss $\alpha(z)$ between two consecutive (k and $(k-1)$) amplifiers is a piece-wise constant function with the loss coefficient α_k in the exponent, giving

$$g(z) = -\alpha(z) + \sum_{k=1}^{N} [\exp(\alpha_k l_a) - 1]\delta(z - kl_a). \tag{12}$$

Here $l_a = L_A/L$ is the normalized amplification period, $\alpha_k[1/km] = 0.05\ln(10)\bar{\alpha}_k[dB/km]$ is the loss coefficient, where $\bar{\alpha}_k$ is the loss characteristic of the fibre given in typical engineering units, the index k accounts for the variances of attenuation in different fibre spans, and δ is the Dirac delta function, showing the discrete nature of the amplification at N points along the fibre. In the case where there is negligibly small variances in the fibre loss from span to span $\alpha_k = \alpha$, and $g(z)$ is periodic with period l_a. When the gain g only depends on z, it is possible to make the following transformation $a(z,t) = u(z,t)\exp(\int_0^z g(z')dz' - \langle g\rangle z)$ into Eq. (2), where the average gain level is given by $\langle g\rangle = \int_0^{l_a} g(z)dz/l_a$. The evolution of the transformed signal envelope $a(z,t)$ is then given by the normalized NLSE with a periodic nonlinear coefficient

$$i\frac{\partial a}{\partial z} + \frac{s}{2}\frac{\partial^2 a}{\partial t^2} + c(z)|a|^2 a = 0, \tag{13}$$

where the periodic function $c(z) = \exp[2\int_0^z g(z')dz' - 2\langle g\rangle z]$, and we have let, similar to the previously discussed limit for analytic solutions to the conservative NLSE, $L = L_{NL} = L_D$. This transformation allows for $c(z)$ to describe the power oscillations between $c(0) = c(l_a) = 1$ and $c(l_a - \epsilon) = \exp[-2\alpha l_a]$ ($\epsilon \ll 1$) due to fibre loss and amplifier gain, which is accounted through the transformation of the pulse power at the locations of the optical amplifiers. Being periodic, the nonlinear coefficient $c(z)$ can be presented through a Fourier series $c(z) = \sum_{m=-\infty}^{\infty} c_m \exp[i2\pi m z/l_a]$, where the Fourier coefficients c_m are easily found as $c_m = (1 - \exp[-2\alpha l_a])/(\alpha l_a + i2\pi m)$. The function $c(z)$ then can be further split into constant and oscillating parts: $c(z) = \langle c(z)\rangle + \tilde{c}(z)$ where $\langle c(z)\rangle = (1 - \exp[-2\alpha l_a])/(\alpha l_a)$ and $\tilde{c}(z) = \sum_{m\neq 0} c_m \exp[i2\pi m z/l_a]$ with $\langle \tilde{c}(z)\rangle = 0$. Following [6,82], the function $a(z,t)$ can be divided into a slowly varying portion $a_s(z,t)$ (the guiding centre soliton) and a rapidly varying portion $a_r(z,t)$ where $\langle a_r(z)\rangle = \int_0^{l_a} a_r(z')dz'/l_a = 0$. It can be shown that the rapidly varying portion $a_r(z,t)$ can be expanded in powers of $l_a \ll 1$ [84]. Substituting $a(z,t) = a_s(z,t) + a_r^0(z,t) + l_a a_r^1(z,t) + O(l_a^2)$ into Eq. (13) and averaging over the amplification period, we obtain at leading order the path average propagation model which is the re-normalized NLSE [50,82–84]

$$i\frac{\partial a_s}{\partial z} + \frac{s}{2}\frac{\partial^2 a_s}{\partial t^2} + \langle c\rangle |a_s|^2 a_s = 0. \tag{14}$$

The next term in the expansion at O(l_a), first found by Kodama and Hasegawa (see e.g. [82,84,85]) gives the leading order rapidly varying portion

$$a_r^0(z,t) = i\left[\frac{1}{2\alpha} + \frac{l_a}{2} - z - \frac{l_a\exp(-2\alpha z)}{1 - \exp(-2\alpha l_a)}\right]|a_s|^2 a_s. \tag{15}$$

Here the evolution of $a_r^0(z,t)$ is for the interval from $z = 0$ to $z = l_a$, then repeated due to periodicity. If the initial conditions for a soliton pulse satisfy the condition $a_r^0(kl_a,t) = 0$ ($k = 1, 2, \ldots$), there will be reduced oscillations caused by the difference of the field $a(z,t)$ from the average, slow varying components $a_s(z,t)$. Indeed, suppression of the rapidly oscillating portion of the pulse becomes an important issue when the amplification period is approximately equal or close to the characteristic nonlinear or dispersion length ($l_a \sim 1$).

Traditional soliton propagation can be affected by various effects such as noise perturbations or pulse-to-pulse interactions, and in many practical situations that rely on stable soliton parameters some form of soliton control is necessary [86]. Noise impacts on solitons can be transferred into statistical variations of soliton parameters including timing (Gordon–Haus–Elgin) jitter [87–90], phase (Gordon–Mollenauer) jitter [5], and other deviations. Integrability of the path-averaged model makes it possible to use well-developed mathematical techniques to analyse the effects of numerous practical perturbations and boundary conditions that might be especially important for soliton lasers. Indeed, guiding centre soliton theory can provide essential insight into the known side-band generation of Fabry–Perot or ring soliton lasers, which can be mathematically modelled with Eq. (1) with gain (12). Due to the periodic gain and loss the path average soliton can develop side-bands in its spectral profile which can lead to instabilities. Here we provide a simple intuitive physical explanation of such an instability. The NLSE fundamental soliton $u(z,t) = \lambda \exp(i\lambda^2 z/2)/\cosh(\lambda t)$ has a wavenumber (propagation constant) $k_{\text{sol}} = \lambda^2/2$, while linear waves have a dispersion relation $k_{\text{lin}} = -\omega^2/2$ (ω being the frequency variable). The periodic variation of the gain and loss produces dispersive perturbations with wavenumber $k_{\text{periodic}} = 2\pi/l_a$. The phase matching condition necessary for providing efficient generation of dispersive waves is $k_{\text{periodic}} = k_{\text{sol}} - k_{\text{lin}}$, leading to the resonance frequency $\omega_{\text{res}} = \sqrt{4\pi/l_a - \lambda^2}$. Assuming a slightly perturbed soliton solution to the NLSE $\lambda \sim 1$, the resonance frequency $\omega_{\text{res}} \gg 1$ for $l_a \ll 1$. Since the spectral density of the fundamental soliton solution is $I(\omega) = |E(\omega)|^2 = \pi^2/(4\cosh^2[\pi\omega/(2\lambda)])$, we see in this limit that $I(\omega_{\text{res}}) \ll 1$ so that the resonance condition is satisfied at frequencies where the soliton spectral density is small. In this case the path-average soliton theory works well and the generation of radiative linear waves is suppressed. Increasing l_a to $4\pi/\lambda^2$ leads to strong phase matching where the soliton spectral density is high and a large fraction of the soliton energy will be leaked away into dispersive waves. This effect is seen in the generation of spectral side bands, also known as Kelly side-bands [91] that are routinely observed in the spectra of soliton lasers. In the physical units L_A is bounded above by $8Z_{\text{sol}} \propto T_{\text{sol}}^2 \propto 1/P_{\text{sol}}$, where T_{sol} and P_{sol} are soliton width and peak power, respectively. This relation restricts the possible pulse outputs from a soliton laser since for a certain cavity length it imposes a lower bound pulse duration before instabilities arise.

1.3. Basic solutions of the GLE

In the previous sections we reviewed important solutions to the conservative NLSE as well as a physical situation with dissipation, however the particular scalings involved allowed for an averaging procedure where the slow dynamics can be described by the conservative NLSE, giving rise to guiding centre soliton solutions. In general, a physical system can have a wide variety of linear and nonlinear dissipative elements. In many situations an averaged model based on the GLE can describe both qualitative and quantitative properties of the system. The normalized general GLE we present here is given by

$$iu_z + \frac{s}{2}du_{tt} + \epsilon|u|^2u = i\left[gu + \nu u_{tt} + F(|u|^2, c_1, c_2, \ldots)|u|^2u\right], \tag{16}$$

where all normalizations are as in Eq. (2), and we see that the GLE differs from the conservative NLSE since the right hand side contains distributed dissipative terms. Specifically, the term gu represents linear gain/loss, the term νu_{tt} represents spectral filtering, or so-called gain dispersion, and the term $F(|u|^2, c_1, c_2, \ldots)|u|^2u$ represents nonlinear gain/loss. The function F is left general here, and depends only on the intensity of the field as well as constant parameters.

When $F(x) = c_1$, Eq. (16) is the cubic GLE (CGLE) which has an important class of solutions that are localized wave-packets with a non-trivial time dependence in the phase. In the optics literature these solutions are called "chirped solitons" $u(z,t) = \eta\exp[iqz]/[\cosh(t/\tau)]^{1+iC}$, where η, τ, C and q are completely determined by the parameters s, d, g, ν, and c_1 in Eq. (16). This is an important characteristic of CGLE solutions which differs from conservative NLSE soliton solutions. For the conservative NLSE, families of solutions exist as long as certain relations between the pulse parameters are satisfied. For solutions to the CGLE, the pulse parameters are completely determined by the equation parameters. The chirped soliton solution was first found by Hocking and Stewartson [92] and then re-derived in the different physical context by Pereira and Stenflo [93]. An important property of these solutions is the nontrivial phase across such pulse solutions, allowing for more complex pulse-like solutions to be found in both the anomalous ($s = 1$) and normal ($s = -1$) dispersion regimes. We will see in the following sections that a non-trivial phase is an important characteristic of dispersion-managed solitons. Another solution of the CGLE is described by the Nozaki–Bekki hole solution [94] $u(z,t) = (\tilde{a}\tanh[k(t - z/V)] + \tilde{b})\exp[i\ln[\cosh(k(t-z)/V)]/k + i\tilde{\psi} + i\tilde{c}z]$, where again the parameters of the solution are completely determined by the equation parameters. This solution has an evident link with a grey-soliton of the conservative NLSE.

An extension of the CGLE is when the function $F(x) = c_1 + c_2x$, giving an additional quintic gain/loss term, resulting in the so-called cubic–quintic GLE (CQGLE). The use of a quintic loss term ($c_2 < 0$) is often used as a stabilization mechanism to prevent pulse collapse (where the pulse develops a singularity at a finite distance z) in the CGLE when $c_1 > 0$. Note however that a stable soliton can also exist under some conditions due to the phase effects without need for an additional stabilizing quintic term in the CGLE [95,96]. As expected, the added quintic term introduces a complexity that restricts the number of analytic solutions that can be found for the CQGLE. One stationary solution to the CQGLE that has recently received much attention in mode-locked fibre lasers operating in the all-normal dispersion regime is a generalization of the Hocking and Stewartson solution ($s = -1$): $u(z,t) = \eta\sqrt{1/(\cosh(t/\tau) + B)} \times \exp[-iC(\ln(\cosh(t/\tau) + B)) + iqz]$ [97,106]. This solution has co-dimension one, meaning that the solution parameters cannot be expressed entirely in terms of the equation parameters, leading to additional assumptions on the equation parameters. No solutions where the solution parameters are completely expressed as a function of the equation parameters have been found to the CQGLE. However, there is an interesting class of approximate solutions found recently with particular relevance to highly chirped pulse oscillators [98–102]. Due to the difficulty in finding analytical solutions to the CQGLE, there has been extensive numerical studies performed over the past two decades, resulting in solitary wave solutions such as stationary, pulsating, chaotic, and exploding solitons [36,103–105]. Further, in addition to these solitary wave solutions there also exist coherent structures of different types such as fronts and domain boundaries, to name a few (see e.g. [10,35,36,106] and references therein).

Finally we mention an interesting asymptotic solution to Eq. (16) where $F(x) = \nu = 0$, $s = -1$, and $g > 0$. Linearly chirped parabolic solutions of the form $u(z,t) = \sqrt{P(z)(1 - t^2/\tau^2(z))} \times \exp[i[C(z)t^2 + q(z)]]$ exist and act as global attractors regardless of the initial conditions. In a similar analysis as that used in [77], the pulse parameters can be shown to evolve self-similarly, with the pulse amplitude and duration increasing exponentially with propagation. Such solutions, so-called "similaritons", have received much attention in applications such as optical processing as well as mode-locked lasers.

2. Dispersion-managed solitons: introduction

2.1. Basics of dispersion management in optical communications and laser applications

Nonlinear distributed systems with periodic variations of one or several key parameters present a very important branch of nonlinear science with a number of practical applications in solid state physics, optics, plasma physics, hydrodynamics, wave physics, and other fields. The impact of nonlinear effects on wave propagation or modifications of the nonlinear wave properties by a medium with periodically varying parameters are two important fundamental problems that have been actively studied in the past decades. In particular, the control of dispersion is feasible in many physical systems. Here we will focus on dispersion-management in optics, specifically on fibre-optics, where dispersion control has achieved a great level of sophistication.

A light pulse is an electromagnetic wave-packet containing a continuum of frequency components. These spectral components travel at different group velocities leading to a spreading of the pulse energy over time as it propagates through the dispersive medium. A characteristic of this effect is quantified by the fibre group velocity dispersion (GVD), which is measured either by the GVD coefficient β_2 [ps^2/km] (picoseconds squared per kilometre) or D [ps/nm/km] (picosecond per kilometre per nanometre). The dispersion parameter β_2 is related to D by $\beta_2 = -\lambda_0^2 D/(2\pi c_l)$, where λ_0 is the central wavelength of the signal and c_l is the speed of light. Roughly speaking, in a optical fibre with dispersion D ps/nm/km, a pulse with a bandwidth of 1 nm will spread in time by D ps over 1 km. Depending on the central wavelength of the optical field travelling in the fibre, dispersion can be positive (anomalous) $D > 0$ ($\beta_2 < 0$), where high frequencies travel faster than lower frequencies, or negative (normal) $D < 0$ ($\beta_2 > 0$), where low frequencies propagate faster than high frequencies. The dispersion of standard transmission single mode fibre (SMF) is positive (normal) for wavelengths shorter than 1300 nm and negative (anomalous) for wavelengths longer than 1300 nm. At the important wavelength 1550 nm, where losses in the fibre are minimized, the dispersion $\beta_2 \sim -20$ ps^2/km. For low signal powers (linear regime) at this wavelength, a 10 ps pulse will spread ∼50 ps, or 5 times its original pulse duration, over 125 km. Further, a 1 ps pulse will undergo 100 times the dispersive spreading as a 10 ps pulse, showing that dispersive broadening becomes increasingly important for shorter pulse propagation. Dispersive broadening has major implications for a variety of applications that use optical fibre, one of which is optical communication systems and the growing demand for its capacity. Increasing the per-channel rates of optical communication systems imposes the use of shorter time slots allocated for each transmitted symbol and, consequently, shorter optical carrier pulses. For instance, in fibre-optic systems operating at the channel rates of 10, 40, 100 and 160 Gbit/s the corresponding temporal interval between neighbouring carrier pulses is 100, 25, 10 and 6.25 ps, respectively. The width of a carrier pulse has to be shorter than this, typically by factor of two or more.

In the linear (low power) propagation regime, compensation of the dispersive pulse broadening can be achieved by using a medium with the opposite sign of dispersion producing the re-compression of the dispersed pulse. Of importance is to nullify (minimize) the total accumulated chromatic dispersion, and the order in which the transmission fibre and compensating devices used is irrelevant. Namely, linear compensation can be done before transmission (pre-compensation), after transmission (post-compensation), in-line or using any combination of those approaches providing the same overall dispersion. The idea to use a specially designed compensating fibre to overcome the dispersion of single-mode fibre has been proposed for transmission in 1980 [107]. The basic dispersion compensation system consists of a transmission fibre (e.g. SMF) and dispersion equalizer fibre with opposite-signed dispersion (e.g. dispersion compensating fibre (DCF)) [107]. The dispersion compensation technique has been used successfully both in long-haul communication systems and in existing terrestrial optical links, most of which are based on standard telecommunication fibre with large dispersion at 1550 nm [5–7]. Although these systems were inspired by ideas from linear propagation, there were some indications that the overall accumulated response (transmission function) of the optical fibre medium was nonlinear at the level of powers used in fibre communications. For example, in a linear communication channel the improvement of the signal-to-noise ratio, a crucial characteristic directly relevant to a quality of transmitted signal, can simply be achieved by increasing the signal power while keeping the noise at the same level. However, in a typical nonlinear fibre communication system the bit-error rate (BER) measured in the optical fibre channel initially improves with growing signal power, reaches a minimum corresponding to the best system performance, then is degraded at higher signal power levels due to nonlinear impairments.

Nonlinearity in optical fibres arises from an instantaneous increase in the refractive index by an amount proportional to the optical power (Kerr effect). The modulation of the optical power leads to the corresponding modulation of the refractive index which in turn leads to a change in the phase of the propagating signal. Nonlinearity affects different signal spectral components, delaying the high-frequency spectral components relative the low-frequency components. When considering nonlinearity in such dispersive systems, a non-trivial interplay between dispersion and nonlinearity determines specific properties of optical signal evolution in the fibre link. Distinct effects occur in the dispersion managed nonlinear regime including intra-channel and inter-channel pulse interactions [108–112], cross-talks [113], four-wave mixing [5,114–117], and stabilization and control by nonlinear gain [118,119]. Indeed, using particular arrangements of the dispersion compensation in the nonlinear system, or *dispersion management*, it is possible to suppress many of these. There are two principal approaches (that often converge) to overcome fibre transmission impairments: in the first (that can be called "linear") both the chromatic dispersion and nonlinearity are treated as detrimental factors, while in the second the nonlinear and dispersive effects might be partially counterbalanced cancelling or suppressing each other (such systems can be called "nonlinear"). In principle, detrimental nonlinear effects in the "linear" systems can be used under proper arrangement to improve transmission characteristics of optical communication systems. We will use here the term *dispersion management* when considering nonlinear systems, in contrast to *dispersion compensation* that is applied to linear systems or linear (low power) operational regimes.

In this review we will focus on dispersion management in optical fibre based systems in telecommunications and laser applications. To give an idea of the breathing nature of pulse solutions in dispersion managed systems, we show a typical example of dispersion management from a communications and laser applications in Fig. 3. Indeed, dispersion management has been crucial for understanding systems in both applications. In recent history of communications systems the role of dispersion and its application has highlighted many rather dramatic twists in the importance of different physical phenomena in optical fibres with a corresponding impact on technologies. First, fibre dispersion was treated as a purely detrimental effect and the development of dispersion-shifted fibre, where a dispersion value close to zero near 1550 nm was proposed. However, later it was found that transmission in fibres with small dispersion suffer from nonlinear four-wave mixing that is dramatically enhanced due to suitable phase matching conditions at small dispersion. Next the proposal of dispersion management with optical fibres with high local dispersion but low net-dispersion was implemented. Recently developments in linear coherent transmission offers a new possibility to compensate dispersion electronically at the receiver, allowing for uncompensated transmission over thousands of kilometres. However, such large dispersive broadening in such systems can lead to the overlapping of a large number of optical bits and create additional irregularities [120]. Further, improvement of the signal-to-noise ratio will inevitably introduce nonlinearity in such systems. We anticipate that future analysis of nonlinear effects in coherent transmission could lead to a better way to manage dispersion. Indeed, development towards new solutions in such communications systems is needed since in the next decade the total capacity of the current fibre transmission systems will be saturated by the ever-increasing amount of Internet applications and data flow. In ultra-short fibre lasers a similar history has highlighted the important role of dispersion management in these inherently dissipative, periodic systems. The first soliton fibre lasers have been constructed entirely of fibre with anomalous group-velocity dispersion to generate fundamental solitons of the NLSE [121]. However, similar to guiding solitons, the very nature of solitons in such periodic systems restricts the parameter regimes possible from such lasers. One of the most effective ways to circumvent the instabilities and limitations imposed by soliton laser operation is to construct fibre lasers with segments of both anomalous and normal GVD, so the cavity consists of a dispersion map [122,123]. Since the pulse solutions (often called "stretched pulses" in the context of laser applications) are compressed and broadened per cavity round trip, such lasers produce pulses where the average pulse duration is increased while the average peak power is decreased when compared with a laser that produces the same energy pulses with uniform dispersion. This has the overall effect of reducing the nonlinear effects and their associated instabilities in the anomalous dispersion fibre. The breathing evolution also disrupts the phase-matching to dispersive waves that occurs in the generation of side-bands. Current mode-locked fibre lasers consist of a cavity without any anomalous dispersion fibre, but rely on other methods for dispersion compensation such as spectral filtering.

Fig. 3 shows two physical examples of the pulse dynamics in dispersion managed optical systems. Clearly these solutions, so-called DM solitons, are different than classical optical solitons (solitons of the NLSE with uniform dispersion) which rely on the continuous balance between the effects of linear dispersive pulse broadening and nonlinearity. Optical pulses propagating in a dispersion-managed system experience a periodic change of their key parameters such as pulse width, power and the phase parameter (chirp), following the periodic variations of the dispersion. The change in the sign of dispersion causes the DM solitons to temporally broaden and re-compress or "breathe" as they propagate. Moreover, the use of periodic distributed Raman amplification in fibre lines makes it possible to control periodic variations of the signal power—the technique is known as nonlinearity management [112,124]. In general, the properties of DM solitons are quite different than conventional NLSE solitons and one of the goals of this paper is to overview the physics and mathematics of DM solitons in the context of transmission and ultra-short fibre lasers extensively studied in the past decades. The key ideas of dispersion management and the dynamics of DM solitons that we plan to discuss in this review is:

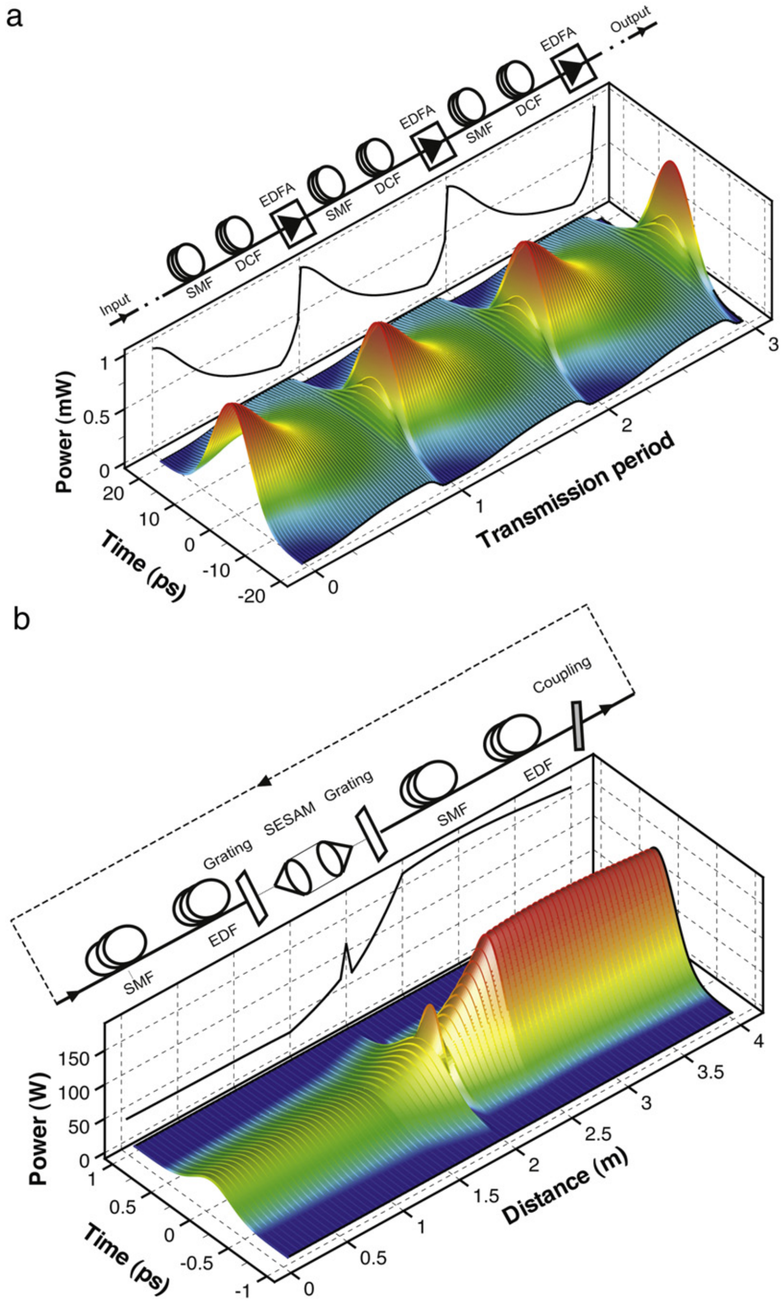

Fig. 3. Typical power evolution in optical systems where dissipative elements are included along with dispersion compensation. (a) Example from a transmission line in optical communications. (b) Example from a mode-locked fibre laser. SMF — single-mode fibre; DCF — dispersion-compensated fibre; EDFA — erbium-doped fibre amplifier; EDF — erbium doped fibre; SESAM — semi-conductor saturable absorber mirror.

- How low net dispersion (also accumulated or average dispersion) of the periodic cell allows one to control effects that are dependent on the overall dispersion of the system.
- How high local dispersion in each section of the dispersion map allows for the control of effects that depend on the local value of dispersion. For instance, phase matching for the efficiency of four-wave-mixing, or dispersive pulse broadening that reduces peak power and, respectively, nonlinear effects.
- In laser oscillators, the generation and management of broadened low peak power pulses may be combined with the extraction of (or compression to) short-duration, high peak power of pulses with comparable energy content.
- The shape and key pulse characteristics such as peak power, width and chirp are not constant during propagation within the periodic cell (e.g. cavity), but experience large oscillations leading to "breathing-like" soliton dynamics.

Please cite this article in press as: S.K. Turitsyn, et al., Dispersion-managed solitons in fibre systems and lasers, Physics Reports (2012), doi:10.1016/j.physrep.2012.09.004

- Dispersion management can be used to increase the energy of the stable breathing pulse compared to the NLSE soliton with the same pulse width at the same average dispersion.
- With dispersion management stable pulses can propagate with any sign of net-dispersion and even at the zero path-average dispersion.

2.2. DM soliton characterization and visualization

There are two main propagation scales in typical DM soliton systems: (i) the "fast" scale corresponds to the DM soliton dynamics which occur over one dispersion map period; and (ii) the "slow" scale corresponds to propagation distances which are much larger than the dispersion map period. Often the fast dynamics can be captured by obtaining evolution equations on key pulse characteristics such as pulse width, peak power, energy, chirp parameter and bandwidth. The particle-like properties of solitons make it possible to derive under some reasonable assumptions a closed system of coupled ordinary differential equations (ODES) that well approximate the key features of soliton dynamics. This important simplification is a direct consequence of the soliton being a wave-packet that can be well-approximated by a finite number of degrees of freedom. Instead of the analysis of partial differential equations that govern the field evolution, one can use a finite set of ODEs to understand the intra-map dynamics. Both the variational method and the method of moments have been used to derive such ODEs for nonlinear Schrödinger-type equations. The variational approach [125] relies on the ability to restate the NLSE in terms of a variational problem in which the Lagrangian is to be minimized for a particular ansatz function. It was first used for NLSE-type equations by Anderson in 1983 [126] and has since been extensively used to model a variety of perturbed NLSE systems (see e.g. [127–130] and references within). The method of moments (or root mean square momentum method), first used in nonlinear optics as early as 1971 [131], quantifies certain pulse characteristics such as pulse duration and peak power in terms of integral (over time) quantities. The governing partial differential equation can be algebraically manipulated resulting in a set of ODEs describing the evolution (in z) of the integral quantities [132]. It is interesting that although both the variational method and method of moments (or RMS momentum method) have been used to accurately describe GLE-based models, to our knowledge a formal mathematical analysis comparing the methods has not been performed outside of a few specific examples.

Here we will focus on work that has been done regarding certain integral quantities called the root-mean-square (RMS) characteristics which has had success describing, among others, pulse characteristics in fibres [133,134]. To describe the key particle-like characteristics of the pulse field $u(z, t)$ we consider the evolution of the following integral quantities

$$T_{RMS}(z) = \left[\frac{\int t^2|u(z,t)|^2dt}{\int |u(z,t)|^2dt}\right]^{1/2} \tag{17a}$$

$$P_{RMS}(z) = \frac{\int |u(z,t)|^4dt}{\int |u(z,t)|^2dt} \tag{17b}$$

$$C_{RMS}(z) = M_{RMS}(z)T_{RMS}(z) = \frac{i}{4}\frac{\int\ t[u(z,t)u_t^*(z,t) - u^*(z,t)u_t(z,t)]dt}{\int |u(z,t)|^2dt} \tag{17c}$$

$$\Omega_{RMS}(z) = \left[\frac{\int |u_t(z,t)|^2dt}{\int |u(z,t)|^2dt}\right]^{1/2}, \tag{17d}$$

which describe the RMS pulse duration T_{RMS}, pulse power P_{RMS}, chirp parameter $C_{RMS} \equiv M_{RMS}T_{RMS}$ and bandwidth Ω_{RMS}. These integral pulse characteristics can be expressed through the corresponding local pulse parameters by considering

$$u(z,t) = \sqrt{P(z)}f\left(z, \frac{t}{T(z)}\right)\exp\left[i\frac{M(z)}{T(z)}t^2\right], \tag{18}$$

with the parabolic (in time t) phase and a power distribution given by function $f(z, t)$. The links between RMS integral quantities and local pulse characteristics are given by

$$T_{RMS}(z) = T(z)\left[\frac{\int x^2|f(z,x)|^2dx}{\int |f(z,x)|^2dx}\right]^{1/2} = T(z)\langle x^2\rangle_f \tag{19a}$$

$$P_{RMS}(z) = P(z)\frac{\int |f(z,x)|^4dx}{\int |f(z,x)|^2dx} = P(z)\langle |f|^2\rangle_f \tag{19b}$$

$$C_{RMS}(z) = M(z)T(z)\langle x^2\rangle_f \tag{19c}$$

$$\Omega^2_{RMS}(z) = \frac{1}{T^2(z)}\frac{\int |f_x(z,x)|^2dx}{\int |f(z,x)|^2dx} + 4M^2(z)\langle x^2\rangle_f. \tag{19d}$$

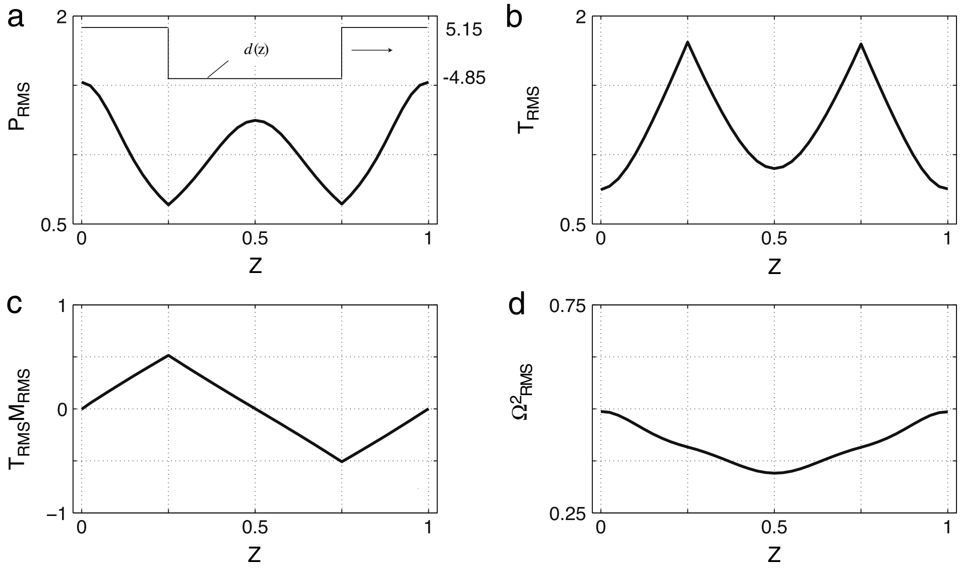

Fig. 4. The slow evolution of the RMS parameters for a typical piecewise constant dispersion map.

In Eq. (19) the integrals depend on z due to the structural function $f(z, t/T(z))$. When the propagation is ideally self-similar $f(z, t/T(z)) = f(t/T(z))$, the integrals (19) do not depend on z. In this case the RMS and local pulse parameters evolve in exactly the same way and are described effectively by the same evolution equations. However, when there is a difference between the RMS and local quantities then it is due to the change in the structural function $f(z, t)$. Indeed, this comparison can be made to describe and quantify slight deviations from true self-similar propagation regimes.

Since the RMS parameters depend on propagation distance it is important to visualize them in the appropriate way. Fig. 4 illustrates how such parameters evolve in a dispersion managed system over one piece-wise constant dispersion map. The evolution of the parameters illuminates that the DM soliton stretch and compress twice per cavity round trip, reach a minimum duration in the middle of each segment, and acquire both signs of chirp, typical of conservative DM solitons. The same information can be visualized in the phase plane of the RMS parameters. Fig. 5(a) shows the phase plane dynamics for a conservative DM soliton as shown in Fig. 4. Here we see the "crescent" shaped phase portrait that is typical of DM solitons, with each curve in the crescent corresponding to a section of anomalous or normal dispersion [135]. In the following section we will show how the evolution of the RMS integral quantities (17) can be presented as a system of ODEs and in some limits solved analytically. This simple and transparent method has been used extensively in DM systems and is especially useful in applied problems where massive multi-parametric optimization modelling is required.

RMS quantities are also important to classify the phase shifts caused by nonlinearity and dispersion per map period. These phase shifts can be quantified by

$$\phi_{NL}(L) = \int_0^L \gamma P_{RMS} dz, \qquad \phi_D(L, t) = \int_0^L \beta_2 \Omega_{RMS}^2 dz, \tag{20}$$

where ϕ_{NL} (ϕ_D) are the accumulated nonlinear (dispersive) phase shifts in a fibre of length L. There are two quantities that are related to the accumulated phase shifts that are commonly used to classify the nonlinearity or dispersive properties of pulse propagation in optical fibre. First, the maximum nonlinear phase shift $\phi_{NL}^{\max} = \mathrm{Max}(\gamma P_{RMS})$ quantifies the variation of the phase across the pulse. If excessive, it can influence the spectral and temporal profiles of a pulse and lead to nonlinear instabilities and pulse break-up or fission. Second, the maximal dispersive phase shift is commonly given by a quantity known as the "map strength". For a k-step piecewise constant dispersion map with GVD coefficients $\beta_2^{(k)}$ and length $L^{(k)}$ for the kth link, the map strength is given by

$$S = \frac{\sum_k |\beta_2^{(k)}| L^{(k)}}{\sum_k L^{(k)}} \times \mathrm{Max}\,(\Omega_{RMS}^2), \tag{21}$$

where $\mathrm{Max}(\Omega_{RMS}^2)$ is the maximum square of the bandwidth in the dispersion map. This definition is an extension of the commonly used map strength definition where $\mathrm{Max}\,(\Omega_{RMS}^2) = \left[\mathrm{Min}\,(T_{RMS}^2)\right]^{-1}$. As we will see, since the DM soliton dynamics relies on the interaction between the peak power and pulse bandwidth, the map strength has an upper bound in its value due to nonlinear instabilities which occur for $\phi_{NL}^{\max} \sim 2\pi$.

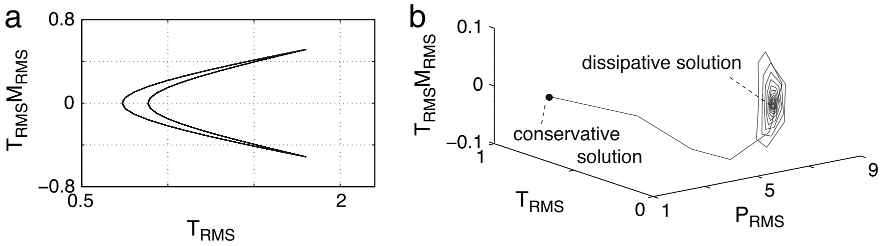

Fig. 5. Visualization of dispersion managed soliton dynamics. (a) Phase plane dynamics showing the evolution of pulse parameters over one dispersion map period for a conservative DM system. (b) Poincaré map showing the stroboscopic long-scale evolution of the pulse parameters at one particular point (shown here in the middle of the anomalous segment) in the dispersion map over many map periods. The examples shown here correspond the conservative case in (a), and a dissipative DM solution whose initial condition is the same as the DM soliton considered in (a). Note the dissipative terms attract the solution to a different point in the phase space.

In addition to the analysis of the fast dynamics in dispersion managed systems, the slow evolution may be described using a variety of mathematical approaches, including, among others, Hamiltonian averaging in the spectral domain, the expansion of the solutions in the basis of Gauss–Hermite functions, averaging based on using a Lie-transformation, and multiple-scale averaging. In this review we do not aim to present all of these important techniques already comprehensively discussed in the literature. However, we will use only some of these various methods that in our view are the most natural to the considered problems and can be presented in a relatively simple and clear way while describing the main physical features of the slow DM soliton dynamics. Such slow dynamics can be visualized at one particular point in the dispersion map, giving a "stroboscopic" evolution, or viewing the solution in terms of a Poincaré map in the periodic system. Fig. 5(b) shows the stroboscopic evolution of the RMS quantities in the conservative case shown in Fig. 5(a) as well as an example where dissipative elements are involved. Here the quantities are shown at a particular point in the map, and for the conservative DM case the initial conditions satisfies the conditions for exact periodic evolution, thus the point in the map stays stationary. However, for the case when dissipative terms are included the flow spirals to a sink point, representing the periodic solution. The flow to a point in the phase space is not always the case, and it is possible to have DM soliton evolution that is not perfectly periodic, which would be represented in the absence of a sink point in such a stroboscopic visualization.

3. Dispersion-managed solitons in Hamiltonian systems

3.1. Introduction and historical perspective

In Section 3 we will overview DM solitons in Hamiltonian systems by considering the rather general model of optical signal propagation in a system with periodic dispersion management and periodic amplification. Similar to the system considered for guiding centre solitons in Section 1.2, the governing equation for such a dispersion managed system is modelled by the normalized NLSE

$$i\,\frac{\partial a}{\partial z} + d(z)\,\frac{\partial^2 a}{\partial t^2} + c(z)|a|^2 a = 0. \tag{22}$$

To reiterate what was presented in Section 1.2, the field transformation and normalizations used in Eq. (22) are

$$a(z,t) = u(z,t) \times \exp\left[\int_0^z g(z')dz' - \langle g\rangle z\right] \tag{23a}$$

$$g(z) = -\alpha(z) + \sum_{k=1}^{N}[\exp(\alpha_k L_a/L) - 1]\delta(z - kL_a/L), \tag{23b}$$

$$d(z) = \tilde{d}(z) + \langle d\rangle = -\frac{(\tilde{\beta}_2(z) + \langle\beta_2\rangle)L}{2T_0^2} = \frac{\lambda_0^2(\tilde{D}(z) + \langle D\rangle)L}{4\pi c_l T_0^2}, \tag{23c}$$

$$c(z) = \tilde{c}(z) + \langle c\rangle = \gamma(z)P_0\,L\,\exp\left[2\int_0^z g(z')dz' - 2\langle g\rangle z\right], \tag{23d}$$

where time, distance, and power have been normalized by T_0, L, and P_0 respectively and the normalized dispersion $d(z) = \tilde{d}(z) + \langle d\rangle$ represents a sum of a periodically varying high local dispersion ($\langle\tilde{d}(z)\rangle = 0$) and a constant residual (average) dispersion ($\langle d\rangle \ll \tilde{d}$). The variation in nonlinearity $c(z)$ is due to different fibres with potentially different intrinsic parameters (such as effective mode area) as well as a periodic (with period L_A/L) contribution due to the power decay from fibre loss as well as lumped amplification. Eq. (22) possesses a conserved quantity $E = \int |a(z,t)|^2 dt$ that is the energy of the system. Optical pulse dynamics in dispersion-managed transmission systems is determined by the combined action of fibre loss, periodic amplification, self-phase modulation and chromatic dispersion. It should be pointed out that these effects are not additive and pulse evolution critically depends on the order in which dispersion compensation is realized. Strong interference of the effects of nonlinearity and varying dispersion leads to a rich variety of possible configurations for dispersion management.

As discussed in Section 1, the various length scales in the model equation (22) determine different operation regimes. In addition to the nonlinear length L_{NL}, amplification length L_A, and local dispersion length L_D, the inclusion of a dispersion map adds two new length scales, that of the residual dispersion length $L_{\langle D\rangle} = T_0^2/(2|\langle\beta_2\rangle|)$ as well as the period of the dispersion map L_{DM}. Consideration of these length scales is the key to understanding the many limits available for pulse solutions to Eq. (22). Some of these limits include

- Lossless ($L_A = 0$) and effectively lossless ($L_A \ll L_{DM}$) systems.
- Typical terrestrial system implementation for $T_0 \sim 10$'s of ps ($L_{DM} = L_A$).
- Short-scale management ($L_{DM} \ll L_A$).
- Strong dispersion management ($L_D \ll L_{\langle D\rangle}, L_{NL}$).
- Weak dispersion management ($L_{DM} \ll L_D, L_{\langle D\rangle}, L_{NL}$).

In the following sections we highlight many aspects of dispersion management. Before we get into the details, it is important to understand the historical perspective of why dispersion management became a relevant subject. Soliton transmission had been theoretically proposed, however some limitations in practical communications systems were soon discovered. In a transmission system, it is important to be able to predict the arrival time of the optical bit as well as distinguish it from other radiation. In soliton transmission systems amplifiers introduce amplified spontaneous emission noise which is added to the signal. The noise modulates the soliton frequency randomly, which leads to random timing jitter through the GVD of the fibre [87–90]. The magnitude of the so-called Gordon–Haus–Elgin timing jitter (or variance of the fluctuation of arrival time of a pulse) is proportional to the GVD of the fibre for pulses of the same width. Thus for a particular pulse width, to reduce the timing jitter one needs have the GVD of the fibre close to zero. In addition to reducing the timing jitter, it is also important to be able to distinguish the optical signal from the noise added by the amplifiers. This ability is quantified by the so-called signal-to-noise ratio [7]. The soliton area theorem states the peak power is proportional to the GVD resulting in an increased signal-to-noise ratio for larger values of GVD for a particular pulse width. Thus by tuning the GVD you can minimize one detrimental aspect for transmission, but only at the expense of maximizing another, imposing a fundamental limit to soliton transmission systems. A natural idea to circumvent these issues was to allow the transmission line to be constructed from alternated fibres with anomalous or normal dispersion. Thus the transmission system can have a low path-averaged chromatic dispersion, but a high local one, thereby suppressing the Gordon–Haus–Elgin timing jitter as well as four-wave mixing simultaneously, but still having high signal-to-noise ratios. In [114] it was proposed to incorporate a section of dispersion compensating fibre into the standard periodic soliton transmission line before each amplifier. This technique was successful as it reduces the power required, compared to an uncompensated (constant dispersion) soliton system, and increases both the maximum transmission distance and the range of pulse widths over which operation is possible [114]. In the first related experimental work [115] dispersion management was shown to lead to a significant reduction of the Gordon–Haus–Elgin timing jitter. In should be pointed out that around the same time as these ideas were developing in transmission systems, similar ideas in ring lasers were also being utilized in the form of stretched pulse generation [136]. In Refs. [137,138], the pulse propagating in such a dispersion-managed transmission system was identified as a new information carrier—a stable periodic breather with features very different from that of the conventional soliton.

Fig. 6 shows an example of the evolution of a traditional DM soliton over one map period from numerically solving Eq. (22) for a lossless system ($c(z) = 1$) with a piece-wise constant dispersion map

$$d(z) = \begin{cases} d + \langle d\rangle, & 0 < z < 0.25 \\ -d + \langle d\rangle, & 0.5 < z < 0.75, \\ d + \langle d\rangle, & 0.75 < z < 1, \end{cases} \tag{24}$$

where the dispersion depth $d = 5$, path average dispersion $\langle d\rangle = 0.15$, and the propagation length $L = L_{DM}$. We see that the DM soliton undergoes self-similar-like compression and broadening. In the logarithmic scale it is seen that at $z = 0$ and $z = 0.5$ (the middle of each segment) there is maximum compression and there exists dips corresponding to points at which the soliton power $|a(z,t)|^2$ approaches zero (and consequently, the logarithm of the power tends to minus infinity) [139]. These oscillations around the main peak present an inherent part of the DM soliton. The DM soliton remains localized and stable during evolution while acquiring an additional phase term after each dispersion map period. As the DM soliton propagates from the centre of the anomalous dispersion segment ($z = 0$), it temporally broadens and then re-compresses until it reaches the centre of the normal dispersion segment ($z = 0.5$), whereupon it begins to broaden again, thereby breathing, as seen in Fig. 6. Numerical simulations and experiments revealed the following main features of the DM soliton which make it quite distinct from conventional solitons

- In strongly dispersion managed systems, the pulse width can experience large oscillations during the compensation period leading to "breathing-like" soliton dynamics. This differs substantially from the path-averaged (guiding-centre) soliton propagation in systems with constant or weakly varying dispersion and from that of the traditional fundamental soliton [46]. Although there is breathing dynamics, it is possible to observe extremely stable propagation in fibre links with strong dispersion management.

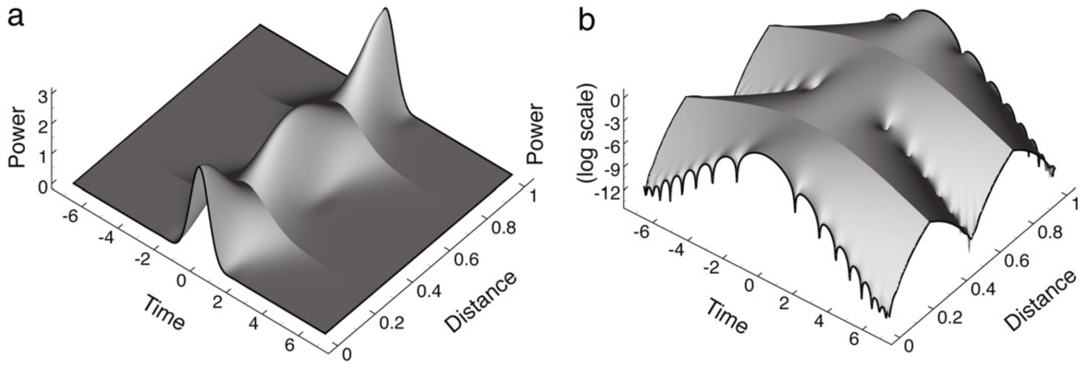

Fig. 6. Breathing dynamics of a DM soliton propagating over one dispersion map period.

- Throughout most of the dispersion compensation period, the DM soliton has a nontrivial phase across it, characterized by the chirp parameter [137,140]. The chirp can reduce the chromatic dispersion penalty as well as suppress pulse to pulse interaction to improve the transmission capacity in systems implementing dispersion management [140]. The initial chirp of the pulse launched into the transmission line was shown to be essential in stable propagation [117,140–143]
- The asymptotic shape of the pulse is not always a hyperbolic secant shape as it is for the NLSE soliton, but varies with an increase of the map strength (21) from a hyperbolic secant shape to a Gaussian shape and to a flatter waveform.
- The pulse shape within the dispersion map varies from a monotonically decaying profile to a distribution with oscillatory tails.
- The time–bandwidth product varies with an increase of the map strength (21) from 0.32 corresponding to the hyperbolic secant NLSE soliton to 0.44 corresponding to the Gaussian pulse and increases further with an increase of the map strength.
- The energy of the stable breathing pulse is well above that of the NLSE soliton with the same pulse width and of the corresponding average dispersion [138]. This energy enhancement leads to an increase of the signal-to-noise ratio with substantial improvement of transmission system performance [115].
- The DM soliton can propagate at both zero and normal path-average dispersion, in contrast to the fundamental soliton that propagates stably only in the anomalous dispersion region [144]. This feature allows the transmission of a finite energy pulse close to zero net-dispersion, suppressing timing jitter.
- The central part of the DM pulse is self-similar, but the far-field oscillating (and exponentially decaying) tails are not.

Because of the various length scales and parameters in dispersion-managed systems, it is important to both use efficient numerical techniques as well as obtain analytical knowledge to both optimize and characterize the system [109,128,145–147]. As we have seen in Section 1, there is a rich basis of mathematical findings with conventional solitons. A natural question is whether such mathematical insight and techniques can be used with DM solitons, since the same NLSE is used to model propagation, only with a slight modification that the dispersion coefficient is dependent on propagation distance. However, as we have just discussed, all the listed features show that there is a distinct difference between DM solitons and conventional solitons of the NLSE. Indeed, the variation of dispersion with propagation distance violates many of the symmetries present in the conservative NLSE. As a particular consequence of this, a model describing the path-averaged (slow) evolution of the breathing DM pulse should differ from that which governs the path-averaged dynamics of the fundamental soliton. In many limits significant analytical insight into the nature of DM solitons and their dynamics can be obtained. For instance, in the effectively lossless limit $L_A \ll L_{DM}$, the effects of periodic amplification and dispersion compensation can be separated [141]. In this case the signal dynamics can be averaged over the amplification period and an averaged propagation equation is described by the lossless limit ($c(z) = \text{constant}$). In the case of weak dispersion management a Lie-transform technique has been applied to describe properties of the DM soliton [148]. For strong dispersion managed systems, the fast scale pulse dynamics were separated from the slow scale pulse dynamics [137], leading to the application of various averaging or multiple scale methods [137,149]. Other pursuits considered the DM soliton as a nonlinear Bloch wave function or, in other terms, as a nonlinear eigenfunction of Eq. (22) with the period L_{DM} that exists in the case of small nonlinearity [150,151]. In the following subsections we will discuss some of most important aspects of DM solitons in Hamiltonian systems that are described by Eq. (22).

3.2. Linear solutions

In the case of strong dispersion management the dispersion map period (or local dispersion length) is much smaller than both the nonlinear and residual dispersion length ($L_{DM}, L_D \ll L_{NL}, L_{\langle D \rangle}$). In this limit the effects of nonlinearity and the residual dispersion are small over one map period and the main factors that affect the pulse evolution during the single period are chromatic dispersion, loss, and amplification. The propagation regime is then quasi-linear and, thus, it is worth to recall the well known exact solution of the linear problem. This will not only provide the right framework for analysis when small nonlinearity and residual dispersion effects are taken into account, but also provides good physical insight into the DM solitons and their relation to localized structures in periodic mediums. When neglecting the nonlinear term in Eq. (22) (note that this also includes neglecting the gain/loss dynamics) there exists the solution

$$a(z,t) = \int_{-\infty}^{+\infty} \hat{a}\,(0,\omega)\exp[i\omega t + i\omega^2 R(z)]\,d\omega, \quad R(z) = \int_0^z d(z')\,dz', \tag{25}$$

where $\hat{a}\,(0,\omega)$ is the Fourier transform of the initial pulse. To give a specific example, for an initial Gaussian pulse $a(0,t) = N\exp(-t^2/2)$, the rapid oscillations of the pulse power and width over the compensation cell from $z = 0$ to $z = L_{DM}$ are given by

$$a(z,t) = |a(z,t)|\,e^{i\Theta(z,t)}, \quad \text{where } |a(z,t)|^2 = \frac{N^2}{\tau(z)} e^{-\frac{t^2}{\tau^2(z)}}, \qquad \Theta(z,t) = \frac{C(z)\,t^2}{\tau^2(z)} - \Phi(z), \tag{26}$$

where $\tau^2(z) = 1 + 4R^2(z)$, $C(z) = R(z)$ and $\Phi(z) = 0.5\,\arctan[2R(z)]$. The spectral evolution is given by

$$\hat{a}(z,\omega) = |a_\omega(z,\omega)|e^{i\Theta_\omega(z,\omega)}, \quad \text{where } |a_\omega(z,\omega)|^2 = N^2 e^{-\omega^2}, \qquad \Theta_\omega(z,\omega) = \Phi(z) - R(z)\times\omega^2. \tag{27}$$

When the dispersion $d(z)$ is exactly compensated ($R = 0$) the linear pulse recovers its initial power, width and chirp periodically. In a system with strong dispersion management and low nonlinearity, at leading order the short scale (on the order of the dispersion map period) pulse dynamics of a DM soliton is approximated by the linear solution (26). Thus we can obtain important insight by recognizing the main features of the solution (26) that we expect will survive, at least in the weakly nonlinear propagation regime. From Eq. (27), we see that the spectral solution to the linear equation is modified only in spectral phase due to dispersion, but the spectral bandwidth does not vary. As will be discussed in Section 3.4, this observation suggests a decomposition in the spectral domain of the rapid (quasi-linear) oscillations of the phase and slow (path-averaged) evolution of the DM soliton for the weakly nonlinear case [129,137,152–155]. Further, we see from Eq. (26) that the dispersion managed pulse to the linear equation has a quadratic (in time) nontrivial phase (linear chirp) and also has a self-similar structure, i.e. the product of the pulse peak power and duration is constant. These basic features should be retained when including small nonlinearity and residual dispersion, at least in the central, energy containing part of the pulse. This gives an alternative way to describe the DM soliton that leads to significant physical insight of the DM soliton. Specifically, let us assume that the field is given by a function of the form

$$u(z,t) = \frac{N}{\sqrt{T(z)}} f(z,x)\,\exp\left[i\frac{M(z)}{T(z)}t^2\right], \tag{28}$$

where $x = t/T(z)$, and f, T, and M are real functions. Inserting (28) into Eq. (22) we find that $T_z = 4d(z)M(z)$ and the evolution of the structural function f is given by

$$i\frac{\partial f}{\partial z} + \frac{d(z)}{T^2}\frac{\partial^2 f}{\partial x^2} - \left[M_z T x^2 - \frac{Nc(z)}{T} f^2\right] f = 0. \tag{29}$$

We see that if $M_z \neq 0$ there exists an effective parabolic trapping potential, and in the linear limit ($c(z) = 0$) Eq. (29) is analogous with the harmonic oscillator in quantum mechanics. In the weakly nonlinear case we can exploit this by assuming that the pulse can be presented in the complete basis of the chirped Gauss–Hermite functions

$$a(z,t) = \frac{N}{\sqrt{\tau(z)}} \sum_{n=0}^{\infty} \frac{a_n}{\sqrt{2^n n! \sqrt{\pi}}} \exp\left[-\frac{t^2}{2\tau^2(z)} + i\,C(z)\,\frac{t^2}{\tau^2(z)} - i(1+2n)\Phi(z)\right] H_n\!\left(\frac{t}{\tau(z)}\right), \tag{30}$$

which are the eigenfunctions to the harmonic oscillator Schrödinger operator. Here $\tau(z)$, $C(z)$ and $\Phi(z)$ are the same as introduced in (26). The function H_n is the nth-order Hermite polynomial and the coefficients a_n are determined by the initial distribution

$$a_n = \frac{\pi^{1/4}}{N\sqrt{2^n n! \pi}} \int_{-\infty}^{\infty} a(0,t) e^{-t^2/2} H_n(t)\,dt. \tag{31}$$

Note that the initial condition used to derive (26) is the zero-mode of this expansion. For the linear case ($c(z) = 0$) any arbitrary combination (i.e. with arbitrary a_n) of the Gauss–Hermite modes presents a periodic solution. These modes do not interact or mix, and the pulse will propagate without distortion. Further, the initial amplitude does not depend in any way on the initial pulse width. In the next subsection we will show that when nonlinearity is included the initial condition is critical for exact periodic pulse evolution.

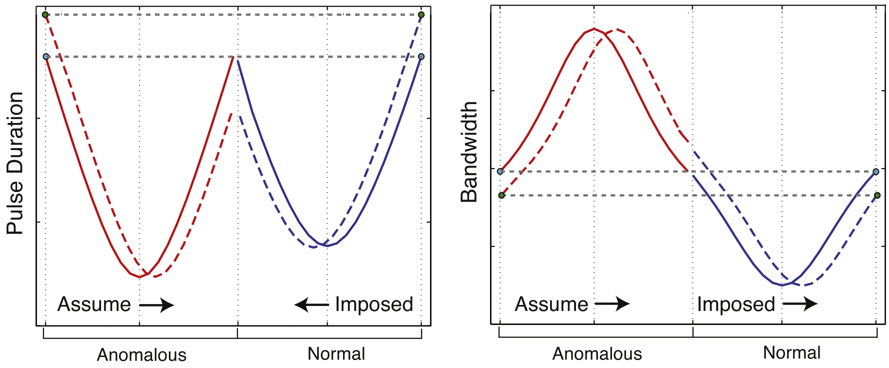

Fig. 7. Typical pulse duration and bandwidth for periodic DM soliton evolution (solid). Hypothetical evolution when it is assumed that CFP in the anomalous GVD segment is moved to the right of the centre of the anomalous GVD segment.

3.3. Initial conditions and chirp-free points for periodic DM soliton evolution

In contrast to the linear case, when nonlinearity is introduced exact periodic propagation will not occur unless a certain relation between the initial pulse amplitude and pulse width is satisfied. If this condition is not satisfied, the nonlinearity will redistribute the energy between different Gauss–Hermite modes of the DM soliton. Often the higher-order modes become an inherent part of the nonlinear solution. This can be understood by noticing that in Eq. (29) nonlinearity modifies the parabolic potential, and the shape of the nonlinear wave is an eigenfunction of the Schrödinger operator with this perturbed periodic potential. An important consequence is that if an initial Gaussian pulse that is not the true DM solution is input into the dispersion managed system, radiation is shed and causes long scale oscillations around some steady state value of the pulse parameters [156]. Such dispersive radiation is an additional source of noise and can degrade system performance. Thus to obtain exact periodic pulse evolution it is necessary to pre-condition the initial pulse to have a certain peak power, pulse duration, phase, and shape for the particular system of interest. Typically the pulse power and duration can be controlled using various optical elements such as amplifiers. Further, it is possible to manipulate the nontrivial phase across the pulse through either some phase modulation or by propagating the pulse in a dispersive medium. The time derivative of the nontrivial phase is defined as the chirp, or instantaneous frequency. Similar to the linear solution (30), DM solitons typically have a quadratic nontrivial phase profile, or linear chirp in the energy-containing core of the pulse. The magnitude of the nontrivial phase across the pulse is quantified by the chirp parameter, which is defined as the coefficient in front of the quadratic term in the phase ($C(z) = M(z)/T(z)$ in Eq. (28)). Pulse pre-chirping by an external modulator or additional fibre propagation can substantially reduce the chromatic dispersion transmission effects relative to the non-pre-chirped case [140].

One of the key characteristics of DM solitons is that the chirp parameter oscillates between positive and negative values. Points of interest for this evolution are so-called chirp-free points (CFPs), where the chirp parameter is zero and the pulse duration and bandwidth achieve an extremum value. Initial studies of DM solitons showed that systems with a periodic dispersion map consisting of two sections of opposite sign dispersion (each segment having arbitrary lengths) required the CFPs to be at the mid-points in each section. This observation highlighted the importance of nonlinearity in the system, since in the linear case the CFP can be anywhere along the dispersion map, and exact periodic evolution requires only perfect dispersion compensation per dispersion map period. A simple intuitive explanation can be understood by observing the pulse duration and bandwidth evolution of a DM soliton per map period in a "lossless" system. To give a specific illustrative example, Fig. 7 shows the DM soliton evolution for a symmetric dispersion map where the lengths of each segment are the same and the CFP is in the middle of each dispersion segment. For the pulse duration, if we assume that the CFP in the anomalous GVD segment is to the right of the anomalous GVD segment centre, the CFP in the normal GVD segment is constrained to move to the left of the normal GVD segment centre to preserve periodic boundary conditions. However, when considering the bandwidth, making the same assumption of the CFP in the anomalous GVD segment imposes that the CFP in the normal GVD segment moves to the right of the normal GVD segment centre to maintain periodic boundary conditions. This leads to a contradiction showing that the CFP must be at the middle of each segment. Indeed, since the pulse duration for DM solitons acts like a even function and that for the bandwidth acts as an odd function, the CFPs are restricted to be in the middle of each dispersion segment for such lossless systems with a symmetric dispersion map. Note that in the linear case this argument does not hold since the bandwidth is a constant value, and thus an even function.

This intuitive argument can be proven rigorously by symmetry arguments on the governing Eq. (22) in the case of lossless or effective lossless limits ($c(z) = 1$). The DM soliton solution is given by the nonlinear Bloch wave-function $a(z, t) = F(z, t, k)\ \exp(ikz)$ with a periodic function $F(z + L, t, k) = F(z, t, k)$ which is governed by

$$i\,\frac{\partial F}{\partial z} - kF + d(z)\,\frac{\partial^2 F}{\partial t^2} + |F|^2 F = 0. \qquad (32)$$

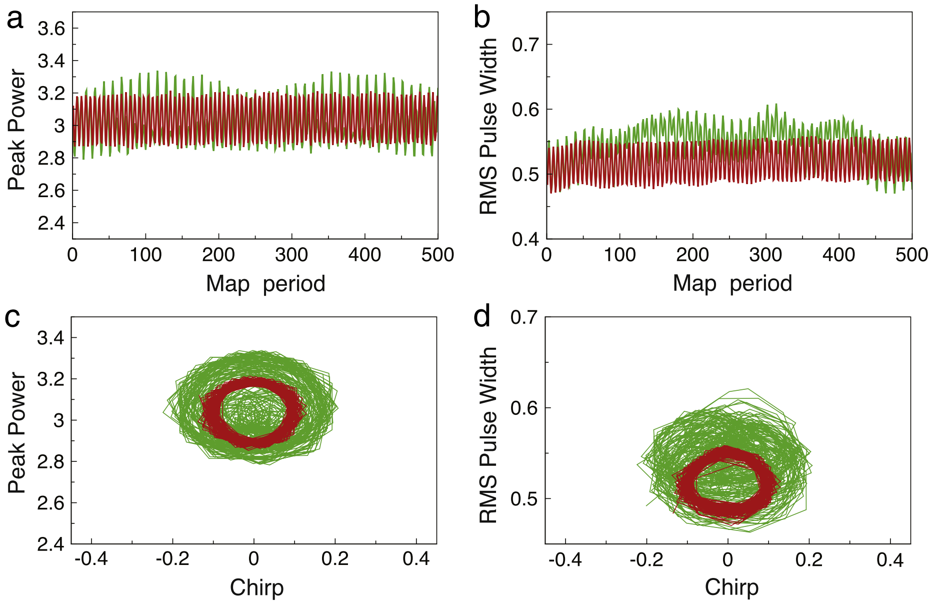

Fig. 8. Stroboscopic (taken at the middle of the anomalous GVD segment) evolution of (a) peak power and (b) RMS pulse width launched either at the CFP in the middle of the anomalous GVD fibre (red) or slightly from the CFP (green). Stroboscopic (taken at the middle of the anomalous GVD segment) evolution in the (c) power, chirp (d) width, chirp phase planes. (For interpretation of the references to colour in this figure legend, the reader is referred to the web version of this article.)

For simplicity, we neglect a certain degeneracy which occurs for strong dispersion maps with zero or normal average dispersion for which two stable periodic solutions can exist with the same pulse energy [157]. Neglecting such degeneracy, the wave-number k uniquely determines the DM soliton solution of Eq. (32) and it can be shown that CFPs are located at the points of symmetry of the function $d(z)$. Specifically, if $F(z,t,k)$ is a solution of Eq. (32) then $F^*(-z,t,k)$ is also a solution providing that the periodic dispersion map obeys the symmetry condition $d(z) = d(-z)$. Since k uniquely determines the DM soliton, $F(z,t,k) = F^*(-z,t,k)$ (note constant phase factors can be neglected due to the gauge invariance of Eq. (32)). Thus at the origin of any symmetrical dispersion map $\mathrm{Im}\,F(0,t,k) = 0$, which shows that the DM soliton will have no chirp at the points of symmetry of the dispersion map. For the specific dispersion map consisting of two pieces of optical fibre, such CFPs are always in the middle of the fibre spans. The uniqueness of the solution plays a crucial role in the proof presented here and does not apply to the case of multi-stability, when two or more stable solutions exist so that it is possible that $F^*(-z,t,k) \neq F(z,t,k)$. Indeed, there are special dispersion maps for which symmetry breaking occurs, in particular when the dispersion is small near the boundary [157].

As mentioned previously, pre-processing for the input signal into a particular dispersion managed system is typically essential to obtain the exact periodic DM soliton. Typically the peak power and pulse duration can be manipulated easily, however modulating the pulse phase and shape can be complicated and often involves expensive optical elements, adding to the cost of the system. Many pulse sources (such as a Ti:Sapphire mode-locked laser) generate Gaussian-type pulses which are transform limited, e.g. they do not have a nontrivial phase across the pulse. For practical dispersion managed systems it is important to achieve DM soliton pulse evolution from a wide variety of unchirped input pulse forms. Here we highlight that the locations of CFPs can be exploited to reduce long scale oscillations that are caused by dispersive radiation being shed due to any small deviations of the input pulse from the true periodic waveform. Fig. 8 considers Eq. (22) with a two step dispersion map (24) with $d = 2.5$ and $\langle d \rangle = 0.075$ and $c(z) = 1$ (lossless case). From our symmetry analysis, we know that the CFP for this system is at the middle of each fibre segment at $z = 0$ and $z = 0.5$. The initial condition is an unchirped Gaussian pulse with pulse duration 0.5. The peak power of the initial condition is found by finding periodic solutions to certain evolution equations governing the key pulse parameters (more details on how this is done will be given in Section 3.5). Fig. 8(a), (b) shows the stroboscopic evolution (taken at the middle of the anomalous GVD segment) of the pulse peak power and RMS pulse width over 500 map periods. The red lines are for the scenario where the initial pulse is launched at the CFP in the anomalous GVD fibre and the green lines are for the scenario where the initial pulse is launched at a point +0.01 units from this point. Long scale oscillations and reduced periodicity is observed when the initial pulse is not launched at the CFP. Fig. 8(c), (d) shows the stroboscopic (taken in the middle of the anomalous GVD segment) evolution in the phase plane, and highlights the increased variation of the pulse parameters when the launch point is not at the CFP. Even in the case where the initial pulse is launched at the CFP there is still some small variations in the pulse parameters, due to the initial pulse shape being Gaussian and is different from the shape of the true DM soliton. Indeed, if the input pulse was the true DM soliton there would be only a point in the phase space, highlighting exact periodic evolution. Note that although we have only considered a lossless system, it has been shown that launching an unchirped pulse at a CFP reduces long scale oscillations of the pulse parameter for various transmission systems, away from the lossless limit ($L_{DM} \sim L_A$) [140,143,157,158].

Although less studied, the analysis of CFPs in dispersion managed mode-locked fibre lasers also has many important implications. For example, CFPs are the optimal locations to place the output coupler since typically this is associated with the shortest pulse durations and the highest available peak power. Thus it could alleviate any post processing from the laser output. In fibre lasers composed of segments of fibres with opposite dispersion, the chirp free points hold the key to optimal out-coupling of the generated DM solitons or dissipative DM solitons. This will be further discussed in the following sections on practical applications of DM soliton theory in lasers.

3.4. Weak dispersion management

The overall impact of the periodic variation of the parameters in Eq. (22) strongly depends on the interplay between different physical effects. In the limit of weak dispersion management, it is natural to assume that the governing dynamics would be similar to that governing conventional solitons of the NLSE. Physically a weakly dispersion managed system exists if the length of the dispersion map L_{DM} is much shorter than both the nonlinear length L_{NL} and the residual dispersion length $L_{\langle D\rangle}$. In this limit, we can normalize Eq. (22) by $L = L_{NL}$ and obtain

$$i\frac{\partial a}{\partial z} + d\left(\frac{z}{\epsilon}\right)\frac{\partial^2 a}{\partial t^2} + |a|^2 a = 0, \tag{33}$$

where the small parameter $\epsilon = L_{DM}/L_{NL} \ll 1$ and $d(z/\epsilon) = d(z/\epsilon + 1)$. Here we have assumed a lossless model ($g(z) = 0$), however it is possible to perform a standard transformation to obtain the same governing equation (33) when the gain balances the loss in each dispersion map [159]. Utilizing the smallness of the parameter ϵ, we let [159,160]

$$a(t, z) = V + \epsilon v_1 + \epsilon^2 v_2 + O(\epsilon^3), \tag{34}$$

where V is the average of a with respect to z over the dispersion map period, so that the expansion terms v_k ($k = 1, 2, \ldots$) represent the fast oscillating part of the solution (similar to guiding-centre theory) satisfying $\langle v_k\rangle_\xi = \int_0^1 v_k\, d\xi = 0$, where $\xi = z/\epsilon$. Taking advantage of the different inherent length scales, it is possible to use a multiple scale expansion [161] where we assume that the oscillating parts v_k can be expressed through the average V and the "fast" variable ξ, while the evolution of V is described by "slow" variables $z_k = \epsilon^k z$, ($k = 0, 1, 2, \ldots$) so that

$$\frac{\partial V}{\partial z} = \frac{\partial V}{\partial z_0} + \epsilon\frac{\partial V}{\partial z_1} + \epsilon^2\frac{\partial V}{\partial z_2} + \cdots. \tag{35}$$

Inserting Eqs. (34)–(35) into (33) gives various terms that can be grouped in powers of ϵ. In order to avoid secular terms at leading order (ϵ^0)

$$i\frac{\partial V}{\partial z_0} + \langle d\rangle\frac{\partial^2 V}{\partial t^2} + |V|^2 V = 0 \tag{36}$$

and

$$v_1 = -\frac{i}{2}[\mu_1(\xi) - \langle\mu_1\rangle_\xi]\frac{\partial^2 V}{\partial t^2}. \tag{37}$$

Here $\langle d\rangle = \langle d\rangle_\xi$ is the average GVD coefficient, and the fast oscillations around the slowly varying field V are proportional to $\mu_1(\xi) = -2\int_0^\xi [d(s) - \langle d\rangle]ds$. Calculating the next two orders gives expressions for v_2, v_3, $dV/dz_1 = 0$, and dV/dz_2 [159]. Substituting the derivatives of dV/dz_0 from (36) and dV/dz_2 into Eq. (35) gives the averaged evolution equation for V

$$\begin{aligned} iV_z + \langle d\rangle V_{tt} + |V|^2 V = \epsilon^2\mathcal{M}\Big[&V^2V^*_{tttt} + 6VV_tV^*_{ttt} + 2(|V|^2)_tV_{ttt} + 5V|V_{tt}|^2 \\ &+ 7V_t^2V^*_{tt} + 10|V_t|^2V_{tt} + \frac{5}{2}V_{tt}^2V^*\Big] + O(\epsilon^3), \end{aligned} \tag{38}$$

where $\mathcal{M} = [\langle\mu_1^2\rangle - \langle\mu_1\rangle^2]/2$ is the variance of μ_1. The form of the solutions to v_1 and v_2 suggests the application of a near-identity transformation where we define a modified field

$$q = V + \epsilon^2\mathcal{M}\left\{\frac{1}{4}V_{tttt} - \frac{1}{2\langle d\rangle}\left[V_t(|V|^2)_t + V(VV_t^*)_t\right]\right\} + O(\epsilon^3). \tag{39}$$

Substituting this into Eq. (38) gives the evolution equation

$$i\frac{\partial q}{\partial z} + \langle d\rangle\frac{\partial^2 q}{\partial t^2} + |q|^2 q = -\epsilon^2\frac{\mathcal{M}}{2\langle d\rangle}\left\{|q|^2 q\frac{\partial^2}{\partial t^2}(|q|^2) + \frac{1}{2}q\frac{\partial^2}{\partial t^2}(|q|^4)\right\} + O(\epsilon^3). \tag{40}$$

This key result shows that a rapidly varying periodic dispersion can be transformed into a NLS equation with perturbations. However, this approximation is no longer valid when $\langle d\rangle \to 0$ since the perturbations become significant in this limit. The fact that rapidly varying dispersion can be shown to be equivalent to perturbations to the NLSE has also been shown in other contexts. Specifically, guiding centre solitons were described using Lie averaging [160] and guiding centre pulse dynamics for systems with mean zero dispersion were described using a near identity transformation and stationary phase asymptotics [162].

To make a connection with the conservative soliton of the NLSE, let the normalized path average dispersion $\langle d\rangle = 1/2$. Using a regular perturbation expansion in Eq. (40), we find

$$q(z,t) = e^{iz/2}\left[\operatorname{sech}(t) + \frac{4}{3}\epsilon^2\mathcal{M}[2\cosh^{-1}(t) - \cosh^{-3}(t) - \cosh^{-5}(t)] + O(\epsilon^3)\right]. \tag{41}$$

Transforming $q(z,t)$ back to $a(z,t)$ using (39) and (34) gives $a(z,t) = P(z,t)\exp(i\phi(z,t))$, where

$$\phi(z,t) = \frac{z}{2} - \frac{\epsilon}{2}\left[\mu_1(\xi) - \langle\mu_1\rangle_\xi\right]\left(1 - 2\cosh^{-2}(t)\right) + O(\epsilon^2) \tag{42a}$$

$$P(z,t) = \cosh^{-1}(t) \times \left[1 + \frac{1}{3}\epsilon^2\mathcal{M}\left[8 + 8\cosh^{-2}(t) - 19\cosh^{-4}(t)\right]\right.$$
$$\left. + \epsilon^2\left(\frac{1}{2}\left[\mu_1(\xi) - \langle\mu_1\rangle_\xi\right]^2 - \left[\mu_2(\xi) - \langle\mu_2\rangle_\xi\right]\right)[4\cosh^{-2}(t) - 5\cosh^{-4}(t)] + O(\epsilon^3)\right]. \tag{42b}$$

We see that weak dispersion management adjusts the NLSE soliton phase (power) by factors proportional to ϵ (ϵ^2) [159,160].

The analytic approximation for the weakly dispersion managed soliton can be used to understand a variety of different aspects of its dynamics. For example, Eq. (42b) shows that the pulse energy

$$\int_{-\infty}^{\infty}|a|^2\,dt = 2\left(1 + \frac{32}{15}\epsilon^2\mathcal{M} + \cdots\right), \tag{43}$$

is enhanced due to weak dispersion management. Considering a particular lossless system with a two-step dispersion map, early numerical studies on DM solitons discovered an empirical expression for the energy enhancement factor [138,141]. For small map strengths the energy of the DM soliton was shown to increase by a term proportional to the square of the map strength. This expression was found to be in excellent agreement with Eq. (43) up to a map strength $S \sim 3$ [159,163]. In addition to energy enhancement, the approximate solution (42) can also be used to find the CFPs of a dispersion managed system. Using (42) in (17) gives the RMS chirp parameter

$$C_{RMS} = -\frac{2}{\pi^2}\epsilon\left[\mu_1(\xi) - \langle\mu_1\rangle_\xi\right]T_{RMS}^2, \tag{44}$$

showing that the CFPs exist at points $\xi = \xi_0$ where $\mu_1(\xi_0) = \langle\mu_1\rangle_\xi$. In a transmission system consisting of a two-step dispersion map with one amplifier per map period, this condition leads to an analytic expression for the distance between the amplifier and each CFP [143,159,164]. Surprisingly, by choosing the ratio between the two dispersion segment lengths properly, the CFP can be independent of the GVD coefficients of the fibre segments [143,159]. These "magic" dispersion segment lengths correspond to a special condition and only depend on the loss coefficient. The observation that special dispersion maps exist having GVD-independent optimal launch points (CFPs) is of crucial importance for WDM soliton transmission systems. Since typically there is a dispersion slope for different transmission channels, each channel has different dispersion characteristics and therefore launched pulses need to be pre-chirped accordingly. However, the existence of these "magic" dispersion maps implies that the pre-conditioning of the launch pulse is insensitive to GVD and thus the same pulse can be input in each channel in the dispersion-managed WDM system.

In general, the asymptotic solution (42) obtained by the multiple-scale analysis and their predictions such as pulse energy enhancement and chirp-free points can be validated with numerical simulations. The solution is formally valid when the dispersion-map period is much shorter than the nonlinear length, however the analytic predictions often give a reasonable comparison to numerical simulations away from this limit. The asymptotic results are useful for providing valuable insights into DM solitons themselves as well as optimizing dispersion-managed soliton systems.

3.5. Fast DM soliton dynamics (over one period)

A DM soliton is made primarily from two main components including a self-similar core and a dispersive pedestal. Fig. 6 highlights these two components, illustrating both the self-similar compression and broadening of the core of the pulse in the normal scale along with a logarithmic scale representation illustrating the dynamics of the pulse tails. It is clear that there exist time values where the pulse power goes to zero (logarithm goes to minus infinity) at propagation distances $z = 0$ and $z = 0.5$. These dips, first discovered in [144], occur in the non-self-similar pulse tails and are an inherent

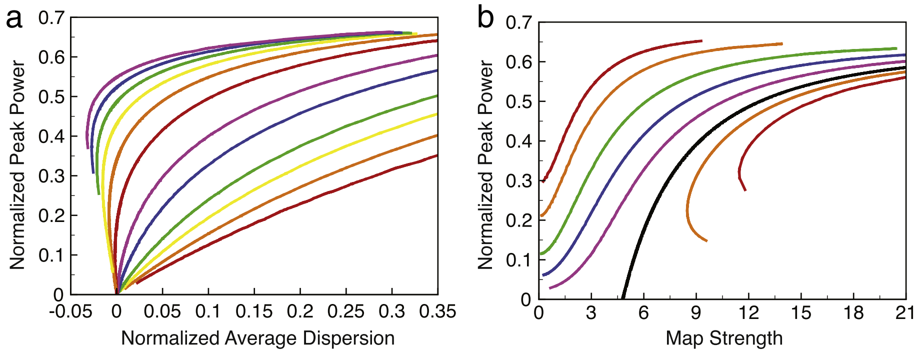

Fig. 9. Solution curves found from solving the TM equations (50). (a) Lines of constant map strength (right to left) $S = 0.5, 1, 1.5, 2, 3, 4, 6, 8, 10, 12, 14, 16$. (b) Lines of constant average dispersion (right to left) $\langle d \rangle = -0.02, -0.01, 0.0, 0.02, 0.05, 0.1, 0.2, 0.3$.

part of the DM soliton. In this section we focus on the "fast" self-similar dynamics of the core of the DM soliton over one dispersion map period. Indeed, since the energy contained in the pulse tails is typically small relative to the energy of the main core, the evolution of the central part of the DM soliton is typically the most important aspect for system optimization and understanding [109,128,145–147].

An advantage of using a phase and/or amplitude modulated optical carrier pulse of a certain shape for the transmission of information (as compared to non-return-to-zero formats where a carrier waveform effectively depends on the information content it carries) is that it can be described by few distinct pulse parameters. Indeed, the particle-like behaviour of the solitary wave signal allows for the use of well developed mathematical methods to understand features of such optical signals and to predict the effects that occur due to practical boundary conditions as well as deviations of real fibre properties from an ideal model. As mentioned in Section 2.2, we can exploit the particle-like nature of DM solitons and describe the fast dynamics of the energy containing core by obtaining evolution equations on key pulse characteristics such as pulse width, peak power, energy, chirp parameter and bandwidth. In this section we present a version of this approach based on both integral pulse characteristics (17) and RMS local pulse characteristics (19) [134,165,166].

3.5.1. Reduced model: TM system

To describe the propagation dynamics of the main energy containing core, we consider the evolution of the integrated quantities defined in Eq. (17). Manipulating the governing equation (22) it can be shown that

$$\frac{dT_{RMS}}{dz} = 4d(z)M_{RMS}(z), \tag{45a}$$

$$\frac{dC_{RMS}}{dz} = \frac{d}{dz}(T_{RMS}\, M_{RMS}) = d(z)\, \Omega^2_{RMS} - \frac{c(z)}{4}\, P_{RMS}, \tag{45b}$$

$$\frac{dP_{RMS}}{dz} = 2d(z)W_{RMS} \tag{45c}$$

$$\frac{d(\Omega^2_{RMS})}{dz} = c(z)W_{RMS}, \tag{45d}$$

where $W_{RMS} = -\int |a|^4[\mathrm{Arg}(a)]_{tt}dt / \int |a|^2 dt$. Although Eq. (45) is general and no assumptions have been made, it lacks closure and thus cannot be solved without some additional assumptions. Observing that the chirp of the typical DM soliton shows a linear behaviour in the region where most of the energy in concentrated, it is possible to make the assumption that $\mathrm{Arg}(a) = M_{RMS}/T_{RMS} \times t^2$, giving $W_{RMS} = -2M_{RMS}P_{RMS}/T_{RMS}$ [167]. Although the assumption that the chirp is linear is only an approximation, it is important to notice that the phase dependence in the integral for W_{RMS} is multiplied by $|a|^4$, which is a fast decaying function. Therefore, the contribution in the integral pulse characteristics due to deviations from a linear chirp is negligible in many practical situations with a highly localized pulse. Inserting W_{RMS} into Eq. (45) we obtain a closed set of the so-called "TM equations" [129,165,166,168])

$$\frac{dT_{RMS}}{dz} = 4d(z)M_{RMS}(z), \tag{46a}$$

$$\frac{dM_{RMS}}{dz} = \frac{d(z)C_2}{T^3_{RMS}} - \frac{c(z)\, C_1}{T^2_{RMS}}, \tag{46b}$$

where the constants are given by the invariant quantities $4C_1 = P_{RMS}(z)\, T_{RMS}(z) = P_{RMS}(0)\, T_{RMS}(0)$ and $C_2 = [\Omega^2_{RMS}(z) - 4M^2_{RMS}(z)]T^2_{RMS}(z) = [\Omega^2_{RMS}(0) - 4M^2_{RMS}(0)]T^2_{RMS}(0)$. The TM system (46) can be solved numerically for a variety of different dispersion maps as well as amplifier distributions. Formally, periodic solutions are necessary ($T(L_{DM}) = T(0)$ and $M(L_{DM}) = M(0)$) for each value of the parameter C_1 (related to pulse energy in dimensionless units). Fig. 9 shows solution curves found by solving for the variables $T(z)$ and $C(z)$, where $T(z) = T_{RMS}$ and $C(z) = M_{RMS}/(2T_{RMS})$ in Eq. (46) for a lossless system ($c(z) = 1$) and two step dispersion map

$$d(z) = \begin{cases} d + \langle d \rangle, & 0 < z < 0.25 \\ -d + \langle d \rangle, & 0.5 < z < 0.75 \\ d + \langle d \rangle, & 0.75 < z < 1. \end{cases} \tag{47}$$

The initial condition was taken so that the initial pulse has a zero chirp ($M_{RMS} = 0$) and the bandwidth and duration such that $C_2 = 1$. The initial power was adjusted through the parameter C_1 until a periodic solution was found. The solution curves are characterized by the average dispersion $\langle d \rangle$ and map strength $S = 2d/[\min(T_{\text{FWHM}})]^2$, where T_{FWHM} is the FWHM pulse duration. The peak power is normalized by a factor $N^2_{\text{norm}} = [\min(T_{\text{FWHM}})]^2/(3.11d)$ so that the normalized power gives the pulse peak power at the CFP in the anomalous GVD fibre segment in fractions of the power of the fundamental soliton of the same FWHM [169]. We see a somewhat surprising property of DM solitons that is distinct from conservative solitons of the NLSE. Above a certain critical map strength there is a region that allows for stable propagation at zero or normal average dispersion [170–172]. This property can be understood by integrating Eq. (45) over one period giving

$$\langle d(z)\, \Omega^2_{RMS}(z) \rangle = \frac{1}{4} \langle c(z)\, P_{RMS}(z) \rangle. \tag{48}$$

When $d(z)$ and $c(z)$ are constant this leads to the expression for the RMS power of the conventional soliton, and it is required that $d > 0$. When both $d(z)$ and $c(z)$ are periodic functions (or c is constant as in the lossless model) one can see that the requirement $d > 0$ for the existence of conventional solitons is replaced by a condition $\langle d(z)\, \Omega^2_{RMS} \rangle > 0$, which, because of the breathing nature of the bandwidth, can be satisfied even when the average dispersion is zero or negative. We also note here that in the case when $d\ (> 0)$ is constant and $c(z)$ is allowed to vary periodically in Eq. (48) we obtain the guiding-centre (path averaged) enhancement factor [5,6]. The curves shown in Fig. 9 were first found via a variational method and compared to full numerical simulation [169]. The numerical simulations showed good agreement however the maximum map strength was shown to be restricted to ~ 13, in contrast to what was found from the reduced TM or variational system. Regardless, the reduced models do an excellent job in capturing the solution curves, highlighting not only the ability for DM solitons to exist at average zero or normal dispersion, but also predicting two solutions for the same energy in the normal dispersion regime [169,171], as well as the reduced peak power variation over a range of average anomalous dispersion values for strong map strengths [169]. For more general dispersion and amplification schemes, the TM equations can also be used for determining the CFPs in various systems (see e.g. [140,173]), making them ideal for optimization purposes.

In addition to obtaining the TM equations through RMS quantities (17) it is also possible to obtain them through local pulse characteristics defined by (19). Inspired by the linear solution, if we assume the solution has a specific form [166]

$$u(z,t) = N\, \frac{f(x,z)}{\sqrt{T(z)}} \exp\left[i \frac{M(z)}{T(z)} t^2 \right], \tag{49}$$

where $x = t/T(z)$, it is possible to separate the self-similar dynamics from the structural form of the pulse. Here the parameter N scales out the pulse power by imposing a normalization condition on the structural function f so that $\int |f|^2\, dx = 1$. Inserting (49) into Eq. (22), and defining the relations (see, e.g., [174])

$$\frac{dT}{dz} = 4d(z)M \tag{50a}$$

$$\frac{dM}{dz} = \frac{d(z)}{T^3} - \frac{pc(z)N^2}{T^2}, \tag{50b}$$

where the parameter p is a constant, gives the governing equation

$$i\frac{\partial f}{\partial z} + \frac{d(z)}{T^2} \left(\frac{\partial^2 f}{\partial x^2} - x^2 f \right) + N^2 \frac{c(z)}{T} \left(|f|^2 f + p x^2 f \right) = 0. \tag{51}$$

The choice of defining the TM equations (50) is arbitrary, but it is encouraged by the TM equations found in Eq. (46) from the RMS integral quantities. Indeed, the system Eq. (50) is exactly the same as an approximate system (46) and the functions T and M are related to T_{RMS} and M_{RMS} through Eq. (19) [167,174]. With the TM equations found using the RMS integral quantities, we assumed a linear chirp to obtain a closed set of equations. For the system (50), there is an assumption based on the arbitrary value of p, which accounts for the strength of the nonlinearity in the chirp parameter evolution. When $p = 0$ system (50) describes linear pulse evolution and Eq. (51) is the evolution equation of a quantum harmonic oscillator with an additional nonlinear term. For an initial Gaussian pulse, the nonlinearity mixes different modes of the linear oscillator, inducing transitions from the ground state (which corresponds to a Gaussian-shaped pulse) to other modes. The constant p in system Eq. (50) can be adjusted to minimize the rate of transitions from the ground state to other modes or, in other words, to make the approximation of the DM soliton solution of the NLSE as close as possible to the ground state of the linear operator. A difference with the local description (50)–(51) from the RMS description (46) is that the evolution of the structural shape of the DM soliton is allowed to evolve and is governed by Eq. (51). Indeed, in some of the early works on DM solitons it was shown that the pulse shape can vary in structure depending on the map strength parameter [138].

3.5.2. One-period solutions of the TM equations

As mentioned in the previous section, the TM equations (50) can describe the fast dynamics of the DM soliton and be a powerful tool in the optimization of dispersion managed systems. In addition to solving them numerically, it is also possible to highlight the nature of the fast DM soliton dynamics by investigating the TM equations (50) analytically as well. It is instructive to find the solutions to Eq. (50) in the linear limit ($p = 0$). Introducing a new variable $R(z)$ so that $d(z) = dR(z)/dz$ with boundary conditions $R(0) = 0$, $T_0 = T(0)$, $M_0 = M(0)$ we obtain

$$T^2(z) = \frac{1 + 4\left(M_0T_0 + R(z)\Omega_0^2\right)^2}{\Omega_0^2} \tag{52a}$$

$$M(z) = \frac{M_0T_0 + R(z)\Omega_0^2}{T(z)}, \tag{52b}$$

where $\Omega_0^2 = T_0^{-2} + 4M_0^2$. Because it is required that the dispersion is completely compensated in the linear system for periodic evolution ($R(z^*) = 0$), we see that $T(0) = T(z^*)$ and $M(0) = M(z^*)$. As a matter of fact, the solutions (52) have already been discussed when considering the analytical solution (26) of the linear Schrödinger equation. These solutions give a good approximation to the fast dynamics in the strong dispersion management limit when the pulse width and chirp are mostly determined by the high local dispersion over one map period. In this limit, it was shown that the solution parameters are close to (52), and the parameters of the linear solution can be viewed as adiabatic invariants of the system which slowly vary due to the small effect of nonlinearity and residual dispersion [175].

For certain dispersion maps it is also possible to solve Eq. (50) analytically. Here we will focus our results on a two-step map

$$\begin{aligned} &d(z) = d_1 > 0, \qquad c(z) = c_1 \quad 0 < z < L_1 \\ &d(z) = d_2 < 0, \qquad c(z) = c_2 \quad L_1 < z < L_{DM}. \end{aligned} \tag{53}$$

Using simple scaling transformations, it is possible to set $d_1 = 1$, $d_2 = -1$ and $L_{DM} = 1$ [176]. The map is then characterized by three parameters: the nonlinear coefficients of the two fibre segments $\sigma_{1,2} = pc_{1,2}N^2$ and the average dispersion $\langle d\rangle = 2L_1 - 1$. Here, for the sake of clarity, but without loss of generality, we only consider the case of "equally nonlinear" fibres, that is, $|\sigma_1| = |\sigma_2| = c$. Consider the trajectory of a one-period solution of (50) in the (T, M) plane. Since CFPs exist at the centre of the dispersion segments, we have

$$L_+(T^*, M^*) = L_1/2, \qquad L_-(T^*, M^*) = (1 - L_1)/2, \tag{54}$$

where the point (T^*, M^*) is the parameter values at the point in the phase plane corresponding to $z = L_1$, and L_+ (L_-) is the length of the anomalous (normal) fibre that takes the solution from the CFP to the point (T^*, M^*). Using symmetry, the distance function can be found analytically to be [150,177]

$$L_\pm = \frac{1}{2V}\left[TM \mp \frac{c}{\sqrt{8V}}\cosh^{-1}\left(\frac{T \pm c/(2V)}{\sqrt{c^2/(4V^2) + 1/(2V)}}\right)\right], \tag{55}$$

where $V(z) = 2M^2 + 0.5/T^2 \mp c/T$. Although it is not so easy to visualize the analytic solutions, Eqs. (54)–(55) provide a straightforward way of finding the single-period solutions of the TM system numerically and similar plots such as Fig. 9 can be achieved. The analytic solution can also be used to obtain the power enhancement factor of DM solitons in certain limits. Specifically, consider the lossless case ($c(z) = \epsilon$) and two step dispersion map (47). In the strong dispersion managed limit when nonlinearity and residual dispersion are small and the leading order dynamics is governed by the high local dispersion over one map period ($\langle d\rangle, \epsilon \ll d$), perturbation theory can be used to find the energy enhancement [150]

$$N^2 = \frac{\langle d\rangle/T_1}{2/\sqrt{1+y^2} - y^{-1}\ln\left(y + \sqrt{1+y^2}\right)}, \quad y = d/(2T_1^2), \tag{56}$$

where T_1 is the DM soliton width in the middle of the anomalous GVD fibre. For a fixed average dispersion, certain map depths $d = d_c \sim 6.64T_1^2$ will cause the denominator in Eq. (56) to be zero and the first order perturbation theory used to obtain this result fails. However, for values $d \ll d_c$, and when the local dispersion is the main effect and the optical pulse behaves almost linearly, the energy enhancement agrees with numerical simulations [150].

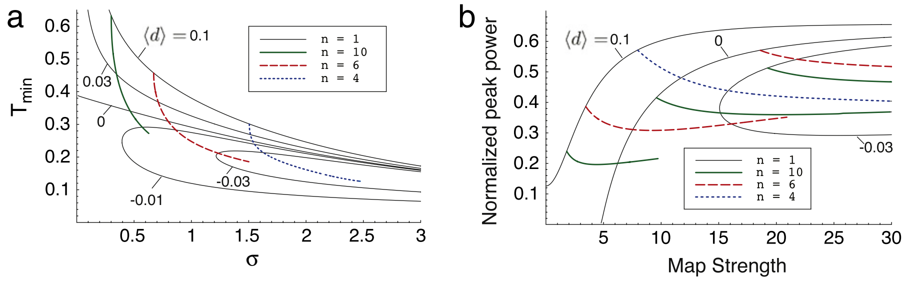

Fig. 10. Solution branches to the TM equations (50) for a lossless system ($c(z) = 1$) with a two-step dispersion map (47). (a) Dependence of minimum T on the energy parameter $\sigma = pN^2/d$. Thin lines correspond to one-period solutions for various average dispersions and thick/dashed lines correspond to multiple-period solutions with $\langle d \rangle = 0.1$. (b) Dependence of normalized power N^2_{norm} on the map strength. Both one-period and multiple-period branches are shown for average dispersion values $\langle d \rangle = 0.1, 0, -0.03$. Normalizations and map strength are the same as in Fig. 9.

3.5.3. Multiple-period solutions of the TM equations

In addition to one-period solutions to the TM equations (50), there is also a class of multiple-period solutions that satisfy the periodic boundary conditions over a multiple number of dispersion maps [176]. We will refer to the index n so that single period solutions (or standard DM solitons) have $n = 1$ and multiple-period (or long-period) solutions have $n > 1$. To compare the characteristics of multiple-period solutions to their one-period DM soliton counterparts, we highlight solutions to the TM equations (50) in the same lossless ($c(z) = 1$) system with a two-step dispersion map (47) as was used in Fig. 9. Fig. 10(a) illustrates the energy dependence of the minimum pulse duration $T_{\min} = \min(T(z))$ per dispersion map period. For one-period DM solitons, $T_{\min}$ tends to a finite value as $\sigma \to 0$ in the case of zero $\langle d \rangle$, and tends to infinity when $\langle d \rangle > 0$. For negative $\langle d \rangle$ the energy dependence of $T_{\min}$ has two branches. The energy dependence of $T_{\min}$ for multiple-period solutions with $n = 10$, $n = 6$ and $n = 4$ at $\langle d \rangle = 0.1$ is also shown in Fig. 10(a) for the same map parameters. We see that at the same energy the minimum pulse duration for multiple-period DM solitons can be almost two times less than the minimum pulse duration for one-period DM solitons. Fig. 10(b) extends Fig. 9(b) to show the dependence of the normalized peak power on the map strength for multiple-period solutions. The multiple periodic lines branch off the lines corresponding to the simple periodic solutions. This plot demonstrates that the peak power of multiple-period solitons can be about 3 times less compared to power of conventional DM solitons at the same map strength.

Although we have discussed multiple-period DM solitons in the context of solutions of the TM equations (50), full numerical simulations of Eq. (22) have confirmed such solutions [176]. The multiple-period solutions found have smaller energies compared to single-period traditional DM solitons. Such multi-period DM solitons can be of interest as carrier pulses in high-speed optical communications employing differential phase-shift-keying formats. Indeed, these multiple-period solutions present an important step in the convergence of the DM soliton concept and the widely used quasi-linear transmission regime. Namely, multiple-period DM solitons have less energy and can experience larger broadening during propagation and, therefore, much more closely mimic quasi-linear propagation regimes compared to traditional DM solitons.

3.6. Path-average theory of the DM soliton

The previously discussed TM equations are appropriate to describe the fast dynamics of the DM soliton. Although these equations are important in describing the pulse characteristics, it does not describe the long scale dynamics or shape of the DM soliton. In general, numerical simulations of Eq. (22) for a particular dispersion managed system can highlight these long scale dynamics. However, in the limit when nonlinearity and residual dispersion are small compared to the high local dispersion, insightful analytics can be performed on the governing equation (22). Specifically, since the nonlinearity and residual dispersion are perturbations, it is possible to use a variety of averaging or perturbation methods to develop a path-averaged description of DM solitons. The dynamics of the DM soliton then can be considered on the fast scale which accounts for the rapid oscillations of the phase, pulse duration and peak power over one dispersion map period, as well as the slow scale dynamics which describe the accumulation of small deviations from the periodic oscillations over many periods (nonlinear/residual dispersion length). In the following sections we highlight two methods that give particular physical insight into the description of the DM soliton and its fast and slow dynamics.

3.6.1. Gabitov–Turitsyn path-average equation

In this section we consider the strongly dispersion managed limit of Eq. (22), where we set $c(z) = \epsilon c(z)$ to emphasis the smallness of the nonlinear coefficient and $\langle d \rangle \ll |d(z)|$. Since we expect the strong local dispersion to determine the leading order linear dynamics, we apply the so-called Floquet–Lyapunov transformation to Eq. (22) [137,178]

$$\hat{a}(z, \omega) = \hat{\phi}(z, \omega)\, e^{-i\omega^2 R_0(z)}, \qquad \frac{dR_0(z)}{dz} = d(z) - \langle d \rangle, \tag{57}$$

where $a(z,\omega)$ is the Fourier transform of $a(z,t) = \int a(z,\omega)\exp[-i\omega t]\,d\omega$. Taking the Fourier transform of Eq. (22) and using the new variables (57) gives

$$i\frac{\partial\hat{\phi}}{\partial z} = \langle d\rangle\,\omega^2\,\hat{\phi} - \epsilon\int G_{\omega 123}\,\delta(\omega+\omega_1-\omega_2-\omega_3)\,\hat{\phi}_1^*\,\hat{\phi}_2\,\hat{\phi}_3\,d\omega_1 d\omega_2 d\omega_3, \tag{58}$$

where $\hat{\phi}_i = \hat{\phi}(z,\omega_i)$, $G_{\omega 123}(z) = c(z)\,\exp\{i\Delta\Omega R_0(z)\}$ with $\Delta\Omega = \omega^2+\omega_1^2-\omega_2^2-\omega_3^2$, and δ is the Dirac delta function. The function $G_{\omega 123}$ depends on the specific combination of the frequencies given by the resonance surface $\Delta\Omega$. Both the Fourier and the Floquet–Lyapunov transform (57) are canonical and the transformed Hamiltonian H is

$$H = \langle d\rangle\int\omega^2|\hat{\phi}|^2 d\omega - \epsilon\int\frac{G_{\omega 123}}{2}\delta(\omega+\omega_1-\omega_2-\omega_3)\hat{\phi}^*\hat{\phi}_1^*\hat{\phi}_2\hat{\phi}_3 d\omega d\omega_1 d\omega_2 d\omega_3. \tag{59}$$

Eq. (58) is an evolution equation where the right-hand side of the equation is small, allowing us to apply Hamiltonian averaging [178]. Using the change of variables

$$\hat{\phi} = \hat{\varphi} + \epsilon\int V_{\omega 123}\delta(\omega+\omega_1-\omega_2-\omega_3)\hat{\varphi}_1^*\hat{\varphi}_2\hat{\varphi}_3 d\omega_1 d\omega_2 d\omega_3, \tag{60a}$$

$$V_{\omega 123}(z) = i\int_0^z [G_{\omega 123}(\tau) - T_{\omega 123}]d\tau + iV_{\omega 123}(0) \tag{60b}$$

$$T_{\omega 123} = \langle G_{\omega 123}\rangle = \int_0^{L_{DM}} c(z)\,\exp\{i\Delta\Omega R_0(z)\}dz \tag{60c}$$

so that $\langle V_{\omega 123}\rangle = 0$, we find that at the leading order in ϵ, a path-averaged equation has the form [137]

$$i\frac{\partial\hat{\varphi}}{\partial z} = \langle d\rangle\,\omega^2\,\hat{\varphi} - \epsilon\int T_{\omega 123}\,\delta(\omega+\omega_1-\omega_2-\omega_3)\,\hat{\varphi}_1^*\,\hat{\varphi}_2\,\hat{\varphi}_3\,d\omega_1 d\omega_2 d\omega_3. \tag{61}$$

Eq. (61), first derived in 1996 [137], is the basic model of the DM soliton theory in the limit of strong dispersion management and can describe many interesting properties of DM solitons [149,178–180]. It has a corresponding averaged Hamiltonian

$$\langle H\rangle = \langle d\rangle\int\omega^2\left|\hat{\varphi}\right|^2 d\omega - \epsilon\int\frac{T_{\omega 123}}{2}\delta(\omega+\omega_1-\omega_2-\omega_3)\hat{\varphi}^*\hat{\varphi}_1^*\hat{\varphi}_2\hat{\varphi}_3 d\omega d\omega_1 d\omega_2 d\omega_3, \tag{62}$$

and can be exploited in a regular way to calculate next order corrections to the averaged model. From Eq. (60c) it is easy to see that the matrix element $T_{\omega 123} = T_{1\omega 23} = T_{\omega 132} = T^*_{23\omega 1}$. Eq. (61) possesses the remarkable property that on the resonant surface $\omega+\omega_1-\omega_2-\omega_3 = 0$ both the matrix element $T_{\omega 123}$ and its derivative over $\Delta\Omega$ are regular. This observation allows us to make the following quasi-identical-like transformation [178]

$$\hat{\varphi} = \hat{q} - \frac{\epsilon}{\langle d\rangle}\int\frac{T_0 - T_{\omega 123}}{\Delta\Omega}\,\hat{q}_1^*\,\hat{q}_2\,\hat{q}_3\,\delta(\omega+\omega_1-\omega_2-\omega_3)\,d\omega_1 d\omega_2 d\omega_3, \tag{63}$$

where $T_0 = T(0)$ and the variable part of the matrix element $T_{\omega 123}$ is now removed. If the kernel function in Eq. (63) is small compared to $\hat{q}$

$$|S(\Delta\Omega)| = \left|\frac{T_0 - T_{\omega 123}(\Delta\Omega)}{\Delta\Omega}\right| \ll 1, \tag{64}$$

then the averaged model can be reduced to the NLSE. However, in general this is not the case and explains why the typical solution of Eq. (61) has a form different from a hyperbolic secant shape [149].

To see how the general mathematical analysis can be used in practical settings, let us consider a few examples. First we analyse a transmission system typical for transoceanic transmission with a two-step dispersion map with the dispersion compensation period $L_{DM} = 2M\times L_A$ km, where L_A is the amplification distance. The fibre has anomalous GVD $d(z) = d + \langle d\rangle$ for the first M amplifiers ($0 < z < L_{DM}/2$) and normal GVD $d(z) = -d + \langle d\rangle$ for the second M amplifiers ($L_{DM}/2 < z < L_{DM}$). Let us normalize the system by the dispersion map period so that $L_{DM} = 1$. The mean-free function $R_0(z)$ in Eq. (57) is $R_0(z) = d\,z - d/4$ if $0 < z < 1/2$ and $R_0(z) = -d[z-1/2] + d/4$ if $1/2 < z < 1$. After some calculations, it can be found that the kernel of the function $T_{\omega 123} = T(\Delta\Omega)$ in Eq. (60c) is

$$T(X) = \frac{G-1}{G\,\ln G}\,\frac{\sin(X\,M)}{M}\,\frac{1}{(1+[2X/\ln G]^2)}\left\{\frac{\cos(X)}{\sin(X)} + \frac{2X}{\ln G}\,\frac{G+1}{G-1}\right\}, \tag{65}$$

where $X = \Delta\Omega L_A d/(2L_{DM}) = \Delta\Omega d/(4M)$ and the gain $G = \exp[2\alpha L_A]$ (α is a fibre loss). It is interesting to look at some particular limits in this general formula. First, if $d = 0$ (uniform dispersion along the system) we reproduce the result of Mollenauer et al. [50,82,83] where $T(\Delta\Omega) = (G-1)/(G\ln G)$ and because T is a constant, the path-averaged model is just the integrable NLSE. Another interesting limit is the "lossless" model ($\alpha = 0$) [138] where $T(\Delta\Omega) =$

$\sin[\Delta\Omega\ d/4]/[\Delta\Omega\ d/4]$. For higher values of $M \gg 1$, it can be shown that the function $T(\Delta\Omega)$ in Eq. (65) approaches the product of $T(\Delta\Omega)$ predicted by the "lossless" model and the path-averaged factor $(G-1)/(G\ln G)$. Indeed, this confirms the fact that periodic amplification (power budgeting) and dispersion compensation can be treated separately in long-haul transoceanic optical communication systems where amplification distance is typically much shorter than the dispersion compensation period.

Next we consider the opposite limit, or so-called short-scale management regime where $L_{DM} \ll L_A$. It is of interest for some applications to find stable propagation regimes with the signals having short pulse durations with low power. Such pulses were found to exist with short-scale dispersion management and supported pulses that could have low enough energy to provide for stable ultra-high-bit-rate transmission [181], thus making such a limit practical. Indeed, optical fibres with $L_{DM} \ll L_A$ have been manufactured [182]. Consider this limit with a two-step dispersion map with dispersion compensation period $L_{DM} = L_A/m$ (or $1/m$ in the normalized units). The normalized dispersion $d(z) = d + \langle d\rangle$ if $k/m < z < (k+0.5)/m$ and $d(z) = -d + \langle d\rangle$ if $(k+0.5)/m < z < (k+1)/m$, where $k = 0, 1, 2, \ldots, m-1$. In this example the mean-free function $R_0(z)$ in Eq. (57) is $R_0(z) = d(z-k/m) - d/(4m)$ if $k/m < z < (k+0.5)/m$ and $R(z) = -d[z-k/m-1/(2m)] + d/(4m)$ if $(k+0.5)/m < z < (k+1)/m$. After some calculations, it can be shown that the matrix element $T_{\omega 123}$ in Eq. (60c) is

$$T(Y) = \frac{G-1}{G\ln G}\,\frac{1}{1+(\frac{4mY}{\ln G})^2}\left[\exp(-iY) + \frac{4mY}{\ln G}\left(\sin(Y)\,\frac{G^{1/(2m)}+1}{G^{1/(2m)}-1} + i\cos(Y)\,\frac{G^{1/(2m)}-1}{G^{1/(2m)}+1}\right)\right], \tag{66}$$

where $Y = d\Delta\Omega/(4m)$. To give an idea as to how far from the conservative soliton solution we are in this particular limit, we can estimate the matrix element of the quasi-identical transformation

$$|S(\Delta\Omega)| \le \left|\int_0^1 \frac{c(z)[\exp(i\Delta\Omega R(z))-1]}{\Delta\Omega}dz\right| \le \int_0^1 |c(z)R(z)|dz \le \max(R)\langle c\rangle = \frac{\langle c\rangle\, d}{4m}. \tag{67}$$

For fixed parameters, increasing the integer m reduces this matrix element and thus the path-averaged model (61) governing DM soliton propagation converges to the integrable NLS equation. We can gain intuitive insight as to why this is by considering Eq. (66). Increasing m (with other parameters fixed) under a fixed characteristic bandwidth of the signal makes an insignificant oscillatory contribution to the kernel. This means that if $T(Y)$ is concentrated in some region ΔY, then for large m the corresponding region in $d\,\Delta\Omega$ will be larger than for small m. For the pulses with the same spectral width this will mean that T is much flatter for large m and, as a matter of fact, for large m, T can be better approximated by a value $T(0)$. As a result, the NLSE model works rather well in this limit and the solution (of the path averaged model!) should be close to a hyperbolic secant soliton solution of the NLSE. In contrast to the lossless model, the evolution of the soliton parameters over one period is highly asymmetric due to the gain and loss. Rapid variations of the pulse width, peak power and chirp are accompanied by the exponential decay of the power due to loss. Nevertheless, numerical simulations have revealed that there exists a true periodic solution that reproduces itself at the end of the compensation cell (in this case, at the end of the amplification period). Note that though it is known that DM solitons have a hyperbolic secant shape for lossless systems in the weak dispersion management limit [137,138,144,163], this particular signal shape is not obvious for such a short-scale management scheme where there is gain and loss as well as different periods of amplification and dispersion compensation.

Although we have shed insight into the average dynamics via the Gabitov–Turitsyn path average equations, it is important to note that various averaging methods have been used to obtain slightly different aspects of DM solitons. These include, among others, additional Hamiltonian averaging procedures [178–180], Lie-transform [183], and multiple-scale expansion [149].

3.6.2. DM soliton expansion in the basis of the chirped Gauss–Hermite functions

An arbitrary input pulse propagating down the dispersion-managed system typically evolves into an asymptotic structure that presents a self-similar rapidly oscillating main peak and a non-self-similar dispersive pedestal [144,152]. As pointed out in Section 3.2, there is an interesting analogy between a DM soliton and the nonlinear macroscopic quantum oscillator. The basic idea is that the periodic variations of the phase (that occur due to periodic oscillations of the dispersion) create an effective parabolic trapping potential. Without nonlinearity any propagating wave is a direct combination of the eigenfunctions of such a quantum oscillator potential—the Gauss–Hermite functions. When nonlinearity comes into play, the energy is redistributed between different modes. It is then quite natural to describe the path average evolution of the DM soliton as some combination of chirped Gauss–Hermite functions. To separate the rapid self-similar dynamics that occurs due to large variations of the local dispersion let us apply the following self-similar transformation to Eq. (22) [142]

$$a(z,t) = \frac{N\,e^{i\frac{M(z)}{T(z)}t^2}}{\sqrt{T(z)}}\sum_{n=0}^{n=\infty} B_n(z) f_n\!\left(\frac{t}{T(z)}\right)e^{i\lambda_n R(z)}. \tag{68}$$

The rapid oscillations of pulse width and chirp are accounted by periodic functions $T(z)$, $M(z)$, and the phase term $R(z)$ where $dR/dz = d(z)/T^2(z) - \langle d/T^2\rangle$. The periodic functions T and M satisfy the TM equations (50) and in the leading order keep the self-similar structure of the DM pulse. The slow evolution is given by the summation of functions $f_n(x)$, which are the orthogonal normalized Gauss–Hermite functions

$$f_n(x) = \frac{1}{\sqrt{2^n n! \sqrt{\pi}}} \exp\left(-\frac{x^2}{2}\right) H_n(x) \tag{69}$$

which satisfy

$$\frac{d^2 f_n}{dx^2} - x^2 f_n = \lambda_n f_n, \quad \lambda_n = -1 - 2n. \tag{70}$$

Here $H_n(x)$ is the nth-order Hermite polynomial and coefficients B_n are given by the ordinary scalar product in $\mathcal{L}^2$ with f_m. Inserting this expansion into Eq. (22) and after scalar multiplication with f_m we obtain

$$i\frac{dB_n}{dz} + \left\langle \frac{d}{T^2} \right\rangle \lambda_n B_n + \beta(z) \sum_{m=0} e^{2i(n-m)R(z)} S_{n,m} B_m + \beta(z) \sum_{m,l,k} e^{2i(n+k-m-l)R(z)} B_m B_l B_k^* V_{m,l,k,n} = 0, \tag{71}$$

where $\beta(z) = c(z)N^2/T^2$ and

$$S_{n,m} = \langle f_m | x^2 f_n \rangle = \int_{-\infty}^{+\infty} f_m(x) x^2 f_n(x) dx, \tag{72a}$$

$$V_{n,m,l,k} = \langle f_m | f_n f_l f_k \rangle = \int_{-\infty}^{+\infty} f_n(x) f_m(x) f_l(x) f_k(x) dx. \tag{72b}$$

Since integrals of the form $\int x^n e^{-\alpha x^2}$ can be calculated analytically, it is possible to determine any $S_{n,m}$ and $V_{n,m,l,k}$.

In contrast to Eq. (22), Eq. (71) can be averaged directly because the large variations of the dispersion are moved to the phase factor proportional to $R(z)$. Although averaging can be performed either using Lie-transform technique [150] or Hamiltonian averaging [175], we can gain important insight on the zero-order term directly. Let us split B_n into slow (U_n) and fast (η_n) varying parts $B_n = U_n + \eta_n + \cdots$ ($d\eta_n/dz \gg \eta_n$) and assume that the rapidly varying part is small compared with slow varying one $\eta_n \ll U_n$. Averaging over one period in the leading order then gives for U_n

$$i\frac{dU_n}{dz} + \left\langle \frac{d}{T^2} \right\rangle \lambda_n U_n + \sum_{m=0} \langle \beta(z) e^{2i(n-m)R(z)} \rangle S_{n,m} U_m + \sum_{m,l,k} \langle \beta(z) e^{2i(n+k-l-m)R(z)} \rangle U_m U_l U_k^* V_{n,m,l,k} = 0. \tag{73}$$

Considering a solution in the form $U_n = F_n \exp(ikz)$, with F_n a constant, we obtain the expansion of the DM soliton in terms of chirped Gauss–Hermite functions. The shape of any DM soliton can be found from a solution of algebraic equations

$$-kF_n + \left\langle \frac{d}{T^2} \right\rangle \lambda_n F_n + \sum_{m=0} \langle \beta(z) e^{2i(n-m)R(z)} \rangle S_{n,m} F_m + \sum_{m,l,k} \langle \beta(z) e^{2i(n+k-l-m)R(z)} \rangle F_m F_l F_k^* V_{n,m,l,k} = 0. \tag{74}$$

Note that although this nonlinear eigenvalue problem looks complicated, this is a set of *algebraic* equations that are much easier to solve compared to finding the DM soliton from original PDE (22). Rapid convergence, which is natural for localized pulse solutions means that the solution should be represented well by a limited number of terms in the expansion. This approach is a rigorous way to describe a family of DM soliton for an arbitrary dispersion map.

To give a specific example, Fig. 11 presents a comparison of the path-average model with direct numerical simulations for an example of a lossless system with two step dispersion map (the same as in Fig. 6). The spectral power (logarithmic scale) of the true DM soliton (solid line), taken at the boundary between the two fibres is compared with the (0 + 4) (dashed–dotted line) and five mode (dotted line) approximations in the expansion using the chirped Gauss–Hermite functions. For comparison, we have also shown the solution of the path-averaged Eq. (61) (dashed line). The inset shows the dynamics over one period of the first nontrivial coefficients in the Gauss–Hermite expansion of the DM soliton. It is seen that both path-average models give quite good approximations of the true DM soliton. Even the two-mode (0 + 4) approximation describes the central part very well.

The expansion in the basis of the chirped Gauss–Hermite functions presents an analytical approximation of the DM soliton describing both the Gaussian core and the oscillating tails, and has been used to describe various properties of the DM soliton [130,142,155,184]. It is powerful in that this method can describe the oscillatory tails and give an estimate as to how accurately the RMS momentum description can be. Further, it can be used in numerical modelling as it reduces the overall dynamics to a system of algebraic equations governing the slow evolution.

Please cite this article in press as: S.K. Turitsyn, et al., Dispersion-managed solitons in fibre systems and lasers, Physics Reports (2012), doi:10.1016/j.physrep.2012.09.004

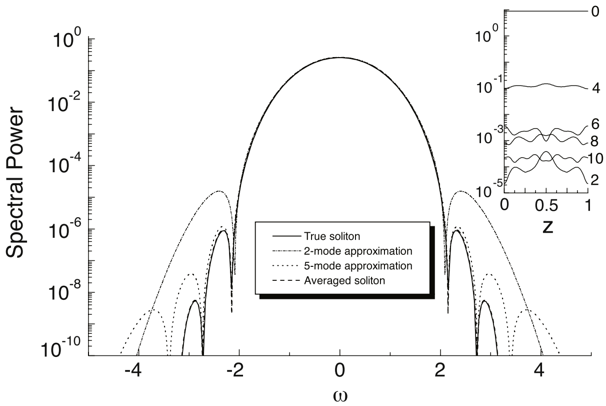

Fig. 11. Spectral power of DM soliton in logarithmic scale: true DM soliton (solid line), solution of path-average Eq. (61) (dashed line), two-mode (dashed–dotted line) and five-mode (dotted line) approximations using a Gauss–Hermite expansion [130]. Inset: dynamics of the first nonzero coefficients in the expansion over one map period.

3.7. Short-scale dispersion management

As previously discussed, a DM soliton has an enhanced power with respect to the fundamental soliton, increasing the signal-to-noise ratio, reducing Gordon–Haus–Elgin jitter, and improving the overall transmission performance. However, this advantage can be a serious drawback for transmission with high bit rates of 40 Gbits/s and more per channel. Data transmission with such high bit rates requires denser pulse packing, leading to shorter soliton pulse durations. Since the energy $E \sim P \times T$ of the DM soliton increases with decreasing pulse duration T (see Fig. 10(a)), the peak power P can become too high to be realized in practice in such high bit rate transmission schemes. Therefore, in designing high-bit-rate soliton-based transmission systems one must keep the soliton power high enough to exploit the advantages of DM soliton propagation but low enough to meet the telecommunication standards for signal power as well as avoid nonlinear interactions between neighbouring pulses.

Traditional dispersion management for long-haul transmission assumes that the dispersion compensation period is much longer than the amplification distance ($L_A \ll L_{DM}$). It is possible to achieve the opposite limit, where $L_{DM} \ll L_A$ by splicing a number of fibre pieces or by building in the periodic change of the dispersion in a continuous manner in producing the fibre. Indeed, existing technologies make it possible to manufacture fibre with the continuous alternation of positive and negative dispersion sections of less than 10 km without any splicing [182]. As was shown in Section 3.6.1 (Eq. (67)), in the so-called short-scale management regime the pulse shape is close to hyperbolic secant shape. Fig. 12 shows an example of the resulting pulse parameter evolution from numerical simulation of the governing equation (22) for a short-scale dispersion map where the amplification distance is $L_A = 40$ km and the dispersion compensation length is $L_{DM} = 4$ km. Rapid variations of the pulse width, peak power and chirp are accompanied by the exponential decay of the power due to loss. Nevertheless, there exists a true periodic solution that reproduces itself at the end of the compensation cell (in this case, at the end of the amplification period). The DM soliton indeed is of hyperbolic secant shape and propagates without radiation [181].

An important feature of the DM solitons in systems with short-scale dispersion management is their reduced power. In contrast to the enhanced power DM soliton that occurs in the most of studied dispersion-managed systems [138], the DM soliton investigated here has a *reduced power* compared with a conventional path-averaged soliton of the same width propagating in a system with the same average dispersion [181]. It is important here to compare the DM soliton power not with the fundamental soliton in a lossless fibre, but with the path-average soliton in a system with uniform dispersion (with the same amplification distance and average dispersion as the system considered here). This reduction in power can lead to the necessary regime in high-speed transmission where the carrier pulse duration must be short enough but the power low enough for practical systems. Indeed, the technique of short-scale or dense dispersion-managed soliton transmission has been successfully achieved at both 80 and 160 Gb/s through numerical simulations [185,186]. An improvement on such a dense dispersion-managed system was proposed where an average dispersion decreasing densely dispersion-managed fibre line was used to substantially improve the performance of high-speed optical transmission systems [187]. Dense dispersion managed systems have been experimentally implemented at very high channel rates [188].

3.8. Other examples of dispersion management

In the past sections we have overviewed many properties of dispersion management mainly with a focus on DM solitons. In this section we want to discuss some other methods of dispersion management used to generate other forms of coherent structures in nonlinear fibre based systems. Dispersion management and tailoring can be used in a similar manner in a variety of materials e.g. in silicon waveguides [189]. The quintessential example is conventional solitons in real systems. As discussed in Section 1, a conventional soliton is a stationary pulse created by the balance between anomalous dispersion

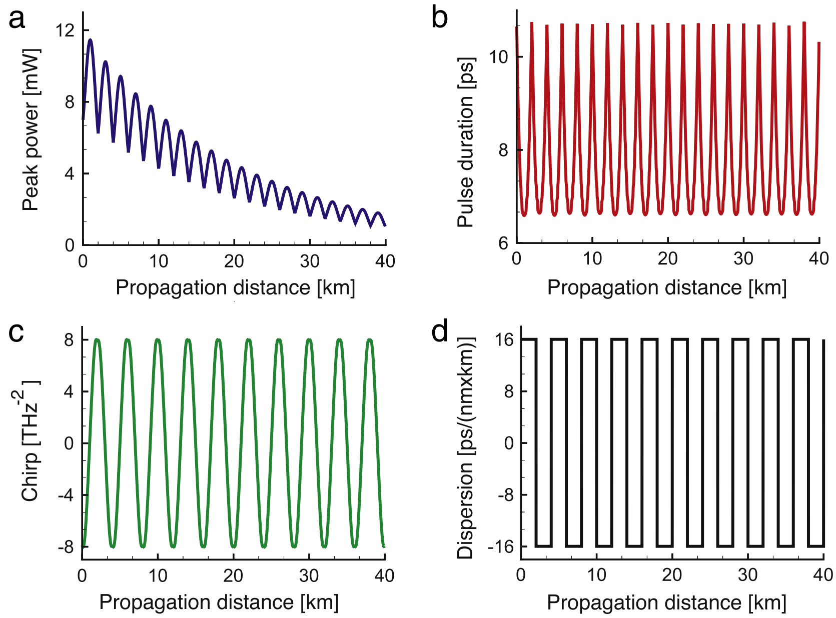

Fig. 12. Evolution of the DM soliton (a) peak power, (b) FWHM pulse duration, and (c) chirp parameter along one section of the transmission system with short-scale dispersion map (shown in (d)). The average dispersion value is $\langle D\rangle = 0.1$ ps/(nm $\times$ km), nonlinear parameter is $\gamma = 2.43$ 1/(W km) and fibre loss is $\alpha = 0.21$ dB/km. The amplification distance is 40 km and the dispersion compensation length is 4 km.

and nonlinearity. In real transmissions and laser systems where the losses are compensated for by lumped amplification, energy of the soliton varies along the propagation distance. The soliton power decreases exponentially as it propagates down the fibre and experiences large nonlinearity just after amplification and reduced nonlinearity in the last part of each amplifier span or cavity round trip. For such systems, some form of dispersion management with an exponentially decaying dispersion is necessary to keep the balance between dispersion and nonlinearity to maintain true static conventional solitons [190–193]. Similar effects can be achieved by a concatenation in series of constant-dispersion fibres (with piecewise decreasing dispersion) to approximate a fibre having exponentially decreasing dispersion.

In addition to conventional soliton propagation in real systems, it is possible to obtain parabolic pulse propagation in fibre-based systems with normal dispersion. High-power parabolic pulse inputs were shown to keep their shape and propagate in a passive fibre [77]. In an amplifying medium operating at normal dispersion (such as a EDFA, Yb-doped fibre, or passive fibres with distributed Raman amplification), parabolic shaped pulses that are linearly chirped were shown to be the global attractors to the system, regardless of the initial condition [194–196]. Indeed, parabolic pulse solutions, or similaritons, were shown to be asymptotic solutions to the NLSE with normal dispersion and constant linear gain [194]. Although these optical pulses are beneficial for high-power amplification and lasers, the active medium can limit the available range of such pulses. There are a number of physical and technical applications (e.g. telecom signal processing) that require a specific parabolic pulse with linear chirp but where noise is to be minimized and high signal power is not necessarily required. A simple alternative method for the generation of such optical signals is through dispersion management in a passive fibre, by means of a dispersion-decreasing fibre (DDF) [197]. To understand the physics behind such a process, it is insightful to look at the governing equation (22) with $d(z) = -|d|p(z)$ and $c(z) = c$, where $p(z)$ is a normalized positive, decreasing function ($p(0) = 1$) and c is a constant. Using the following change of variables $\zeta(z) = \int_0^z p(z)\,dz,\quad q(\zeta,t) = a(z,t)/\sqrt{p(\zeta)}$ Eq. (22) is transformed into the NLSE with constant coefficients and effective gain

$$i\frac{\partial q}{\partial \zeta} - |d|\frac{\partial^2 q}{\partial t^2} + c|q|^2 q = -\frac{i}{2}\frac{p_\zeta}{p}q.$$

The right hand side shows the connection of the governing NLS equation with a decreasing dispersion ($p_\zeta < 0$) and amplification. Indeed, when $p_\zeta/p = -\Gamma_0$ is constant, exact asymptotic solutions are known [194]. This corresponds to $p(\zeta) = \exp[-\Gamma_0\zeta]$, so that the dispersion is an exact hyperbolic profile $p(z) = 1/(1+\Gamma_0 z)$. Assuming a hyperbolic dispersion profile the new variables can be found explicitly as $\zeta(z) = \ln(1+\Gamma_0 z)/\Gamma_0$, $q(\zeta,t) = a(z,t)\sqrt{1+\Gamma_0 z} = a(z,t)\exp(\Gamma_0\zeta/2)$, with fibre length in the new variables to be $\zeta(L) = \ln(1+\Gamma_0 L)/\Gamma_0$. In the case of lossless DDF, mathematically, indeed, these two problems are the same: the initial pulse evolves into a parabolic pulse when $L \to \infty$. To physically generate a DDF it is possible to use a tapered fibre with an appropriately varying core diameter. The zero dispersion point depends on the fibre diameter and changes during the pulling process. Smaller absolute values of dispersion correspond to the larger core diameters (in the normal dispersion region). Therefore, for the purposes of parabolic pulse generation, light should be launched into the taper from the narrow edge. Input and output diameters of the fibre can be tailored to achieve the desirable dispersion curve (i.e. hyperbolic profile). Typically, a difference of diameters is smaller than 10 μm (with the dispersion-shifted fibre diameter of about 120 μm) and higher-order dispersion terms and fibre nonlinearity with a good accuracy can be considered to be constants along the fibre for the fixed wavelength. The effects of higher-order dispersion and fibre loss imposes certain constraints on using tapered fibre for parabolic pulse generation. It has been demonstrated that though parabolic pulse generation in DDF is similar to the case of active fibre, the impact of TOD is critical for the DDF case and it is mandatory either to apply a scheme with a very accurately designed taper fibre length or to use a dispersion flattened DDF [198].

Above we have considered dispersion management with optical carrier pulses that are so-called "bright" solitons, which decay to zero as $|t| \to \infty$. Dispersion management can also be applied to another type of solitons, so-called dark solitons where the soliton is a CW wave with a dip in the constant power distribution (see [56,57,199–202] and references therein). The DM dark soliton in a fibre laser has similarities both with CW operation (far from the dip in power) and pulsed operation (in the power dip), and investigations of their properties in transmission systems have been made [203–206]. In recent work a dark DM soliton was reported as the attracting state in a dispersion managed erbium-doped fibre laser operating with a net-normal GVD [207]. It was shown that dispersion management could not only reduce the pump power threshold for the dark soliton formation in a fibre laser, but also stabilize the single dark soliton evolution in the cavity. It was also found that the formation of the DM dark soliton has lower pump threshold as compared with a similar dark soliton formation in an all-normal dispersion fibre laser. In general, dark solitons in dispersion managed fibre lasers can be quite stable and less sensitive to environmental perturbations [207].

In addition to tailoring the dispersion to obtain coherent structures, other aspects of dispersion management have been investigated. Dispersion management of parabolic pulses [208], and dispersion control in highly nonlinear fibres [209–213] have recently been explored. The use of a cascade of nonlinear optical fibres was used to drive a soliton system to an exact (regular) Cantor set fractals. Dispersion management was used to produce the fission of picosecond solitons in a fibre with a sinusoidal variation of the core diameter along the longitudinal direction of propagation [214]. The fission of high-intensity solitons caused by both the variation of the fibre dispersion and stimulated Raman scattering was demonstrated. Dispersion management can be used in such systems to control the number of output pulses and their frequencies even under the strong effect of the Raman scattering. The nonreciprocal effects and pulse compression due to the longitudinal oscillations of the fibre dispersion were experimentally demonstrated [215,216].

Finally, we mention a few studies involving the random nature of dispersion. The effect of random dispersion is important as short-range correlated uniform noisy fluctuations in the dispersion coefficient is inherent in many types of optical fibres [217–221]. Such random fluctuations broaden and eventually destroy initially ultra-short pulses. However, under the constraint that the integral of the random component of the dispersion coefficient is set to zero (pinned) periodically or quasi-periodically along the fibre, the dynamics of the pulse propagation changes dramatically [218]. For the case that randomness is present in addition to constant positive dispersion, the pinning restriction significantly reduces average pulse broadening. In periodic managed systems with some random deviations in the periodicity of the dispersion, the DM soliton can lose stability over certain parameter regimes [222].

3.9. Mathematical studies of dispersion-managed systems

So far in this review we have focused mainly on some of the key physical aspects of DM solitons. Over the years there has been extensive mathematical research on DM solitons and their dynamics. For completeness of presentation we briefly list some of the mathematical studies of the dispersion-managed systems without going into specific details that can be found in the papers listed in this section. Despite numerous physical and engineering papers, it is surprising that there are only few rigorous mathematical results concerning the existence and smoothness of DM soliton solutions. Existence and smoothness of weak solutions of the Gabitov–Turitsyn equation (61) had first been rigorously studied in [223] in the case of positive average dispersion and in the case of zero average dispersion in [224]. Interesting mathematical results concerning the existence and fine properties of DM solitons such as the exponential decay in both the time and frequency domains have been studied in [225–230]. Perturbation theory for DM solitons has been developed in [231,232]. A number of mathematical problems related to DM solitons dynamics have been considered [162,219,220,233–252]. The stability of DM solitons has been analysed within both a Gaussian variational approximation and an integral evolution model [253]. In the case of the normal average dispersion regime there are two DM soliton solutions having different pulse durations and energies at a fixed propagation constant. It was rigorously shown that the DM soliton with shorter pulse width (and a larger energy) is unstable while the other DM soliton solution with a smaller energy (and longer pulse width) is stable, but hits a resonance with excitations of the dispersion map [253]. In addition to DM solitons themselves, statistical properties of DM solitons in the presence of additive noise have been studied in a number of publications (see e.g. [254–266] and references therein).

4. Dispersion-managed solitons in dissipative systems

As discussed in the previous section, the dispersion-managed pulse is a stable periodic breather with features very different from that of the conventional soliton. In practical real world applications, signal transformation along the fibre line is not only caused by varying chromatic dispersion and nonlinearity, but also by dissipation and amplification. As examples, we refer back to Fig. 3 which shows two examples where dissipative elements occur periodically in the optical system. In long-haul lightwave communication systems the utilization of periodically installed in-line erbium-doped fibre optical amplifiers compensates the carrier signal attenuation in the transmission fibre. Similarly, mode-locked fibre lasers employ rare-earth doped fibre segments to provide the necessary gain to compensate the energy loss from output coupling and other nonlinear dissipative elements that promote self-starting pulse formation from initial amplitude fluctuations. In general, analytical progress becomes increasingly difficult when the dissipative terms have a nonlinear nature. However, there are some important limiting cases where the pulse dynamics can be described. In this section, we will describe dispersion management in dissipative systems where, in contrast to Section 3 the dissipative terms may be more complicated than Eq. (23b). First, we will review dissipative solitons and parabolic solutions in the context of an averaged Ginzburg–Landau equation. Then we will describe dispersion-management in the presence of distributed energy perturbations, and develop a description of dissipative DM solitons. We will then discuss dissipative dispersion-managed solitons where the discrete nature of the dissipative elements is maintained. Finally, we will discuss the intra-map pulse dynamics of such solutions.

4.1. Distributed Ginzburg–Landau equation and solutions

The complex Ginzburg–Landau equation (CGLE) was originally proposed as a phenomenological approach in the context of phase transitions [30], and is arguably one of the most-studied nonlinear models in the physics community. It describes on a qualitative, and often quantitative level a vast variety of physical phenomena, from nonlinear waves to second-order phase transitions, superconductivity, superfluidity, Bose–Einstein condensation, liquid crystals and strings in field theory [35]. It arises, in particular, as a first-approximation "envelope" (or "amplitude") equation that governs the non-equilibrium dynamics of nonlinear systems in the presence of gain/loss, depending on the specifics of the physical problem. For optical systems, the CGLE has been used to describe phenomena such as optical pulse transmission and, in particular, to model mode-locked lasers, where there exist both linear and nonlinear dissipative elements in the system [36,98,267–271].

4.1.1. Dissipative soliton solutions

In general, a pulse will change by some amount ΔU as it goes through each optical element in the periodic system. Significant mathematical insight can be obtained from averaged models when all discrete optical elements can be included in a fully distributed way. Of critical importance to this approach is that in such a system the maximum nonlinear phase shift $\phi_{NL}^{\max}$ a pulse accumulates over one period in the optical system is less than $\sim 2\pi$. In such a limit an average equation can be obtained in the form of a complex Ginzburg–Landau equation (CGLE). The most well-known example in this context was developed by Hermann Haus and is referred to as the "master equation" of passive mode-locking [267] (in dimensional units)

$$iU_z - \frac{1}{2}\beta_2 U_{tt} + \gamma|U|^2U = i\left[(g-\Gamma)U + \frac{1}{\Omega_g^2}U_{tt} + \delta|U|^2U\right]. \tag{75}$$

On the left hand side of Eq. (75) the dispersion and nonlinear coefficients are the average values of these parameters in the optical system. The parameter $g-\Gamma$ [dB/m] is the average constant gain/loss of the cavity, Ω_g [THz] is related to the width of a parabolic (in the frequency domain) filtering action, and δ (>0) [1/(W m)] is the nonlinear gain coefficient determining the strength of the saturable absorber action. Although the nonlinear cubic dissipation term is qualitative and simplifies the details of the particular nonlinear gain/loss element in the optical system, it provides a model that can be explored analytically. Specifically, exact stationary solutions exist to Eq. (75) of the form

$$U(z,t) = \sqrt{P}\ \mathrm{sech}\,(t/\tau)^{1+iC} \times e^{i\phi z} \tag{76}$$

where the parameter P, τ, C and ϕ are all real constants measuring the peak power, pulse duration, chirp parameter, and phase, respectively. Using the solution (76) in Eq. (75) we obtain the set of nonlinear algebraic equations

$$\phi\tau_0^2\Omega_g^2 - \left[D(1-C^2)+2C\right]\frac{\tau_0^2}{\tau^2} = 0, \qquad D(2-C^2) + 3\bar{\gamma}\frac{\tau}{\tau_0} - 3C = 0 \tag{77a}$$

$$(g-\Gamma)\Omega_g^2\tau_0^2 + \left[2DC + (1-C^2)\right]\frac{\tau_0^2}{\tau^2} = 0, \qquad (2-C^2) + 3DC - 3\bar{\delta}\frac{\tau}{\tau_0} = 0, \tag{77b}$$

where the nondimensional parameters $D = \beta_2\Omega_g^2/2$, $\bar{\gamma} = \gamma\Omega_g^2 E\tau_0/6$, and $\bar{\delta} = \delta\Omega_g^2 E\tau_0/6$ have been defined and τ_0 and $E = 2P\tau$ are the characteristic pulse duration and energy, respectively. Figs. 13–14 show the solution parameters for a wide range of parameters. The bandwidth is found from the relation $\mathcal{B} = \tau_0\,\mathrm{arcosh}(\cosh(\pi C)+2)/(\pi^2\tau)$ [272–274]. Fig. 13 shows the solution of (77) for a circumstance where the pulse energy E, filter width Ω_g, and nonlinear gain coefficient δ are fixed, and the GVD parameter β_2 and nonlinear coefficient γ are varied. When the nonlinearity parameter $\bar{\gamma} \neq 0$, there is a zero-chirp solution in the anomalous dispersion regime when $D\bar{\delta} + \bar{\gamma} = 0$ (black line). Typically the shortest pulse durations with the smallest chirp occur in the anomalous dispersion regime and these solutions are close to fundamental

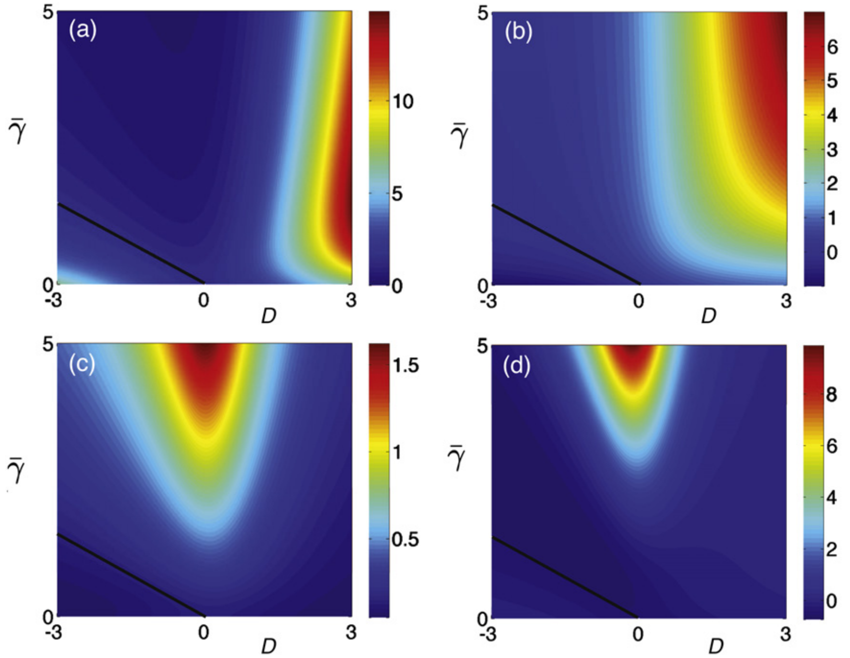

Fig. 13. Solution to the system (77) for (a) duration τ/τ_0, (b) chirp parameter C, (c) bandwidth $\mathcal{B}$, and (d) gain parameter $(g - \Gamma)\Omega_g^2\tau_0^2$ with $\bar{\delta} = 0.5$.

solitons, which rely mainly on the balance between dispersion and self-phase modulation while the dissipative terms play a secondary role. In contrast to the NLSE, the master mode-locking model permits bright soliton solutions of the form Eq. (76) at zero and normal dispersion ($D \geq 0$). Pulse solutions in the normal dispersion regime have larger pulse durations and chirp parameters. The bandwidth $\mathcal{B}$ is maximized for slightly positive dispersion, with the maximum increasing for larger values of the nonlinear coefficient $\bar{\gamma}$. The linear gain coefficient $g - \Gamma$ determines whether the background noise will grow or decay. From Fig. 13(d) we see that this growth rate is typically smaller in the anomalous GVD regime, and increases drastically around $D = 0$ for large values of the nonlinear coefficient. To investigate the role of gain dispersion, Fig. 14 shows the solution to (77) for a circumstance where the GVD coefficient is set to zero ($D = 0$), the parameter $\Omega_g\tau_0$ and pulse energy E are fixed, and $\gamma\Omega_g$ and $\delta\Omega_g$ are varied. The boxes marked "I" and "II" correspond to regions of strong and weak gain filtering, respectively. When there is strong filtering (the gain bandwidth is narrow) the pulse duration is broad and the chirp parameter increases for lower values of $\bar{\delta}$. When there is weak spectral filtering, the pulses have a short duration and are slightly chirped. For all solutions the pulse bandwidth mostly depends on the nonlinear parameter $\bar{\gamma}$, with broader bandwidths for larger values of $\bar{\gamma}$, and the gain coefficient decreases for higher values of the nonlinear gain coefficient $\bar{\delta}$. Fig. 15 shows examples of typical temporal and spectral power profiles of solution (76) for both anomalous and normal dispersion. For highly chirped pulses typical in the normal dispersion regime, the spectral power is squared off with steep edges. Such solutions were experimentally realized in a solid-state laser system with net normal dispersion [275].

In addition to the existence of pulse solutions (76), it is also important to understand their stability. Fig. 13(d) and 14(d) shows the gain parameter which must be negative if the pulse is to be stable against buildup of low amplitude noise between pulses. Indeed, it is possible to obtain negative net gain for various parameters. The mathematical conditions for the net gain to be negative were found in [267], however this analysis did not characterize the stability of the pulse itself. Using soliton perturbation theory techniques and neglecting the filtering and nonlinear gain/loss terms, solutions (76) to Eq. (75) were shown to be unstable in the anomalous dispersion regime ($\beta_2 < 0$) when $g - \Gamma > 0$ [276]. An extension of this work included the addition of a saturable gain

$$g = g(z) = \frac{G_0}{1 + E(z)/E_{\text{sat}}}. \tag{78}$$

The saturable gain model (78) assumes that the gain response of the medium T_g is slow when compared to the time between successive pulses T_R. This is a reasonable assumption since for typical amplifiers $T_g \sim$ microseconds, where $T_R \sim$ nanoseconds for many optical systems such as mode-locked fibre laser resonators. In such a limit the gain saturates due to the total energy $E(z) = \int_{-\infty}^{\infty} |U(z,t)|^2 dt$ in the amplifying medium. The energy saturation parameter $E_{\text{sat}} = P_s^{(g)} \times T_R$, measured in nanojoules, is determined by the saturation power of the gain medium $P_s^{(g)}$ and the repetition rate of the optical system T_R. The parameter G_0, measured in dB/m, is the small signal gain parameter. Including this saturation gain model allowed for the stabilization of the pulse solution (76) in the anomalous dispersion regime ($\beta_2 < 0$) for a small regime of parameter space [277].

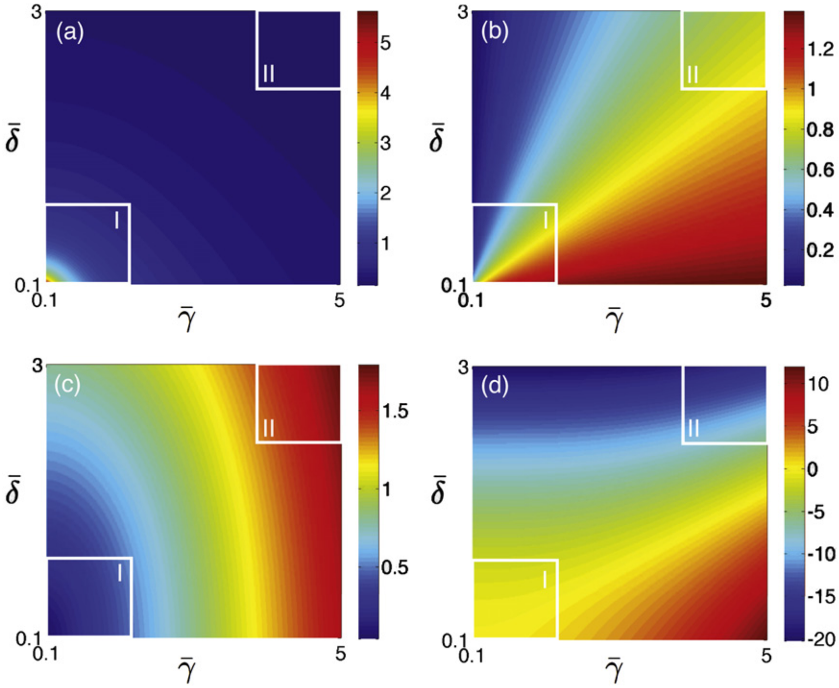

Fig. 14. Solution to the system (77) for (a) duration τ/τ_0, (b) chirp parameter C, (c) bandwidth $\mathcal{B}$, and (d) gain parameter $(g - \Gamma)\Omega_g^2\tau_0^2$ with $D = 0$.

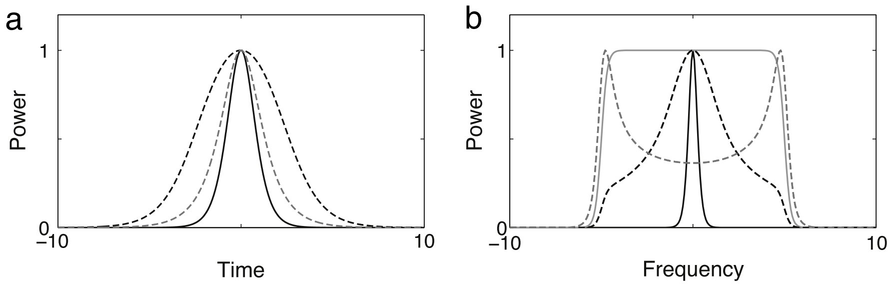

Fig. 15. Hyperbolic secant solutions (76) for $P = 1$, $\tau = 1$, $C = 0$ (solid black) and $C = 5$ (solid grey) in both the (a) temporal and (b) spectral domains. The dashed profiles are examples of highly chirped solutions to the CQGLE [97–101].

Although the master model developed by Haus highlights important qualities about pulse solutions of the form (76), the range of parameters where stable solutions exist is highly restricted. To increase the range of stable solutions, a quintic loss term is often added to the right hand side of Eq. (75), giving the so-called cubic–quintic GLE (CQGLE). Although the quintic term saturates the nonlinear gain and allows for a broader parameter space where solutions are stable, chirped hyperbolic secant solutions (76) are no longer exact solutions. However, the general trends shown in Figs. 13–14 remain consistent with steady state pulse solutions to the CQGLE. Specifically, pulses in the anomalous dispersion regime have low chirp values and tend to be short, whereas pulses in the normal dispersion regime have a large chirp and tend to be broad. The CQGLE has been extensively studied numerically over the past two decades and interesting behaviour has been found describing, for example, stationary solutions, pulsating solitons, chaotic solitons, soliton explosions and soliton interactions [36,103–105,278].

Recent progress in ultra-fast lasers has produced high-energy, highly chirped pulses in chirped-pulse oscillators and all-normal dispersion lasers [279,280]. These highly chirped pulses have features that cannot be predicted by the cubic GLE and its solutions (76). Specifically, the spectral power profile of the pulse solutions is distinctly different in shape from those predicted by the solution (76). Modifications of the flat-top spectrum predicted by (76) include a parabolic-top with squared off sides or high fringes on the edge of the spectra with a dip in the middle (see Fig. 15). A generalization of the Hocking and Stewartson solution to the CQGLE $U(z,t) = \sqrt{P/(\cosh(t/\tau) + B)} \times \exp[-iC(\ln(\cosh(t/\tau)+B)) + i\varphi z]$ has the ability to reproduce such spectral profiles depending on the parameter $-1 < B < \infty$ [97]. This solution has co-dimension one, meaning that the solution parameters cannot be expressed entirely in terms of the equation parameters leading to additional assumptions on the equation parameters. However, it has been successful in qualitatively predicting various modes of operation of all-normal dispersion mode-locked fibre lasers, such as flat top pulses, giant chirp solutions, and the onset of multi-pulsing. It was also used to characterize the intra-cavity dynamics and the role of spectral filtering in such optical systems [281]. Recently these solutions have been employed with the CQGLE to extend the so-called soliton area theorem. In contrast to the typical soliton area theorem which states that the energy is inversely proportional to the pulse duration, for a particular set of parameter values the modified area theorem predicts that the pulse energy varies linearly with pulse duration [282]. In another approach, approximate solutions to the CQGLE have been found which exhibit some qualitative features of the experimentally realized pulses [98–100,102]. These solutions allow for relevant regions in the parameter space to be mapped out, and the approximate solutions have been extended for the more general case when the cubic–quintic dissipative terms are replaced with a Lorentzian function [101].

4.1.2. Similariton solutions

High power optical pulses with a parabolic intensity profile and a linear frequency chirp propagate without typical wave-breaking instabilities in a passive optical fibre operating in the normal dispersion regime [77]. This insight encouraged the study of ultrashort pulse propagation in a normal dispersion optical fibre amplifier which can be described by Eq. (75) with $\beta_2 > 0$, $\Omega_g \to \infty$ and $\delta = 0$. Remarkably, regardless of the initial input pulse, the pulse naturally evolves towards a parabolic pulse profile with a quadratic phase if $g - \Gamma > 0$ and retains this structure even as it is continued to be amplified to high powers [194]. Fig. 16(a) shows the typical pulse evolution and highlights the pulse evolution of a initial Gaussian shape. The inset shows the final parabolic pulse and the linear chirp profile (derivative of the phase) across it. Indeed, regardless of the initial pulse shape these chirped parabolic pulses act as the global attractor to the system in the asymptotic limit. Assuming a self-similar parabolic solution of the form

$$U(z,t) = \sqrt{P_p(z)\left[1 - \frac{t^2}{\tau_p^2(z)}\right]} \times e^{iC_p(z)t^2} \tag{79}$$

into Eq. (75) ($\Omega_g \to \infty$ and $\delta = 0$) and letting $1/\tau^2 \ll C^2$ in the asymptotic limit gives

$$\frac{dP_p}{dz} = 2\beta_2 PC + 2(g-\Gamma)P, \qquad \frac{d\tau_p}{dz} = -2\beta_2\tau C, \qquad \frac{dC_p}{dz} = 2\beta_2 C^2 - \gamma\frac{P}{\tau^2}. \tag{80}$$

These equations have analytical solutions

$$P_p(z) = A_0^2\, e^{4(g-\Gamma)z/3}, \qquad \tau_p(z) = \frac{3\sqrt{\gamma\beta_2/2}}{g-\Gamma}A_0\, e^{2(g-\Gamma)z/3}, \qquad C_p(z) = -\frac{g-\Gamma}{3\beta_2}, \tag{81}$$

where $A_0 = [2(g-\Gamma)E_{\rm in}/\sqrt{\gamma\beta_2/2}]^{1/3}/2$ and $E_{\rm in}$ is the input pulse energy. From Eq. (81), the bandwidth can be calculated to be $\omega_p = \sqrt{2\gamma/(5\beta_2)}\,A_0\exp[2(g-\Gamma)z/3]$. In the presence of gain ($g - \Gamma > 0$), the peak power, pulse duration and bandwidth increase exponentially and only depend on the amplifier parameters and input pulse energy. Further, the chirp parameter approaches a constant value that is proportional to the gain coefficient and inversely proportional to the GVD coefficient. The asymptotic nature of this solution is reflected in the fact that the pulse characteristics approach Eq. (81) regardless of the initial pulse shape. Fig. 16(b) highlights the attractive nature of the asymptotic parabolic pulse solution. Shown is the phase space representation with the phase variables given by the ratio of the RMS pulse duration and bandwidth (see Eq. (17)) to their asymptotic values τ_p and ω_p respectively. The results are obtained from solving Eq. (75) with initial Gaussian pulses of the form $u(0,t) = \sqrt{E_{\rm in}/[\sqrt{\pi}\tau_p(0)]}\,\exp[-t^2/(2\tau_p^2(0))]$ ($E_{in} = 100$ pJ) with FWHM pulse durations varying over the range 150 fs to 1 ps in a 5 metre amplifier. It is clear that although different input pulses follow different evolution trajectories, they are all attracted to the asymptotic similariton solution (the point (1, 1) in the phase plane) with sufficient propagation distance. The important fact that these solutions act as *global* attractors to the system allows for them to be used in a variety of optical systems ranging from laser applications to signal processing.

4.2. Dispersion management with distributed dissipative elements

Distributed models such as the master equation and CQGLE describe the average dynamics of an optical system which physically contains lumped elements. In some systems it is remarkable how well these equations describe the overall physics under certain conditions. However, to incorporate more realistic pulse dynamics in the overall optical system it is important to include physical effects whose influence depends on propagation distance within the optical system. Here we consider pulse evolution in such optical systems with a dispersion map with the dissipative terms averaged over the whole optical system, resulting in the normalized governing equation

$$iu_z + d(z)u_{tt} + \epsilon|u|^2u = i\left[(g(z) - l_0)u + \nu g(z)u_{tt} + \frac{l_0}{p_s}F(|u|^2/p_s)|u|^2u\right], \tag{82}$$

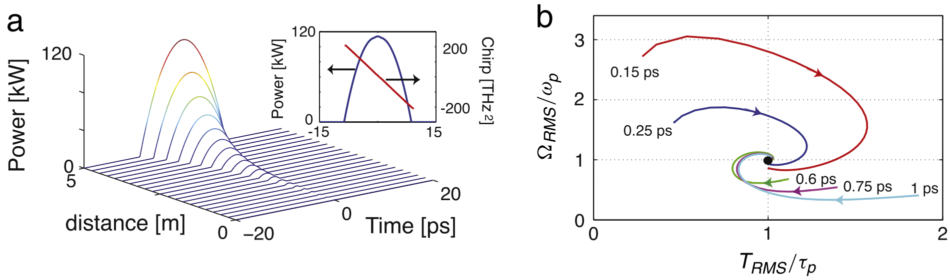

Fig. 16. (a) Solution from Eq. (75) with initial Gaussian pulse of energy 100 pJ and FWHM pulse duration 500 fs over 5 m of propagation. The parameters are $\beta_2 = 0.025$ ps^2/m, $\gamma = 0.005$ 1/(W m), $g = 0.95$ 1/m, $\Gamma = \delta = 0$, and $\Omega_f \to \infty$. Inset: power and chirp profiles after 5 m propagation distance. (b) Phase portrait with normalized RMS pulse duration and bandwidth phase variables from similar numerical simulations as in (a), but with varying initial FWHM pulse durations ranging from 150 fs to 1 ps.

with a saturable gain

$$g(z) = \frac{g_0}{1 + E(z)/e_s}. \tag{83}$$

Here all normalizations are as in Eq. (2), with the length $L = L_{DM}$ being the length of the dispersion map. Without loss of generality and for continuity with Section 3, we consider mainly the symmetric map

$$d(z) = \begin{cases} d + \langle d \rangle, & 0 < z < 0.25 \\ -d + \langle d \rangle, & 0.5 < z < 0.75, \\ d + \langle d \rangle, & 0.75 < z < 1. \end{cases} \tag{84}$$

The additional normalized dissipative parameters $g_0 = LG$, $e_s = E_{\rm sat}/(P_0 T_0)$, $l_0 = L\Gamma$, $\nu = 1/(\Omega_g^2 T_0^2)$, and $p_s = P_s/P_0$ are the normalized small-signal gain coefficient, saturation energy, unsaturated loss coefficient, gain bandwidth parameter, and saturation power, respectively. Here G (in 1/metre) is the linear gain from amplification, Γ (in 1/metre) is the distributed losses, $E_{\rm sat}$ (in picojoules) is the saturation energy of the gain medium, Ω_g (in THz) is related to the amplification bandwidth, and P_s (in W) is the saturation power for the nonlinear gain/loss element such as a saturable absorber. The nonlinear gain/loss element is characterized by the general function F, which in certain limits gives different Ginzburg–Landau type equations. For example, if F is constant, then Eq. (82) has the form of the cubic GLE, where if F is linear it is the CQGLE.

The dissipative terms in Eq. (82) play an important role in the scalings considered and are responsible for major differences between solutions to Eq. (82) and conservative DM solitons considered in Section 3. Conservative DM solitons experience no gain or loss and must be launched with the appropriate energy and chirp corresponding to the particular dispersion map. In contrast, when dissipation is included as in Eq. (82) the dissipative terms will select the appropriate pulse evolution such that the total gain and losses experienced by the pulse will approximately balance. This continuous energy balance is a direct consequence of the proposed distributed model and is distinctly different than models where the dissipative terms are represented in a lumped way. From Eq. (82), the evolution of the energy $E = \int_{-\infty}^{\infty} |u|^2 dt$ is given by

$$\frac{1}{2}E_z = \left[\frac{g_0}{1 + E/e_s}(1 - \nu\,\Omega_{RMS}^2) - l_0\right]E + \frac{l_0}{p_s}\int_{-\infty}^{\infty} F(|u|^2/p_s)|u|^4 dt, \tag{85}$$

where Ω_{RMS}^2 is the RMS bandwidth parameter defined in Eq. (17d). It is clear from Eq. (85) that the pulse energy is increased by the linear gain, while it is reduced by linear loss and gain filtering. Depending on the form of $F(x)$, the energy is increased or decreased by the nonlinear dissipative term. Typically the linear gain and loss will balance so that $E \sim e_s(g_0 - l_0)/l_0$, giving a peak power and pulse duration that typically do not satisfy the requirements for periodic breathers in the conservative DM case. However, exact periodic breathers are still possible due to dissipative effects.

4.2.1. Detailed effects of dissipative terms

Using the same symmetric map (84) as was presented for much of the analysis in Section 3, we highlight how each dissipative term in Eqs. (82)–(84) will effect the pulse evolution. In the simplest case, when only gain saturation is included the initial condition is amplified until the pulse energy reaches a constant value of $E = e_s(g_0 - l_0)/l_0$, giving a total gain $g(z) - l_0 = 0$. The dissipation will amplify or attenuate any initial condition so that the pulse energy is attracted towards this value. Once the energy saturation level has been achieved, the conservative components completely drive the breathing dynamics. Since the energy level is typically not the same as that required for exactly periodic pulse evolution, the breathing dynamics is not periodic (Fig. 18(a)) and resembles a conservative DM soliton started from non-ideal initial conditions. Including a general nonlinear gain element representing, for instance, the action of a saturable absorber in the optical system can lead to stable periodic breathers for a large range of parameter space. Fig. 17 shows the solution of Eqs. (82)–(84) with a Lorentzian nonlinear gain function $F(x) = 1/(1 + x)$. The periodic breather stretch and compress twice per cavity round

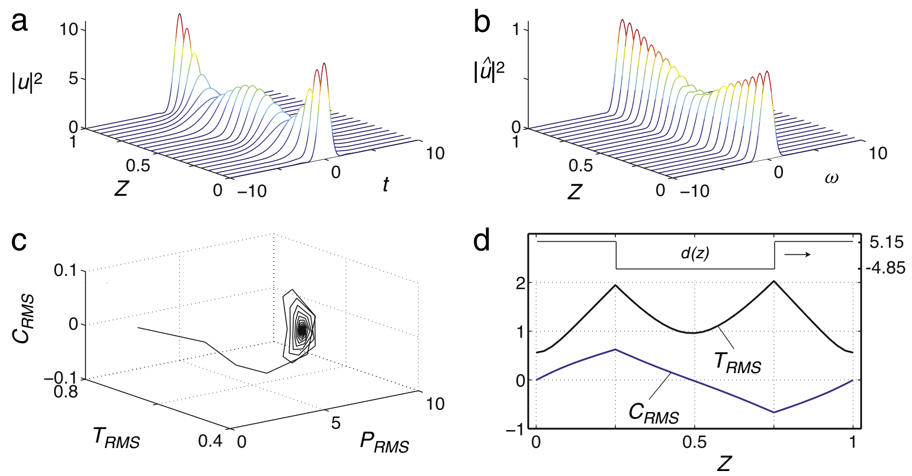

Fig. 17. (a) Temporal and (b) spectral evolution of the power per map period once steady state evolution is achieved from the solution to Eqs. (82)–(84) with $d = 5$, $\langle d \rangle = 0.15$, $\epsilon = 1$, and dissipative parameters $g_0 =$, $l_0 = 0.7$, $e_s = 2$, $p_0 = 10$, and $\nu = 0$. The nonlinear gain function is $F(x) = 1/(1 + x)$. (c) Poincare map taken in the middle of the anomalous dispersion segment. (d) Intra-map evolutions of the RMS pulse duration and chirp parameter once steady state evolution is reached.

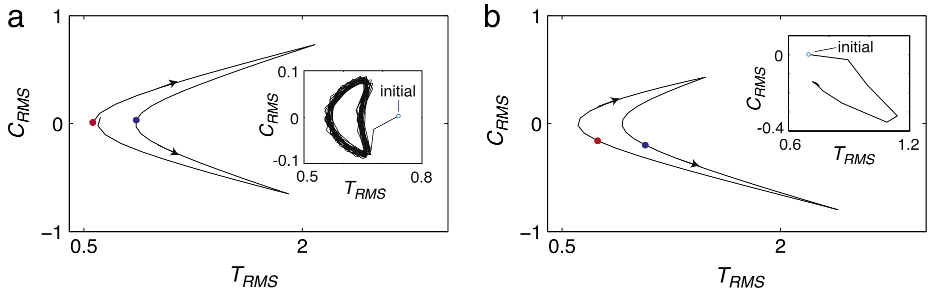

Fig. 18. Phase plane and Poincare map (insets) taken at the middle of the anomalous GVD segment for the solutions obtained from Eqs. (82)–(84) with the same parameters as in Fig. 17 but with (a) $F(x) = \nu = 0$ and (b) $F(x) = 1/(1 + x)$ and $\nu = 0.3$. The red (blue) dots on the phase plane correspond to the middle of the anomalous (normal) GVD segments. (For interpretation of the references to colour in this figure legend, the reader is referred to the web version of this article.)

trip, reach a minimum duration in the middle of each segment, and acquire both signs of chirp. Fig. 17(c) shows the RMS characteristics in a Poincare map at the specific point in the middle of the anomalous GVD segment ($z = 0$). Clearly the intra-map pulse dynamics is attracted to a periodic breather, represented by the attracting node in the phase plane. Indeed, the nonlinear gain is a key element to obtain solutions that are attractors to the system. This is due to the fact that the nonlinear gain element increases the energy of the pulse, effectively decreasing the saturated gain $g(z)$ (see Eq. (83)). Once the gain level has been saturated, the overall linear gain $g(z) - l_0 < 0$. In contrast to conservative DM solitons as well as solutions where only gain saturation is included, the dispersive radiation is attenuated making the evolution exactly periodic.

If spectral filtering is included ($\nu \neq 0$), then additional losses will occur when the pulse bandwidth approaches the gain bandwidth (see Eq. (85)). When $F(x) = 0$, this loss mechanism is compensated by the linear gain $g(z) - l_0 > 0$. In this case the dispersive radiation is amplified, eventually degrading the pulse. When nonlinear gain is included ($F(x) \neq 0$), stable periodic breather solutions exist over a wide range of parameter space. As before, the periodic breather stretches and compresses twice per cavity round trip, however the minimum pulse duration is not necessarily in the middle of each segment due to the phase modulation induced by gain filtering. It is interesting that strong gain filtering in a symmetric dispersion map can have a similar effect as a non-symmetric dispersion map since it moves the zero-chirp points away from the middle of each fibre segment. Fig. 18(b) illustrates the phase plane and Poincare map dynamics for simulations of Eqs. (82)–(84) with strong gain filtering. Clearly the symmetry in the phase plane is lost due to the action of the gain filtering. In general the pulse energy can be increased by increasing the small signal gain g_0 or saturation energy e_s. This results in increased peak power, shorter pulse duration as well as larger spectral breathing ratios. As these parameters are increased, the pulse will eventually break up due to nonlinear instabilities when $\phi_{NL}^{\max} \sim 2\pi$ in the anomalous GVD segment. This puts a restriction on both peak power and pulse energies available.

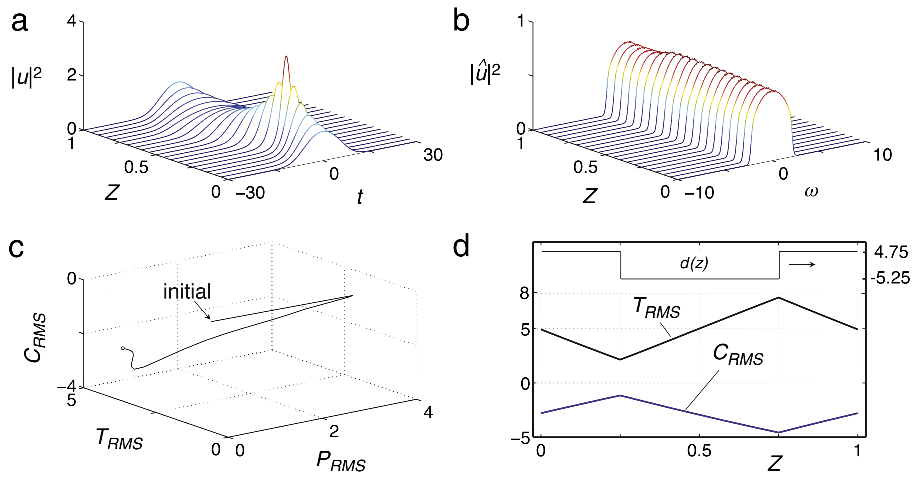

Fig. 19. (a) Temporal and (b) spectral evolution of the power per map period once steady state evolution is achieved from the solution to Eqs. (82)–(84). Here equation parameters are the same as in Fig. 17, but with large net-normal dispersion $\bar{d} = -0.25$ and gain filtering parameter $\nu = 0.1$. (c) Poincare map taken in the middle of the anomalous dispersion segment. (d) Intra-map evolutions of the RMS pulse duration and chirp parameter once steady state evolution is achieved.

4.2.2. Positively chirped DM solitons

We have so far investigated dissipative DM soliton solutions for a particular dispersion map with net-anomalous dispersion. Similar to conservative DM solitons, these solutions exist for dispersion maps with different dispersion depths in the net-anomalous, zero, and *small* net-normal dispersion regime. As discussed in Section 3, conservative DM solitons do not exist for dispersion maps with large net-normal dispersion. However, the addition of dissipative elements allows for highly chirped pulses with distinctly different pulse evolution to exist at larger net-normal dispersions. These solutions mainly rely on linear processes, with the dispersive pulse frequency chirp being the dominating effect driving the evolution. As an example, consider the previously considered dispersion map (84) with $d = 5$, but now with large net-normal dispersion $\langle d\rangle = -0.25$. Fig. 19 illustrates the pulse evolution once it has settled to its steady state. The pulse dynamics is distinctly different than conventional DM solitons. Here the temporal pulse profile goes between a parabolic and Lorentzian shape while the pulse power spectrum is nearly parabolic. The fact that the pulse spectrum changes very little highlights the fact that linear processes dominate over nonlinearity. The pulses are attracting solutions (Fig. 19(c)) and in each map period the pulse stretch and compress once, have minimum duration at the beginning of the normal dispersion segment, and are positively chirped throughout the dispersion map (Fig. 19(d)).

Analytical insight of the pulse evolution once it is in its steady state (when the dissipative terms are small) can be obtained for these solutions by doing an amplitude/phase decomposition on the left hand side of Eq. (82) of the form $u(z,t) = \sqrt{P(z,t)} \times \exp[i\phi(z,t)]$ giving

$$P_z = -2d(z)[P\phi_t]_t \tag{86a}$$

$$\phi_z = d(z)\left[\frac{\partial_t^2\sqrt{P}}{\sqrt{P}} - \phi_t^2\right] + \epsilon P. \tag{86b}$$

In the limit where the square of the chirp ϕ_t^2 is much greater than the other terms in Eq. (86b), there are exact solutions of the form

$$P(z,t) = \frac{a(z)}{1 + t/\tau(z)}, \qquad \phi(z,t) = C(z)\frac{t^2}{\tau^2(z)}, \tag{87}$$

where the peak power, pulse duration and chirp parameter are given by (for the case of the piece-wise constant dispersion map (84))

$$a(z) = \frac{a_0\tau_0^2}{8d(z)C_0 z + \tau_0^2}, \qquad \tau(z) = \frac{1}{\tau_0}(8d(z)C_0 z + \tau_0^2) \qquad C(z) = \frac{C_0}{\tau_0} \times \tau(z). \tag{88}$$

Here a_0, τ_0 and C_0 (< 0) are the initial values of the pulse parameters at the beginning of each map period. Note that the pulse power has a Lorentzian shape (in time) and the chirp is linear. Further, the peak power has a $1/z$ dependence while the pulse duration and chirp parameter are linear, with the slope being determined by the product $d(z) \times C_0$. Note that if $1 \ll \tau$, the Lorentzian power profile can be expanded and approximated by a quasi-parabolic profile.

Please cite this article in press as: S.K. Turitsyn, et al., Dispersion-managed solitons in fibre systems and lasers, Physics Reports (2012), doi:10.1016/j.physrep.2012.09.004

4.2.3. Extended TM equations with distributed dissipative terms

Similar to the conservative case, it is useful to understand the RMS pulse characteristics (17) when investigating the solutions of Eqs. (82)–(84). Taking into consideration the dissipative terms on the right hand side of Eq. (82) and making the same assumption about the phase profile of the pulse ($= M_{RMS}/T_{RMS} \times t^2 = C_{RMS}/T^2_{RMS} \times t^2$), we obtain

$$\frac{dT_{RMS}}{dz} = 4d(z)\frac{C_{RMS}}{T_{RMS}} - \frac{\nu g}{T^2_{RMS}}\left[-1 - T^2_{RMS}\Omega^2_{RMS} + I_1\right] + \frac{l_0}{p_s T_{RMS}}\left[I_2 - T^2_{RMS} I_3\right] \tag{89a}$$

$$\frac{dC_{RMS}}{dz} = d(z)\Omega^2_{RMS} - \frac{\epsilon}{4}P_{RMS} + \nu g\left[I_4 + 2C_{RMS}\Omega^2_{RMS}\right] + \frac{l_0}{p_s}\left[I_5 - 2C_{RMS} I_3\right] \tag{89b}$$

$$\frac{P_{RMS}}{dz} = -4d(z)\frac{C_{RMS}P_{RMS}}{T^2_{RMS}} + 2(g - l_0)P_{RMS} + 2\nu g\left[I_6 + \Omega^2_{RMS}P_{RMS}\right] + \frac{2l_0}{p_s}\left[2I_7 - PI_3\right] \tag{89c}$$

$$\frac{d\Omega^2_{RMS}}{dz} = -2\epsilon\frac{C_{RMS}P_{RMS}}{T^2_{RMS}} + 2\nu g\left[\Omega^4_{RMS} - I_8\right] - \frac{l_0}{p_s}\left[I_9 + \Omega^2_{RMS} I_3\right]. \tag{89d}$$

where $I_1 = \int t^2|u_t|^2 dt/E$, $I_2 = \int t^2|u|^4 F(|u|^2/p_s)dt/E$, $I_3 = \int |u|^4 F(|u|^2/p_s)dt/E$, $I_4 = i\int t(u_{tt}u_t^* - u_{tt}^* u_t)dt/(2E)$, $I_5 = i\int t|u|^2 F(|u|^2/p_s)(uu_t^* - u^* u_t)dt/(2E)$, $I_6 = \int |u|^2(uu_{tt}^* + u^* u_{tt})dt/E$, $I_7 = \int F(|u|^2/p_s)|u|^6 dt/E$, $I_8 = \int |u_{tt}|^2 dt/E$, $I_9 = \int F(|u|^2/p_s)|u|^2(u_{tt}^* u + u_{tt}u^*)dt/E$. The dissipative terms introduce new momenta and thus a closed system of equations is not possible. Alternatively, we can reduce the system of equations (89) to describe the key pulse parameters by assuming a specific structural form of the pulse. Although this will introduce an additional approximation since, in addition to a quadratic phase profile across the pulse we are assuming a power profile as well, all RMS integrals can be explicitly computed resulting in a closed system of ordinary equations. For example, if we assume a chirped-Gaussian pulse of the form

$$\sqrt{P(z)}\ \exp\left[-\frac{t^2}{2\,\tau(z)^2}(1 - iC(z)) + i\varphi(z)\right], \tag{90}$$

it is easy to compute from Eq. (17) the RMS pulse characteristics $T_{RMS} = \tau/\sqrt{2}$, $C_{RMS} = C/4$, $P_{RMS} = P/\sqrt{2}$, and $\Omega^2_{RMS} = (1 + C^2)/(2\tau^2)$ as well as the moments I_1 through I_9. Substituting these values into Eq. (89) gives

$$\tau_z = 2d(z)\frac{C}{\tau} - \nu g\frac{1}{\tau}(C^2 - 1) + \frac{l_0}{\sqrt{\pi}p_s}P\tau\, Q_1(P/p_s) \tag{91a}$$

$$C_z = [2d(z) - 2\nu gC]\frac{1 + C^2}{\tau^2} - \frac{\epsilon}{\sqrt{2}}P + \frac{2l_0}{\sqrt{\pi}p_s}CP\, Q_1(P/p_s) \tag{91b}$$

$$P_z = -2d(z)\frac{CP}{\tau^2} + 2(g - l_0)P - 2\nu g\frac{P}{\tau^2} + \frac{2l_0}{\sqrt{\pi}p_s}P^2\, Q_2(P/p_s), \tag{91c}$$

where $g = g(P, \tau) = g_0/(1+P\tau\sqrt{\pi}/e_s)$, $Q_1(x) = \int F(xe^{-s^2})e^{-2s^2}(2s^2 - 1)\, ds$ and $Q_2(x) = \int F(xe^{-s^2})e^{-2s^2}(2\sqrt{2}\, e^{-s^2} - 1)\, ds$. The nonlinear gain terms Q_1 and Q_2 depend on the particular form of $F(x)$ as well on the ratio of the power P to the saturation power p_s. For the case of the cubic GLE where $F(x) = 1$, $Q_1 = -\sqrt{\pi/2}/2$ and $Q_2 = 2\sqrt{2\pi/3} - \sqrt{\pi/2}$, whereas for the cubic–quintic GLE where $F(x) = 1-x$, $Q_1 = -\sqrt{\pi/2}/2+(2\sqrt{\pi/27})x$ and $Q_2 = 2\sqrt{2\pi/3}-\sqrt{\pi/2}-(2\sqrt{\pi/2}-\sqrt{\pi/3})x$. For a nonlinear gain of a saturable type $F(x) = 1/(1 + x)$, Q_1 and Q_2 can be computed numerically (Fig. 20) and are monotonic functions that asymptotically go to zero for large P/p_s. It is interesting that Eq. (91c) is the same as that obtained using the variational method with the same Gaussian ansatz (90). Indeed, both the RMS momentum method and the variational method has been used extensively to study nonlinear pulse dynamics in nonlinear optical systems, and in particular dispersion managed solitons.

A comparison between the RMS pulse parameters from full numerical simulations of Eqs. (82)–(84) and the reduced equations (91) is shown in Fig. 21. The peak power P, pulse duration τ and chirp parameter C from the solutions to Eq. (91) have been converted to their RMS counterparts. The pulse parameter evolution over one map period after steady state evolution has been achieved is shown in Fig. 21(a). The Poincare map illustrated in Fig. 21(b) is taken at the middle of the anomalous GVD segment, and shows that the reduced model has an attracting solution to the Poincare map and is in reasonable agreement with full numerical simulations. If we let the absolute difference $\Delta = |Q_{RMS}(0) - \tilde{Q}_{RMS}(0)|$, where $Q(0)$ ($\tilde{Q}(0)$) is the RMS pulse parameter found from full numerical simulations (reduced model simulations), we see that although $\Delta < 0.2$ for T_{RMS} and C_{RMS}, $\Delta \sim 1$ for P_{RMS} (Fig. 24(b) inset). This is due to the variance of the temporal pulse shape from a Gaussian profile at this point in the Poincare map. Indeed, the value of Δ for P_{RMS} is much less at other points in the map. Although the reduced model is constrained by the ansatz assumption, it is remarkable how accurately it models the full equation dynamics. The long-scale RMS pulse characteristics are attracted to a periodic evolution when nonlinear gain is included, and will have some error depending on the shape of the temporal and spectral power profile. For instance, for typical DM soliton evolution such as shown in Fig. 17, the reduced system represents the evolution better than for the

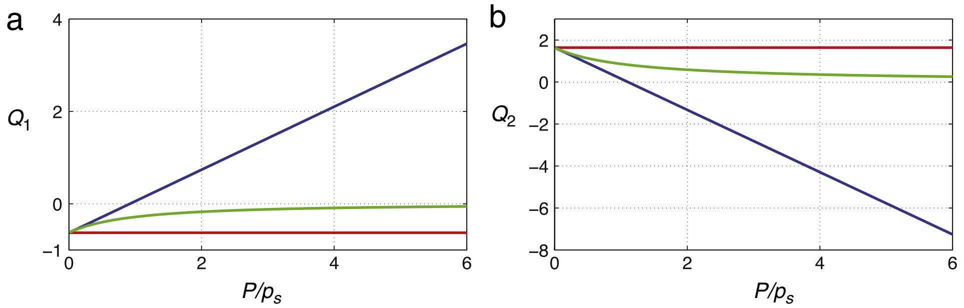

Fig. 20. Nonlinear gain functions (a) Q_1 and (b) Q_2 in Eq. (91) for the cubic GLE where $F(x) = 1$ (red), the cubic–quintic GLE where $F(x) = 1 - x$ (blue), and a saturable GLE where $F(x) = 1/(1 + x)$ (green). (For interpretation of the references to colour in this figure legend, the reader is referred to the web version of this article.)

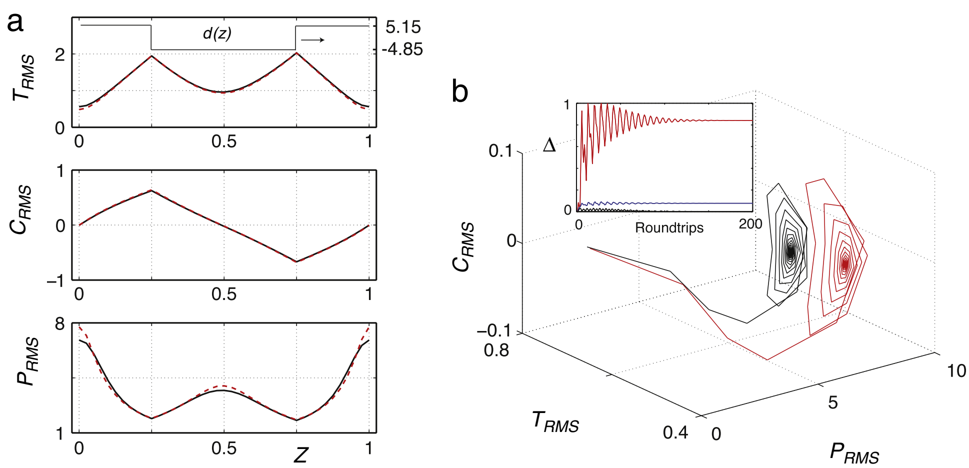

Fig. 21. (a) RMS pulse parameters over one map period once steady state evolution is achieved and (b) Poincare map taken at the point in the middle of the anomalous GVD segment from direct simulation of Eqs. (82)–(84) (black) compared with that found from the reduced model equations (91) (red). Inset: the Δ values are shown for the RMS pulse parameters T_{RMS} (blue), P_{RMS} (red), and C_{RMS} (black). All parameters are the same as in Fig. 17. (For interpretation of the references to colour in this figure legend, the reader is referred to the web version of this article.)

positively chirped pulse evolution shown in Fig. 19. This is expected since for typical conservative DM soliton evolution the temporal and spectral pulse profiles stay close to a Gaussian shape, where for positively chirped pulse evolution they can be different. However, even in the case of positively chirped pulse evolution the pulse parameters are reasonably described by the reduced equations with an error of ∼10%. Indeed, the reduced model equations (91) qualitatively describe the key features of the distributed dispersion managed model, and can be used for the exploration of pulse dynamics in the large parameter space of Eqs. (82) and (84).

4.3. Dispersion management with discrete dissipative elements

Although the governing equations (82)–(84) can represent the average dynamics of many optical systems, it is often not capable of fully characterizing the intra-cavity dynamics. This is because the distributed model averages all dissipative terms so that the gain balances the losses. In practical systems, the dissipative elements may occur at a specific point in the dispersion map, altering the pulse evolution significantly. Indeed, it is possible to obtain large pulse fluctuations per cavity round trip and pulse shaping can be dominated by either large phase or amplitude modulations. Since it is a highly nonlinear system, the strength and the location of the dissipative elements can have a significant influence on pulse evolution. In such systems the validity of averaged models such as Eqs. (82)–(84) is in question. In addition to fibre propagation, here we consider the effects the pulse experiences when some action is induced by discrete dissipative elements. Specifically we will describe pulse propagation in optical fibre modelled by Eqs. (82)–(84) with $F(x) = 0$ and where $g_0 = 0$ for a passive fibre and $g_0 \neq 0$ for an active fibre. Along with the fibre propagation equations we will include key discrete elements such as a saturable absorber, output coupler, and spectral filter. Indeed, these elements are used in a variety of different optical systems ranging from telecommunication to laser applications. These elements can have a complicated interaction with the optical pulse in which various physical processes need to be considered. Here we will simplify our analysis of such discrete elements by describing the discrete elements by simple transfer functions, where certain macroscopic parameters

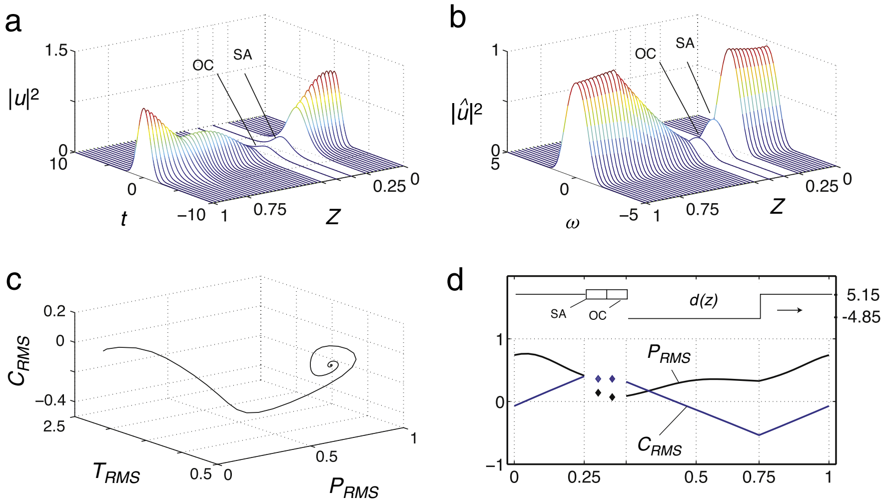

Fig. 22. (a) Temporal and (b) spectral evolution of the power per map period once steady state evolution is achieved from the solution to Eqs. (82)–(84) with discrete actions Eq. (92)–(93). Here $F(x) = 0$, $d = 5$, $\langle d \rangle = 0.15$, $\epsilon = 1$, and dissipative parameters $g_0 = 0$ in the anomalous GVD segment, $g_0 = 4$ in the normal GVD segment, $l_0 = 0.1$, $e_0 = 2$, $\nu = 0.05$, $q_0 = 0.5$, $p_s = 3$, and $R = 0.5$. The saturable absorber and output coupler are after the anomalous GVD segment. (c) Poincare map taken in the middle of the anomalous dispersion segment. (d) Intra-map evolutions of the RMS pulse duration and chirp parameter once steady state evolution is reached.

determine the overall action. In many optical systems it is necessary to have some form of saturable absorber that attenuates low intensities while passing high intensities. This has been used to "clean up" high intensity pulses by attenuating unwanted noise in communications systems or to initiate pulse formation in mode-locked lasers. In the case of a fast saturable absorber, the self-amplitude modulation induced on the pulse follows the intensity profile of the pulse itself. In this limit a generic nonlinear transfer function of the form [33,269]

$$u_f(t) = \left[1 - \frac{q_0}{1 + |u_i(t)|^2/p_s}\right] \times u_i(t), \tag{92}$$

can be used to describe the action of the saturable absorber. Here u_i (u_f) is the input (output) field, q_0 is the unsaturated loss due to the absorber, and $p_s = P_{sat}/P_0$ is the normalized saturation power. Note that this transfer function effectively promotes high intensities while attenuating lower intensities of the pulse. Often it is necessary to output some of the signal in the optical system. The discrete action of the output coupler can be approximated by a simple scalar multiplication of the field

$$u_f(t) = \sqrt{R} \times u_i(t). \tag{93}$$

In this approximation we are assuming that the output coupler is only an amplitude modulation and any phase modulations are assumed to be small, so that the laser output field would be given by $\sqrt{1 - R} \times u_i(z, t)$. Finally, we consider the discrete action of a spectral filter $\hat{A}(\omega)$ on the pulse. Indeed, spectral filtering has been implemented and analysed in dispersion-managed transmissions systems [283–285]. The pulse form is modified in both amplitude and phase and can be written as

$$u_f(t) = \int_{-\infty}^{\infty} \hat{u}_i(\omega) \times \hat{A}(\omega)\ e^{-i\omega t} d\omega, \tag{94}$$

where $\hat{u}(\omega)$ denotes the Fourier transform of $u(t)$. Including all effects of pulse propagation in passive and active fibres as well as the discrete elements of the saturable absorber, output coupler, and spectral filter can describe various optical systems which have a wide variety of pulse solutions and evolutions. As an example, we consider the propagation equations (82)–(84) ($F(x) = 0$) along with the discrete elements (92)–(93). Fig. 22 shows an example of the resulting pulse evolution from numerical simulation consisting of the same symmetric dispersion map as has been considered previously. The piece of normal GVD fibre is a doped fibre segment providing gain. A saturable absorber and output coupler follow the passive segment. The final steady state pulse evolution is obtained from any initial field, including white-noise. Thus the pulse evolution is, in a global sense, the final attracting state. The RMS pulse characteristics evolve in a similar way as to that for typical DM solitons. However, the RMS peak power is largely attenuated after the discrete elements and changes the zero-chirp point away from the centre of each fibre segment. This is to be expected since the presence of the discrete elements effectively breaks the symmetry of the dispersion map. Further, the discrete elements cause the pulse to undergo large changes in its pulse parameters, however the pulse shape remains of Gaussian form. In this limit an extension of the reduced system of Eq. (91) can be used. Indeed, this can be especially useful when considering discrete dissipative elements since all system parameters as well as the geometry of the optical system can lead to a complex multi-parametric problem.

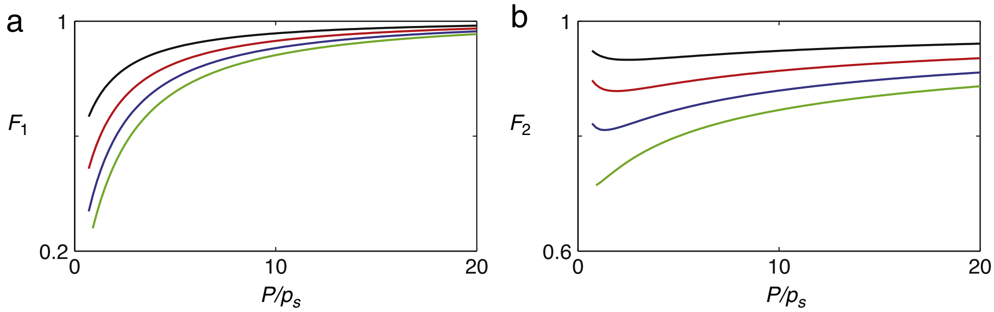

Fig. 23. (a) Peak power and (b) pulse duration response (96) of the discrete saturable absorber for $q_0 = 0.3$ (black), 0.5 (red), 0.7 (blue) and 0.9 (green). (For interpretation of the references to colour in this figure legend, the reader is referred to the web version of this article.)

4.3.1. Extended TM equations with discrete dissipative elements

A simplified model can be used by extending Eq. (91) to include the discrete nature of the dissipative elements. This is possible if each element is assumed not to change the pulse temporal and spectral profile. Using this approximation it is possible to describe large variations in the pulse characteristics per pass through a discrete element. For the Gaussian ansatz (90) considered previously, the pulse characteristics in fibre can be described by Eq. (91) (with $F(x) = 0$) and the transfer functions can be expressed as jump conditions on the pulse parameters $[\tau_i, C_i, P_i] \to [\tau_f, C_f, P_f]$, where the subscript "i" ("f") represents input (output) parameter values. To see how the pulse parameters change due to the saturable absorber transfer function (92), we approximate the function

$$\left[1 - \frac{q_0}{1 + \frac{P_i}{p_s} e^{-\frac{t^2}{\tau_i^2}}}\right] \sqrt{P_i}\, e^{-(1-iC_i)\frac{t^2}{2\tau_i^2}} \sim \sqrt{P_f}\, e^{-(1-iC_f)\frac{t^2}{2\tau_f^2}}. \tag{95}$$

Using a linear least squares fitting routine, we numerically find that the parameters can be mapped using the functions [286]

$$P_f/P_i = F_1(q_0, P_i/p_s), \qquad \tau_f/\tau_i = F_2(q_0, P_i/p_s), \qquad C_f/C_i = \tau_i^2/\tau_f^2, \tag{96}$$

where F_1 and F_2 are shown in Fig. 23. The modulation of P_f is independent of the input pulse duration τ_i, where the output pulse duration depends linearly on the input duration. Further, under this approximation the saturable absorber is only an amplitude modulator and changes the chirp parameter only due to the change in pulse duration. The simple form of the output coupler (93) translates only to a scalar multiplication of the peak power

$$P_f = R \times P_i. \tag{97}$$

In general the application of a discrete spectral filter will cause modulation in both the amplitude and phase parameters. Indeed, it can cause a significant change in the pulse shape depending on the particular shape and characteristics of the input pulse and filter. To gain insight into the action of the spectral filter on a pulse, we assume a Gaussian profile for the spectral filter $\hat{A}(\omega) = \exp(-\omega^2/(2\Omega_F^2))$ so that the integral (94) can be calculated analytically for a chirped Gaussian pulse (90). Taking the Fourier transform of (90), multiplying by $\hat{A}(\omega)$ and integrating, we obtain a Gaussian pulse with modified parameters

$$P_f = \sqrt{\frac{1 + C_i^2}{a^2 + C_i^2}} \times P_i, \qquad \tau_f = \sqrt{\frac{a^2 + C_i^2}{a(1 + C_i^2)}} \times \tau_i, \qquad C_f = \frac{C_i}{a}, \qquad \Omega_f^2 = \frac{\Omega_i^2}{a} \tag{98}$$

where $\Omega_i^2 = (1 + C_i^2)/(2\tau_i^2)$ and $a = 1 + 2\Omega_i^2/\Omega_F^2$. Note that as $\Omega_F \to \infty$, $a \to 1$ resulting in no modification of the pulse parameters. If the filter bandwidth is less than or comparable to the pulse bandwidth ($1 < a$), the action of the spectral filter will reduce the pulse bandwidth by a factor of $1/\sqrt{a}$. Further, for highly chirped input pulses where $C_i \gg 1$, the action of the spectral filter also reduces the pulse duration by the same factor. This is a similar action as that of an anomalous dispersion fibre and the use of spectral filters to compensate dispersion will be used in this context in the next section.

Fig. 24 shows the comparison of the pulse parameters from the full numerical simulation of Eqs. (82)–(84) shown in Fig. 22 and from solving the reduced system (91) ($Q_1 = Q_2 = 0$) and discrete operations (96)–(97). The initial condition for the reduced model was $[\tau_0, C_0, P_0] = [3,\ 0,\ 0.01]$. As with the reduced model with distributed dissipative elements, it is remarkable how accurately it models the full equation dynamics. It is clear from Fig. 24(a) that similar to conservative DM solitons, the pulse compress twice per cavity round trip and acquires both signs of chirp. The saturable absorber and output coupler reduce the peak power of the pulse, however they only slightly perturb the pulse duration and chirp parameter once the pulse has settled into its stable periodic state. Fig. 24(b) highlights how this is the attracting solution to the Poincare map of the reduced system, and it is in agreement with full numerical simulations. As in the previous section, if we let the absolute

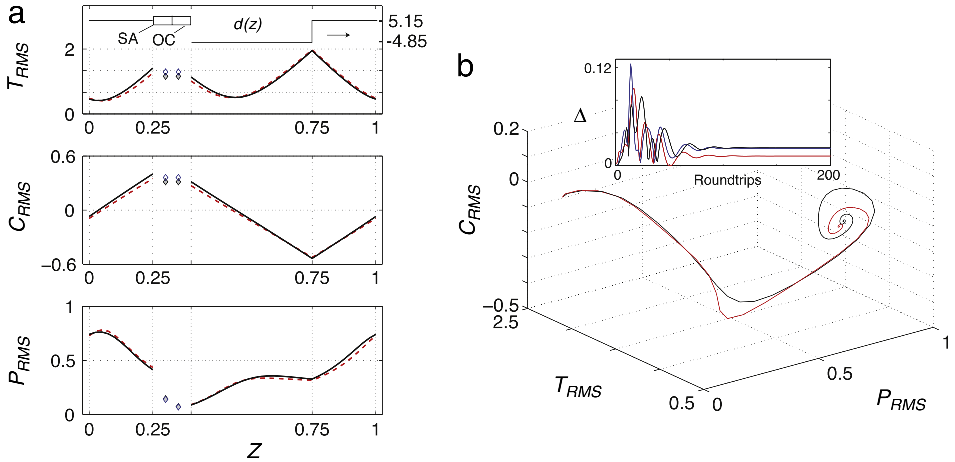

Fig. 24. (a) RMS pulse parameters over one map period once steady state evolution is achieved and (b) Poincare map taken at the point in the middle of the anomalous GVD segment from direct simulation of Eqs. (82)–(84) with discrete actions Eq. (92)–(93) (black) compared with that found from the reduced model equations (91) with discrete transfer functions Eq. (96)–(97) (red). Inset: absolute errors Δ are shown for the RMS pulse parameters T_{RMS} (blue), P_{RMS} (red), and C_{RMS} (black). All parameters are the same as in Fig. 22. (For interpretation of the references to colour in this figure legend, the reader is referred to the web version of this article.)

difference $\Delta = |Q_{RMS}(0) - \tilde{Q}_{RMS}(0)|$, where $Q(0)$ ($\tilde{Q}(0)$) is the RMS pulse parameter found from full numerical simulations (reduced model simulations), we see that $\Delta < 0.12$ for all RMS quantities (Fig. 24(b) inset).

There are many optical systems where a Gaussian pulse form in both the temporal and spectral domains is violated. The reduced model can be used for a wide variety of pulse ansatz, which only varies the coefficients in Eq. (91). However, it is interesting that the Gaussian ansatz used to obtain the reduced model (91) and (96)–(98) does remarkably well in characterizing pulse dynamics even when the pulse is not of Gaussian form. The accuracy of the reduced model in characterizing the pulse evolution allows for one to model such optical systems at a reduced computational price. Specifically, using the reduced system one has to solve the (3×3) system (91) followed by scalar multiplications for the discrete elements per round trip. In contrast, simulations of the full equations (82)–(84) involve solving an $(N \times N)$ system (N large) after discretization (See Section 6). Thus the reduced model has been used in a variety of contexts and has an important practical application in exploring the large parameter space in such optical systems.

4.3.2. Dispersion management via discrete spectral filtering of highly chirped pulses

Using optical fibre with alternating signs of dispersion for dispersion management is a standard method that has been implemented in numerous optical systems. However, the use of anomalous dispersion fibre can generate unwanted instabilities and limit system performance. For instance, the use of anomalous dispersion fibre limits the peak power of the pulse due to severe pulse degradation when the maximum nonlinear phase shift $\phi_{NL}^{\max} \sim 2\pi$. Such instabilities can be avoided in the normal dispersion regime. Pulse propagation in the normal dispersion regime in a passive fibre can be understood from the RMS equation (89) with $d(z) < 0$ and ignoring all dissipative terms. The linear dynamics governs the chirp parameter to negative values, causing the peak power to decrease while the pulse duration increases. Nonlinearity enhances the decrease (to more negative values) in the chirp parameter while increasing the pulse bandwidth. In general, such pulses will have a potentially large nontrivial phase profile across it while avoiding soliton-like instabilities. Pulse propagation in normal dispersion optical fibre has been studied extensively and initial high intensity parabolic pulses were shown to propagate in a self-similar manner without wave-breaking [77]. Indeed, there are many periodic optical systems such as lasers or telecommunications applications where there is incentive to avoid soliton-like instabilities and thus anomalous GVD fibre. In these cases pulse propagation in normal GVD fibre is a plausible solution, however some dispersion compensation is still necessary.

An alternative method to achieve dispersion compensation while avoiding nonlinear penalties is the discrete application of a spectral filter. As mentioned in the previous section, the analytics of a Gaussian filter on a chirped-Gaussian pulse shows the action of the spectral filter on a highly chirped pulse can significantly reduce the pulse bandwidth and the pulse duration if the ratio $\mathcal{B} = \Omega_F^2/\omega^2 < 1$. Thus spectral filtering can provide the necessary effective dispersion compensation for systems that rely on only components with normal GVD. In addition to compensating the pulse duration and bandwidth the spectral filter can also act as a re-shaping mechanism. Since the temporal and spectral shape of an initial pulse in optical fibre is an important characteristic that will determine the pulse evolution, it is important to consider how a spectral filter reshapes certain input pulses. Fig. 25 shows how a highly chirped hyperbolic secant pulse (76) and parabolic pulse (79) is reshaped after the application of a Gaussian filter $\hat{A}(\omega) = \exp(-\omega^2/(2\Omega_F^2))$ as well as a square shaped filter $\hat{A}(\omega) = 1$ for $|\omega| < \sqrt{2\log(2)}\,\Omega_F$, $\hat{A}(\omega) = 0$ otherwise. For small bandwidth ratios $\mathcal{B} \ll 1$ the pulse inherits the shape of the filter. This

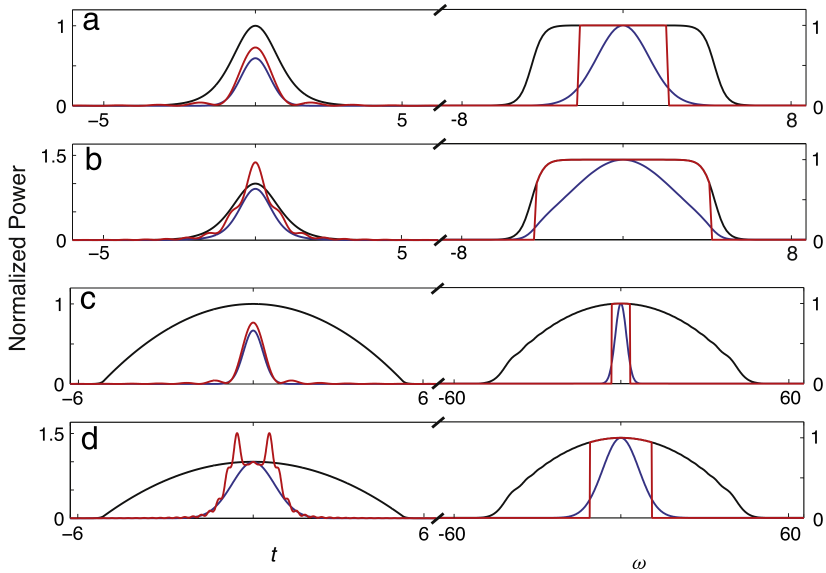

Fig. 25. Normalized temporal and spectral power profiles after the application of a spectral filter. The resultant pulse profiles are obtained from Eq. (94) with a spectral filter of square (red) and Gaussian (blue) shape on initial highly chirped (a, b) hyperbolic secant profile (76) with $P = 1$, $\tau = 2$, and $C = 5$ and (c, d) parabolic profile (79) with $P = 1$, $\tau = 5$, and $C = 5$. The spectral filter bandwidth $\Omega_F = 4$ (a, c), 10 (b, d). (For interpretation of the references to colour in this figure legend, the reader is referred to the web version of this article.)

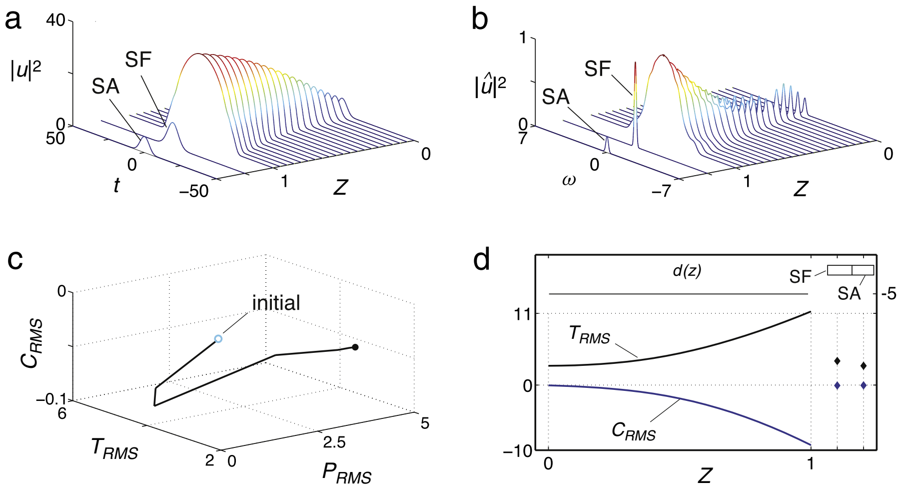

Fig. 26. (a) Temporal and (b) spectral evolution of the power per map period once steady state evolution is achieved from the solution to Eqs. (82)–(84) with discrete actions (92) and (94). Here $F(x) = 0$, $d_2 = -5$, $l_1 = 0$, $\epsilon = 1$, and dissipative parameters $g_0 = 2.5$, $l_0 = 0$, $e_0 = 600$, $\nu = 0$, $q_0 = 0.8$, $p_s = 3$, and $\Omega_F = 0.3$. The spectral filter and saturable absorber follow the normal GVD segment. (c) Poincare map taken in the middle of the anomalous dispersion segment. (d) Intra-map evolutions of the RMS pulse duration and chirp parameter once steady state evolution is reached.

leads to a Gaussian (sinc) temporal power profile for the Gaussian (square) filter (Fig. 25(a), (c)). The mimicry of the filter shape can occur for much larger bandwidth ratios $\mathcal{B}$ for chirped hyperbolic secant pulses than for chirped parabolic pulses due to the flatness of the spectral profile. Although a Gaussian shaped filter usually preserves a high quality temporal pulse shape, a square shaped filter can lead to degraded (Fig. 25(b)) or even non pulse-like temporal profiles (Fig. 25(d)) for $\mathcal{B} \sim 1$. Fig. 25 illustrates how the reshaping of a pulse by a spectral filter primarily depends on the bandwidth ratio parameter $\mathcal{B}$, as well as the shape of the input pulse and spectral filter.

Recently the idea of using a spectral filter for dispersion compensation has been utilized on similariton pulses [287]. To highlight this pulse-shaping mechanism, we look at a series of fibre amplifiers operating at normal dispersion. Following each fibre amplifier is a spectral filter and a saturable absorber. Fig. 26 shows the solution from Eqs. (82)–(84) with discrete operations (92) and (94) once the evolution has reached its steady state from segment to segment. The spectral filter was assumed to have a Gaussian shape $\hat{A}(\omega) = \exp[-\omega^2/(2\Omega_F^2)]$. In the optical fibre the pulse is attracted to its similariton state with parabolic temporal and spectral profiles. Here the bandwidth ratio $\mathcal{B} \ll 1$, so the strong spectral filter significantly

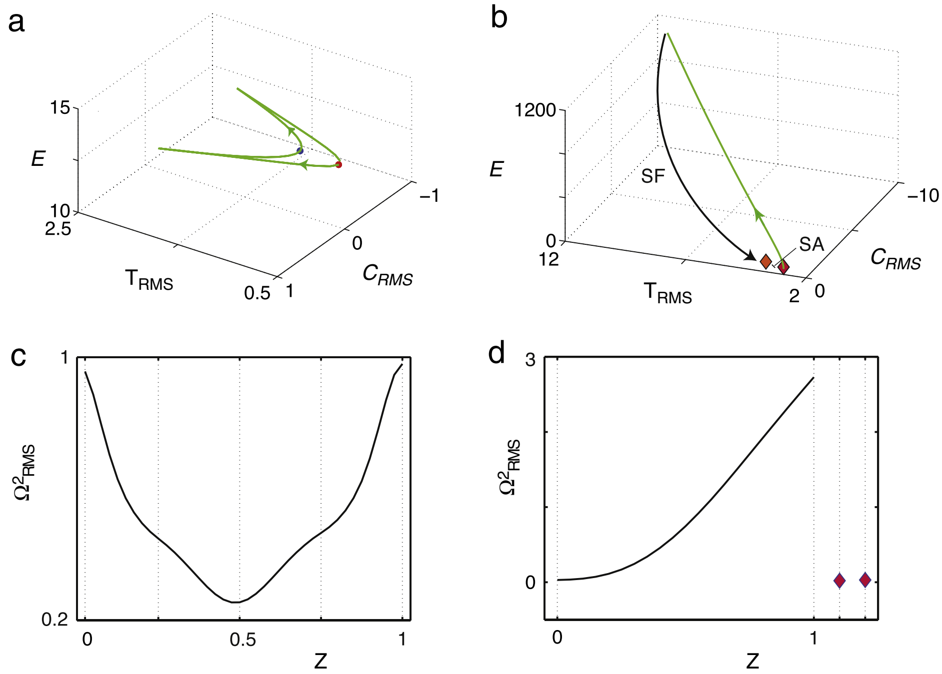

Fig. 27. Pulse RMS quantities energy E, pulse duration T_{RMS}, and chirp parameter C_{RMS} phase plane along with the RMS bandwidth parameter evolution from the data obtained in (a, c) Fig. 17 and (b, d) (a, c) Fig. 26. The RMS parameters are shown over one map period once steady state evolution is obtained.

reduces the pulse duration and bandwidth [287]. Further, the spectral filter shapes the pulse from a parabolic profile to a Gaussian. However, because the similariton state is an attractor in the fibre (see Section 4.1.2), the initial shape of the pulse is not critical. For the parameters used here, the saturable absorber has little influence on pulse propagation and mainly attenuates dispersive radiation generated in the filtering process. A key feature is that this form of dispersion management allows for high peak powers (high energies for the same pulse duration) since a spectral filter avoids nonlinear penalties associated with anomalous dispersion fibre segments.

4.4. *Intra-cavity dynamics of dissipative DM solitons*

Dissipative DM solitons can rely on dissipative processes for dispersion management. This can produce distinctly different intra-map pulse evolutions when compared to its conservative counterparts. Of critical importance is the evolution and sign of the chirp parameter, which drives the pulse dynamics. We can see from Eq. (91) that the sign of $\beta_2 C$ determines if the pulse amplitude and duration increases or decreases. Also from Eq. (91) we see that the evolution of the chirp parameter in optical fibre consists of three important effects: (i) the product of the GVD parameter and the pulse bandwidth; (ii) the product of the nonlinear coefficient and the pulse power; (iii) the product of the ratio of the pulse bandwidth to the gain bandwidth and the chirp parameter. It is the interaction of these terms that determine the intra-map evolution of the pulse parameters. In typical DM soliton pulse evolution, effect (i) (the product of the dispersion and pulse bandwidth) are much larger than other terms, so the slope of the chirp parameter largely depends only on the GVD coefficient. A dispersion map is implemented to compensate the accumulated dispersion and the chirp parameter oscillates between positive and negative values. The pulse stretches and compresses twice per map period, reaches minimum duration in the middle of each segment, and acquires both signs of chirp.

As we have discussed in the previous sections, it is possible not only to compensate dispersion with optical fibre but with bulk elements as well. Although it detracts from an all-fibre format, bulk components such as diffraction gratings, prism pairs, and spectral filters can be used. Often, it is advantageous to use such bulk dispersion compensators to avoid instabilities caused by the fibre medium. For instance, the inclusion of an anomalous GVD segment for dispersion compensation limits the peak power of the pulse, since a large pulse bandwidth is required to obtain an oscillatory chirp parameter. Such large bandwidths leads to spectral pulse splitting and pulse break-up in the temporal domain. However, if only normal dispersion fibre and the appropriate bulk dispersive compensating elements are used then such limitations will be avoided.

Fig. 26 illustrates how a discrete dispersion compensating element such as a spectral filter can be used. The pulse evolution for such systems is distinctly different from typical DM soliton evolution since for these systems the sign of the chirp is always one sign, so the pulse duration and bandwidth increase monotonically in fibre and are compensated at the discrete point. A comparison of the two types of evolution is illustrated in Fig. 27. The pulse RMS quantities per map period once steady state evolution has occurred are shown in a relevant phase plane for the simulations considered in Fig. 17

(Fig. 27(a)) and Fig. 26 (Fig. 27(b)). In Fig. 27(a) the pulse parameters evolve adiabatically since the dispersion compensation is provided by the optical fibre. Due to the chirp parameter changing sign, the pulse bandwidth decreases in the first half of the map and increases in the second half (see Fig. 27(c)). Fig. 27(b) shows the non-adiabatic nature of discrete dispersion compensation. The periodic application of the spectral filter and saturable absorber (once per round trip) actively controls the pulse parameters. After application of the spectral filter, the phase point is moved to the red diamond. The saturable absorber moves the phase point to the blue diamond, where then the solution evolves along the flow line shown. The chirp parameter never changes sign and the pulse bandwidth increases in the optical fibre, only to be compensated by the discrete action of the spectral filter (see Fig. 27(d)). The geometrical picture presented in the phase planes in Fig. 27 gives a way to understand the intra-map pulse evolutions and identify the main differences between continuous and discrete dispersion compensation in such systems.

5. Applications of dispersion management in ultrafast pulsed fibre lasers

As we have seen in this review, dispersion management is a key route for manipulating optical pulses for some desired output in ultra-fast optics. In particular, dispersion management has been extensively used in optical systems that amplify short pulses. For example, in 1985 the concept of chirped pulse amplification (CPA) [288] was proposed to allow ultrashort pulses to be amplified to energy levels previously precluded due to damage threshold in the amplifying medium. A grating pair disperses the input pulse spectrum and temporally stretches the pulse while lowering the peak power, making the pulse safe for amplification. After amplification, a second pair of gratings reverses the dispersion of the first pair, and re-compresses the pulse. CPA is the current state of the art technique for pulse amplification which many high power amplifier and laser systems utilize. Another important example occurs in mode-locked lasers. Dispersion plays a key role in such pulse sources as they can generate pulse durations less than 10 fs. Therefore, dispersion management is particularly important in systems with short optical pulses, e.g. in femtosecond lasers. Femtosecond mode-locked fibre lasers represent a distinctive example of a practical application of the soliton theories providing a constructive impact on laser science and nonlinear physics. Typical femtosecond mode-locked fibre lasers comprise of an active fibre acting as an amplifying medium, a dispersion compensating element (e.g. diffractive grating pairs, passive fibres, etc.) and a saturable absorber element providing pulse formation from initial white-noise and stable mode-locking operation. Femtosecond laser operation is largely determined by the interplay between dispersion and nonlinearity, and these physical effects can be increasingly important when aiming to generate femtosecond pulses with high pulse energies. Indeed, for such oscillators that aim to generate high energy pulses, the pulse undergoes significant temporal and spectral breathing per cavity round trip. The field of high-energy pulse generation from mode-locked fibre lasers is very active, and much of the current state-of-the-art techniques can be found in [151,211,289–306].

Since Kerr-lens mode-locking of Ti:Sapphire lasers was discovered in 1991 [307], novel dispersion compensation methods based on chirped and double chirped mirrors were developed. Currently solid-state mode-locked lasers based on semi-conductor saturable absorber mirrors (SESAM) technologies can produce ultrashort pulses with pulse durations that range from nanosecond to a few femtoseconds with average powers reaching up to 10 μJ, depending on the different laser materials, dispersion, and saturable absorber parameters. Because of their broad output pulse capabilities, ultrafast solid state lasers continue to be the work horse for short pulse generation, and there have been many reviews written on the subject [308–310]. To manage the GVD in such lasers, various bulk optical elements have been used, including prism pairs, grating pairs, dispersion compensating mirrors (DCM) [311], Gires–Tournois interferometer (GTI) mirrors, and slabs. Commercial gratings, DCMs and GTI mirrors are readily available for femtosecond lasers in the near infrared.

Mode-locked fibre lasers have many practical advantages over solid-state lasers such as superior wave-guide properties, reduced thermal effects, power scalability, and integrability with other telecom components. In 1984 the concept of pulse generation using the optical soliton was realized in a laser format to generate pulses from 100 fs to 1 ps depending on the length of the cavity [121]. In 1992 the first all-fibre ring cavity produced stable soliton pulses [312]. This, and many other mode-locked fibre lasers that followed, used an operating wavelength of 1.55 μm where an Erbium-doped fibre was used as an amplifying medium and standard telecom fibres have anomalous dispersion and low loss. Although these lasers were able to produce stable femtosecond pulses, the output pulse characteristics are restricted by fundamental properties of the soliton. Similar to guiding centre solitons in optical communications [82,83], a soliton becomes highly unstable due to side-band instabilities when the period of perturbations approaches $8Z_0$, where $Z_0 = T_0^2/(2|\beta_2|)$ is the soliton period and T_0 is the pulse duration [91]. Because a mode-locked laser periodically perturbs the pulse at the cavity round-trip length L, the shortest soliton that can be supported stably must have $T_0^2 = |\beta_2|L/4$. For a fibre laser composed of standard optical fibre operating at 1.55 μm (where $\beta_2 \sim -0.02$ ps^2/m) of length $L = 1$ m, this restricts the pulse duration to ∼70 fs. If we require 10 fs pulses from the cavity the length of the fibre should be reduced to $L = 2$ cm, which is not very practical. This instability thus imposes a lower limit for the achievable pulse duration with a soliton laser. In addition to this lower bound for the pulse duration, the pulse energy is bounded above due of the delicate balance between dispersion and nonlinearity which gives the soliton area theorem $E_{\text{sol}} = |\beta_2|/(2\gamma T_{\text{sol}})$. Since the pulse duration is typically limited to ∼100 fs due to the aforementioned side-band instabilities, the pulse energy from such lasers is bounded above by ∼0.1 nJ. To eliminate some of the restrictions on the pulse output when using fibre for the waveguide medium, some form of dispersion management can be used. Indeed, recently dispersion management has been a key route in obtaining a broad range of pulse characteristics from mode-locked fibre lasers. Dispersion management in such lasers can be accomplished by the same bulk optics that was used in solid-state lasers, however this increases the cost and size of the system as well as introducing alignment issues. For instance, a typical grating-pair compensator or prism sequence with separation up to 1 metre is required for adequate control of dispersion in a fibre-based cavity. As discussed in previous sections in this review, the development of dispersion compensating fibre allowed for all-fibre dispersion management. Dispersion compensation with optical fibre has also been achieved in lasers by means of chirped fibre Bragg gratings [313–315], photonic crystal fibres [316–318] or solid (hollow) core photonic bandgap fibres [319,320], however, the practical value of these solutions is still to be evaluated.

In the following sections we highlight some examples where dispersion management has been used to provide non-soliton pulse evolution in a mode-locked fibre laser. Our modelling will be based on previously described scalar equations in this review. Specifically, pulse propagation in a rare-earth doped fibre can be modelled with a normalized equation

$$iU_z - \frac{1}{2}\beta_2 U_{tt} + \gamma |U|^2 U = i\Big[(g(z) - \Gamma)U + \frac{g(z)}{\Omega_g^2} U_{tt}\Big], \tag{99}$$

with the saturating gain

$$g(z) = \begin{cases} g_0/\,[1 + E/E_s] & \text{for active fibre,} \\ 0 & \text{for passive fibre.} \end{cases} \tag{100}$$

In addition to fibre propagation, the pulse experiences action induced by the discrete elements such as a saturable absorber, output coupler, and spectral filter in mode-locked fibre lasers. Indeed, it is necessary to have some form of a saturable absorber (intensity discrimination) to promote pulse generation over continuous wave operation. A variety of different saturable absorber mechanisms have been achieved and applied in a fibre based system including, among others, nonlinear polarization rotation [321–325], nonlinear interferometry [326–329], semiconductor saturable absorber (SESAM) [310,330,331], and carbon nanotubes [332,333]. The saturation of an absorber can be described by [33]

$$\frac{dq(t)}{dt} = -\frac{q(t) - q_0}{\tau_A} - \frac{q(t)\,|U(t)|^2}{\tau_A P_s}, \tag{101}$$

where $q(t)$ is the saturable absorber loss coefficient that does not include any nonsaturable losses, $|U(t)|^2$ is the time-dependent power incident on the absorber, q_0 is the modulation depth, P_s is the saturation power and τ_A is the recovery time. By solving Eq. (101) we can determine the saturable absorption $q(t)$ as a function of time and the input field. The output pulse power can then be found from the relation $|U_f|^2(t) = [1 - q(t)]|U_i|^2$, where U_i (U_f) is the input (output) field. In the case of a fast saturable absorber, the absorber recovery time τ_A is much faster than the pulse duration T_0 ($\tau_A/T_0 \ll 1$). Thus, we can assume that the absorption instantaneously follows the absorption of a certain power $|U(t)|^2$ and Eq. (101) reduces to

$$0 = -[q(t) - q_0] - \frac{q(t)\,|U(t)|^2}{P_s} \tag{102}$$

giving a transfer function (92). The discrete action of the output coupler can be approximated by a simple scalar multiplication of the field (93), where we have assumed that any phase modulations caused are small, so that the laser output field would be given by $\sqrt{1-R} \times U_i(z, t)$. Finally, we consider the discrete action of a spectral filter $\hat{A}(\omega)$ on the pulse. The pulse form is modified in both amplitude and phase and can be calculated by Eq. (94). Including all effects of pulse propagation in passive and active fibres as well as the discrete elements of the saturable absorber, output coupler, and spectral filter allows for stable and robust mode-locking in a variety of experimentally realized configurations. Here we use this modelling to describe some relevant dispersion managed laser systems and the various intra-cavity pulse evolutions possible.

5.1. *Stretched pulses in mode-locked fibre lasers*

To overcome the limitations imposed by soliton mode-locking on the pulse width and energy, one can employ positive dispersion in the laser cavity. The earliest attempt minimized pulse shaping in optical fibre by using short lengths of positive dispersion Er^{3+}-doped fibre along with prisms for negative dispersion in a linear cavity [325]. This technique demonstrated pulse durations of 84 fs with 10 pJ of energy, however the laser was not self-starting. Shortly after this, Tamura et al. introduced the stretched-pulse technique, where an all-fibre ring cavity is comprised of segments of alternately large positive and negative dispersion fibre [122]. This technique of dispersion management lead to pulses of 100 fs duration in the negative dispersion segment, leading to a large amount of spreading. In contrast to soliton propagation, the pulse width changed by an order of magnitude within the cavity, which served to lower the average peak power when compared with that of a static transform-limited pulse at the same average dispersion. As with conservative DM solitons, the breathing nature of the intra-cavity pulse effectively reduces the net nonlinear phase shift per pass, allowing for higher energy pulses with larger bandwidths. Further, the alternating dispersion reduces the phase-matched coupling to resonant sidebands giving cleaner spectra with less dispersive radiation between pulses.

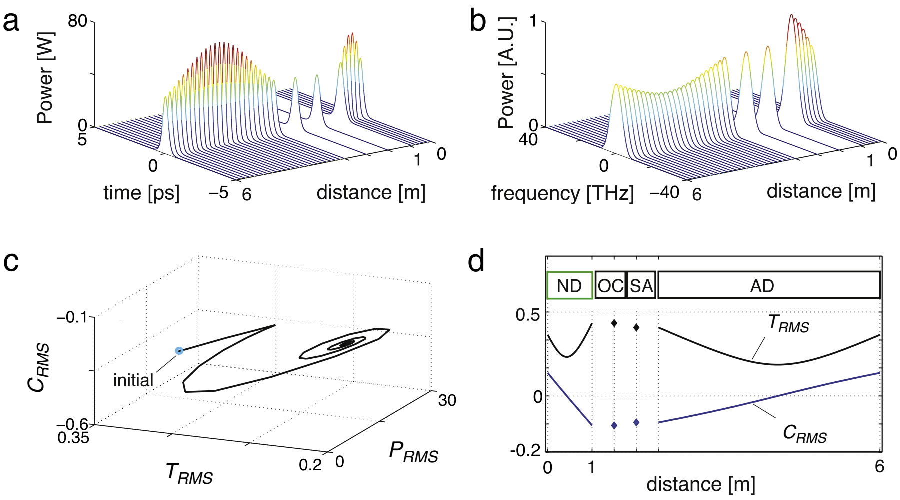

Fig. 28. (a) Temporal and (b) spectral evolution of the power over one round trip once steady state evolution is achieved from the solution to Eqs. (99)–(100) with discrete actions (92) and (93). A doped-fibre with parameters $\beta_2 = 0.1$ ps^2/m, $\gamma = 0.005$ 1/(W m), $g_0 = 2.76$ 1/m (corresponding to 12 dB total gain), $E_s = 1$ pJ, $\Omega_g = 10$ THz, and $L = 1$ m is followed by an output coupler with $R = 0.9$ and a saturable absorber with $q_0 = 0.3$ 1/m and $P_s = 3$ W. The saturable absorber is followed by 5 m of passive fibre with $\beta_2 = -0.022$ ps^2/m and $\gamma = 0.005$ 1/(W m). (c) Poincare map taken at the beginning of the normal dispersion segment. (d) Intra-cavity evolutions of the RMS pulse duration and chirp parameter once steady state evolution is reached.

Variations on this mode-locked laser were done by the group at MIT to obtain higher energy output pulses [123]. These included using the light normally absorbed by the intracavity polarizer as the output to generate pulses with energies greater than 0.5 nJ and pulse durations less than 100 fs after external chirp compensation [334,335] as well as replacing the pump laser with a commercial MOPA to obtain a pulse energy up to 2.25 nJ [336]. Since this work in the mid-1990s, further use of stretched pulse operation for other mode-locked fibre laser systems have been made. For instance, in a fibre laser using a nonlinear optical loop mirror (NOLM) stretched pulse operation produced 100 fs pulses with 1 nJ energy, constituting a 30-fold increase in pulse energy over previously reported femtosecond fibre lasers with a NOLM [329].

Fig. 28 shows an example of the resulting pulse evolution from the numerical simulation of (99)–(100) with discrete actions (92) and (93) for a similar experimental set up as in [122]. The laser consists of 1 m of Er-doped fibre operating at normal dispersion giving ∼12 dB of gain. After the gain segment there is an output coupler and saturable absorber which is then followed by 5 m of negative dispersion passive fibre. The initial condition is white-noise, thus the pulse evolution is the final attracting state. It is clear from Fig. 28(d) that, similar to conventional DM solitons, the pulse compress twice per cavity round trip and acquires both signs of chirp. Indeed, the chirp oscillating between positive and negative values is the hallmark signature of stretched pulse operation. The output coupler and saturable absorber reduce the peak power of the pulse, however they only slightly perturb the pulse duration and chirp parameter once the pulse has settled into its stable periodic state. In such a configuration the output is taken at the end of the gain fibre where the peak power is low and the chirp is large. Since the chirp is largely linear, it can be compressed with an external dispersive delay line composed of fibre, prisms or gratings.

It is interesting that at the same time stretched pulse propagation in mode-locked fibre lasers was being investigated, much attention was being given to DM solitons in optical communications. Obviously they are closely connected, and much of the theory presented for conservative DM solitons can be applied to stretched pulse propagation when the dissipative terms are balanced or much smaller than the conservative components of the system. An analytic theory was developed in the mid-1990s to describe stretched pulse mode-locking that used a distributed GLE with a Taylor series expansion of the saturable absorber and self phase modulation coefficients around the peak of the pulse [136], allowing for chirped Gaussian solutions to be found. This analysis considers the nonlinearity and residual dispersion to be small perturbations, restricting the regime of applicability. Further analytical studies with this model investigated the noise characteristics of such stretched pulse lasers [337,338]. Recently interest has arisen in how dissipative terms can potentially act as a stabilization mechanism to support higher energy pulses with shorter pulse durations in a stretched pulse configuration. It was shown from a distributed GLE equation that stretched pulses with high map strengths can be stabilized by dissipative terms, leading to the potential generation of stable, short pulses with high energy using dispersion management [339]. The intracavity pulse dynamics was described by a reduced model for stretched pulse lasers when a more realistic model with lumped dissipative elements were included [286,340].

5.2. *Spectral filtering ultrashort pulses in lasers operating in the normal dispersion regime*

Solid state lasers were shown to produce highly chirped, relatively long pulses operating in the normal dispersion regime from additive-pulse mode-locked [341] and self-mode-locked Ti:sapphire lasers [307]. These pulses were experimentally characterized with a Kerr-lens mode-locked Ti:sapphire laser and showed that for small positive GVD they had the form of chirped hyperbolic solutions (76) [275]. These pulses relied on the balance of gain dispersion (or filtering) to compensate the broadened bandwidth caused by the normal GVD. In agreement with the analytic theory or mode-locking proposed by Haus et al. [267,268], the pulse energy increased for larger values of (positive) dispersion. This inspired a generation of Kerr-lens mode-locked lasers operating in the positive dispersion regime, able to reach peak powers that exceed several megawatts and pulse energies up to 100 nJ [342]. By using chirped multilayer mirrors to achieve net positive dispersion so-called chirped pulse oscillators generated pulse energies approaching 1 μJ [99,343].

Achieving such operation regimes in a stretched pulse configuration is not possible since such large peak powers will induce soliton-like instabilities such as spectral pulse splitting and pulse break-up in the anomalous GVD segment. Elimination of the anomalous dispersion segment of a fibre laser is only possible if the pulse-shaping is not reliant on the cancellation of phase modulations from GVD and self-phase modulation. Parabolic self-similar pulse propagation in normal GVD fibre was used in a laser resonator in Ref. [344–346]. These lasers largely relied on known propagation in optical fibre operating in the normal GVD regime with the pulse duration increasing and chirp parameter going to zero for reasonable propagation lengths in passive fibre [77]. In Ref. [344,345] the dispersion is compensated for by a linear dispersive delay line and 100 fs pulses with energy as high as 14 nJ were achieved. In Ref. [346] the dispersion is compensated with a grating pair and produces ∼200 fs pulses with 4 nJ energy. The pursuit of higher energy pulses suggested laser cavities with larger positive dispersion, or the elimination of an anomalous GVD segment altogether. A laser without anomalous GVD would presumably have to exploit dissipative processes for some form of dispersion compensation. It has been recently found that this is indeed possible, in a variety of ways. First it was shown that, as in the case of solid-state lasers, so-called ''gain-guided solitons'' existed in an all-normal dispersion laser cavity [347]. These solutions were static solitons and relied on the balance of gain filtering with spectral broadening due to the normal GVD of the fibre. Shortly after this finding, Chong et al. proposed the incorporation of a spectral filter in an all-normal dispersion laser [280]. This was hugely successful in achieving higher energies as these lasers produced pulses with energies above 20 nJ and peak powers greater than 100 kW with standard fibre operating at 1 μm [348]. Recently, in another attempt to eliminate the anomalous GVD segment in a mode-locked fibre laser, a laser cavity that supports amplifier similaritons was been theoretically proposed [287] and experimentally realized [349,350]. Similar to what is observed in Section 4.3.2, this laser relies on strong spectral filtering a similariton pulse generated in a doped fibre operating at normal dispersion.

To highlight the pulse dynamics in a similariton laser, Fig. 29 shows an example of the resulting pulse evolution from numerical simulation of (99)–(100) with discrete actions (92)–(94)) for a similar experimental set up as in [350]. The laser consists of 4 m of Yb-doped fibre operating at normal dispersion at $\lambda_0 = 1$ μm, giving ∼17 dB of gain. In the optical fibre the pulse is attracted to its similariton state with parabolic temporal and spectral profiles. After the gain segment there is an output coupler, spectral filter and saturable absorber. The spectral filter was assumed to have a Gaussian shape $\hat{A}(\omega) = \exp[-\omega^2/(2\Omega_F^2)]$. Since the bandwidth ratio $\Omega_F^2/\Omega_{RMS}^2 \ll 1$, the spectral filter significantly reduces the pulse duration and bandwidth as well as shapes the pulse from a parabolic profile to a Gaussian, as highlighted by the insets in Fig. 29(a), (b). The saturable absorber has little influence on pulse propagation and mainly is needed for the self-starting and attenuation of dispersive radiation generated in the filtering process. Fig. 27(d) shows that the chirp parameter never changes sign and decreases to more negative values in the optical fibre. This causes both the pulse duration and bandwidth to increase, only to be compensated by the discrete action of the spectral filter (see Fig. 27(d)). This is distinctly different from lasers relying on self-similar propagation in passive normal GVD fibre [344] since the bandwidth is able to have huge breathing ratios > 20–40. Since the chirp is largely linear at output, it can be compressed with an external dispersive delay line composed of fibre, prisms or gratings. In this laser configuration there is no anomalous dispersion fibre segment, allowing for high peak powers (6 kW) and large intracavity pulse energies up to 25 nJ. One of the key advantages of using optical fibre is the potential for scalability. Indeed, these fibre lasers relying on all-normal GVD pulse propagation has recently lead to pulse energies approaching 1 μJ by using large-mode-area fibres [351]. An excellent recent review of high-energy femtosecond fibre lasers operating at normal dispersion can be found in Ref. [352]. Recently ultra-wide bandwidth pulse generation has been achieved in similariton mode-locked lasers by including a highly nonlinear fibre in the resonator [353]. This was shown to extend the pulse bandwidth well beyond the gain bandwidth while keeping the chirp of the pulse approximately linear, allowing for significant compression.

Theoretical efforts to describe highly chirped pulse solutions of lasers that consist of all-normal dispersion fibre have been made and are mentioned in Section 4.1.1. Gain-guided solitons are well described by chirped soliton solutions of the CGLE in the normal dispersion regime. Pulse solutions in all-normal dispersion lasers relying on spectral filtering but not on similariton pulse dynamics have been found to resemble an exact solution of the CQGLE [97], or approximate solutions to various Ginzburg–Landau equations in the case of highly-chirped solutions [98–100]. Although these solutions can only represent the average pulse dynamics per cavity round trip, they have had success in describing such oscillators. Indeed, it is surprising that such averaged models capture some of the physical trends since there are typically hundreds of nonlinear lengths ($\phi_{NL} \gg 1$) in the length of the cavity, making the validity of a distributed model a serious question. Investigations into the intra-cavity dynamics due to the spectral filter was initiated, however still relied on a distributed model [281,354]. To obtain a more quantitative agreement with experiment, the intracavity pulse dynamics was described including the discrete nature of the dissipative elements. Analytical results on self-similar mode-locking [340], all-normal dispersion lasers [286], and similariton lasers [287] were obtained.

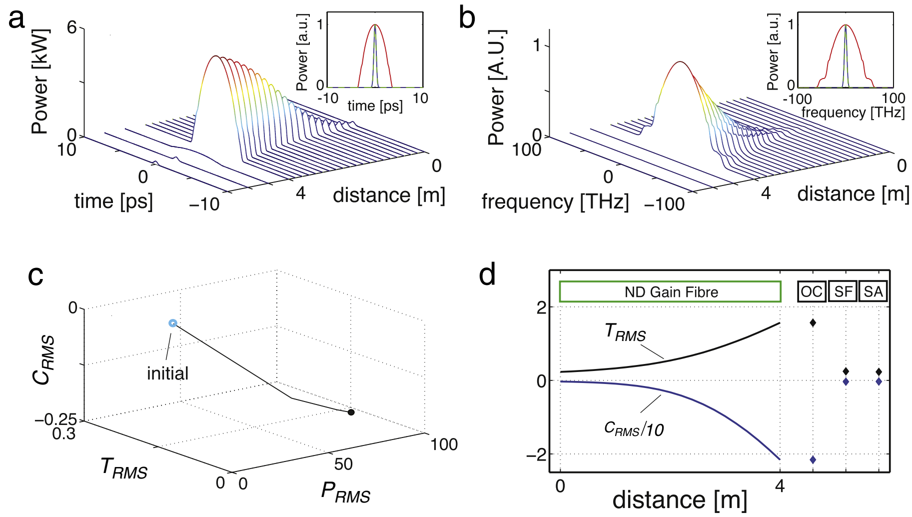

Fig. 29. (a) Temporal and (b) spectral evolution of the power over one round trip once steady state evolution is achieved from the solution to Eqs. (99)–(100) with discrete actions (92)–(94). A doped-fibre with parameters $\beta_2 = 0.025\text{ps}^2/\text{m}$, $\gamma = 0.0047$ 1/(W m), $g_0 = 1$ 1/m (corresponding to 17.37 dB total gain), $E_s = 10$ nJ, $\Omega_g = 100$ THz, and $L = 4$ m is followed by an output coupler with $R = 0.2$, a Gaussian spectral filter with FWHM $10\sqrt{2\log(2)} \sim 11$ THz and a saturable absorber with $q_0 = 0.9$ 1/m and $P_s = 3$ W. (c) Poincare map taken at the beginning of the normal dispersion segment. (d) Intra-cavity evolutions of the RMS pulse duration and chirp parameter once steady state evolution is reached.

5.3. Linear mode-locked fibre laser systems based on SESAMs

Since the development of semiconductor saturable absorber mirrors (SESAMs) [355], they have been widely used for passive mode-locking of many kinds of solid-state and fibre lasers [310,330,356,357]. This is primarily due to the ability to engineer the linear and nonlinear optical properties over a wide range, allowing for more freedom in the specific laser cavity design. The recovery time, saturation fluence, and absorption loss are controllable by proper device design, epitaxial device growth, post-growth heat treatment, or ion implantation. A detailed description and guideline how to design a SESAM for passive mode-locking for different laser parameters is given in recent book chapters [358,359]. Indeed, the ability to tune the design parameters of SESAMs allows them to have many advantages over other saturable absorber methods such as additive pulse mode-locking [360], Kerr-lens mode-locking [307,361], or nonlinear polarization rotation [321,324,325]. Further, exploiting the SESAM as a cavity mirror in a linear laser configuration results in compact size and in environmentally stable devices.

Although first implemented in solid-state mode-locked lasers [330], because of the aforementioned advantages SESAM technology has also been used in mode-locked fibre lasers operating over a broad wavelength range [293,331,362,363]. Understanding how the saturable absorber recovery time and saturation energy of the SESAM in Eq. (101) can effect a particular fibre laser system is important for optimization. A general analysis of the difference between fast and slow saturable absorbers has been examined theoretically and numerically [364]. In addition to the saturable absorber parameters, the operation regimes of mode-locked fibre lasers heavily depends on the dispersion management of the cavity as well. Stretched pulse operation has been obtained in linear SESAM based mode-locked fibre lasers operating with both fast and slow saturable absorbers [362]. Here we discuss numerical modelling results of such a linear laser configuration as shown in Fig. 30 [365]. The cavity consists of an output coupler at one end, followed by a 1.5 m long passive fibre operating at normal dispersion, 0.5 m long active fibre operating at normal dispersion, a grating pair that provides anomalous GVD with negligible nonlinearity, and a SESAM at the other end of the resonator. The pulse propagation in the optical fibre was modelled with Eq. (99)–(100) with an additional third order dispersion term [366]. The parameters for the fibre are $\gamma = 0.005$ 1/(W m), $\beta_2 = 0.02$ ps^2/m and $\beta_3 = 5 \times 10^{-5}$ ps^3/m. The active fibre segment has a gain of $g_0 = 5.5$ dB/m, bandwidth of 11.4 THz (corresponding to 40 nm) centred at 1027 nm and gain saturation $E_s = 0.2$ nJ, corresponding to a round trip time of 20 ns and gain saturation power $P_s^{(g)} = 10$ mW. The grating pair was modelled by solving Eq. (99) with $\gamma = g_0 = 0$ and $\Gamma \neq 0$ such that $\beta_2 = -0.046$ ps^2 is the total anomalous GVD provided and the linear losses were below 20%. The total GVD per cavity round trip is anomalous with $\beta_2^{net} = -0.038$ ps^2. The SESAM is modelled by (101) with non-saturable loss of $q_0 = 0.3$, energy saturation $E_{sat} = 0.5$ pJ, and recovery time $\tau_A = 10$ ps. From an initial white noise distribution the attracting state of the laser is a pulse with temporal shape that is well approximated by a Gaussian shape and the spectral profile has sidebands caused by the periodic perturbations in the system, similar to conventional soliton mode-locking. Fig. 30(b)–(e) shows the RMS pulse characteristics (17) over one round trip once stable mode-locking has been achieved. The pulse parameters largely vary per cavity round trip and are heavily influenced by the particular discrete elements. In particular, the dispersion compensation by the grating pair causes the chirp parameter to have both positive

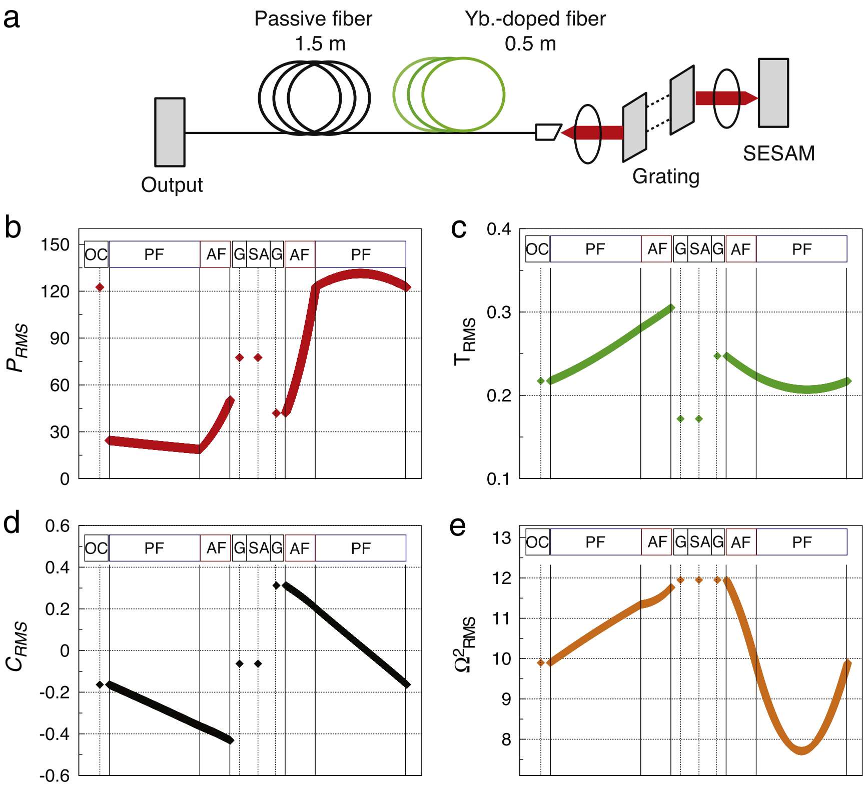

Fig. 30. (a) Linear laser configuration. RMS (a) power, (b) pulse duration, (c) chirp parameter and (d) bandwidth for a typical parameter regime where stable single pulse mode-locking is achieved. OC: output coupler; PF: passive fibre; AF: active fibre; G: grating; SA: saturable absorber (SESAM).

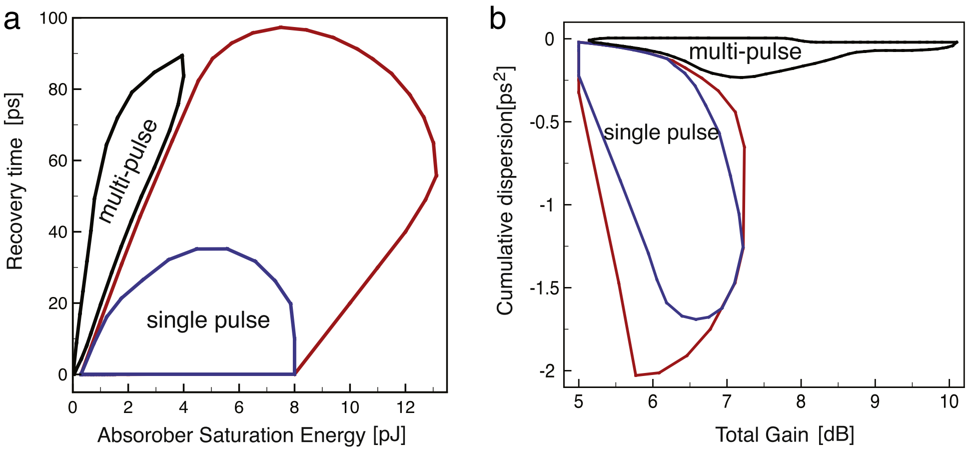

Fig. 31. Regions of stable single and multi-pulse regimes for the laser configuration and parameters shown in Fig. 30 but with SESAM modulation depth $q_0 = 0.1$ and varying (a) SESAM saturation power and recovery time and (b) total gain and cumulative dispersion controlled by the grating pair.

and negative values, making it a typical dispersion managed system. The pulse duration reaches the minimum value at the chirp-free point located at ∼3 m, 1 m after the second pass through the grating pair.

To highlight the role of the SESAM and grating pair, we consider the laser configuration shown in Fig. 30(a) and vary the SESAM parameters, dispersion provided by the grating pair, and total gain around similar values used for stable mode-locking shown in Fig. 30(b)–(e). Fig. 31 shows the results of extensive numerical modelling (with the same equations as in Fig. 30) to determine regimes with stable single and multiple pulse generation. The data generated here is quite extensive and compromises of 1620 (a) and 1770 (b) simulations, each corresponding to a single point in the areas of Fig. 31. The initial field distribution in the laser cavity is white noise and the simulations carried out until the field attains the steady state, which is determined numerically [365]. The curves in Fig. 31 separate regions where a different number of pulses exist in the cavity. The area confined within the red curve corresponds to single pulse generation, while the area confined by the black line corresponds to two and three pulses circulating in the cavity. The area bounded by the blue curve is for single pulse generation with a higher tolerance level on the variation of output parameters to reach steady state [365]. Multiple-pulse regimes are sensitive to initial noise and, consequently, in the same area two and three pulses could be generated depending on particular noise structure in a given trial of mode-locking start-up. Fig. 31(a) shows the pulse regimes for the parameters used in Fig. 30 but with variable SESAM parameters in Eq. (101). We see that a high saturation energy and small recovery time favour single pulse operation. Fig. 31(b) shows the pulse regimes for the parameters used in Fig. 30 but with a variable net dispersion which is achieved by adjusting the dispersion provided by the grating pair, as well as the total gain. We see that stable single-pulse regime exists with net anomalous dispersion with a total gain between 5 and 7.5 dB. Increasing the gain leads to multi-pulse mode-locking for small anomalous dispersion. The resultant pulse dynamics of such a linear mode-locked oscillator is critically controlled by the dispersion the grating pair provides as well as the dissipative parameters of the SESAM. Although we have shown stretched pulse operation here, tuning these parameters allows for different operation regimes to be obtained, as was observed experimentally in a similar laser design [367].

6. Numerical methods

In this section we briefly overview some relevant numerical methods to NLS and dispersion managed NLS systems. Numerical modelling of the field evolution in time or propagation in space in nonlinear dispersive media plays an important role in modern nonlinear science. Numerical experiments support and quite often precede theoretical findings. There are many examples of systems in optics that require intensive numerical modelling. For example, in optical communications systems it is important to simulate the propagation of an initial signal and repeat such simulations many times to take into account certain statistical uncertainties such as noise or other random parameters along the fibre line. Further, for optimization purposes a large number of system parameters should be varied to find the optimal system performance. Direct approaches compute every possible combination of system and signal parameters and select the set of parameters that leads to the best system performance. However, due to the rather long transmission distances and a large bandwidth of the optical signals, such numerical simulations are very time consuming and requires efficient computational algorithms. Much work has been done over the years on the key models considered above, and new numerical techniques have been used to approach the many challenges posed in dispersion managed systems (see, for instance [368]). Here we do not intend to present a comprehensive review of all numerical approaches used in this field, but rather a highlight of some of the key algorithms used in our groups. We first provide an overview of the key numerical methods for solving the NLSE, with details given on the well known split-step Fourier method and finite-difference scheme of a high order accuracy. Next we discuss the numerical algorithm to find solutions to the Gabitov–Turitsyn equations in the spectral domain. We then discuss an algorithm to construct exact DM-soliton solutions and finally we conclude with a discussion on solving periodic boundary value problems for the TM equations.

6.1. Numerical algorithms to solve NLS-type equations

Due to the nonlinear nature of the NLSE, analytic progress can be challenging. Numerical simulations have always played an important role in understanding the behaviour of NLS-type systems, and indeed initial observations of localization came from numerical simulation results themselves [1]. The NLSE has been solved numerically using a number of methods, including the split-step method [369,370], finite-difference schemes [371–378], the finite element method [379–381], the discontinuous Galerkin method [382,383], spline collocation [384,385], split-step finite-difference [386,387], symplectic (spectral and finite difference) methods [388–391], as well as using the various steps of the inverse scattering transform [392]. Efficient numerical routines to solve the NLSE is still an active area of research. A recently developed method to construct an unconditionally stable explicit high-order discretization of the NLSE was proposed in [393]. The technique devised a numerical scheme based on spectral spatial discretization and the extraction of the linear semigroup dependence of the numerical solution which provides unconditional stability along with increased truncation order in z. A comparison with the SSFM was made and showed that the third order semigroup extraction method is more efficient than methods considered in [371]. Often it is important to consider coupled NLS equations (CNLS) [366] for various applications in optical communications, nonlinear optical devices and fibre lasers (especially mode-locked fibre lasers based on nonlinear polarization rotation). A variety of the numerical approaches to solve the CNLS equations, which are similar to the methods used to solve the scalar NLSE, have been proposed, including finite difference schemes [372,394–396], both the Galerkin method [397] and discontinuous Galerkin method [383], parallel split-step Fourier method [398], generalized hyperbolic function transformation method [399], a linearly implicit conservative method [400], multi-symplectic methods [401,402], the Chebyshev spectral collocation method [403], as well as different split-step schemes such as finite difference [387,404].

Among the earliest methods used to solve the NLSE numerically are the split-step and Fourier methods used by Hardin and Tappert [369] and Lake et al. [370]. Taha and Ablowitz [371] made a classical comparative analysis of numerical methods to solve the NLS equation. In their fundamental review they considered a number of different numerical algorithms for solving the nonlinear Schrödinger equation, including the classical explicit (three-level) method, the hopscotch method, the

Please cite this article in press as: S.K. Turitsyn, et al., Dispersion-managed solitons in fibre systems and lasers, Physics Reports (2012), doi:10.1016/j.physrep.2012.09.004

implicit–explicit method, Crank–Nicolson implicit scheme, the Ablowitz–Ladik scheme [405], the split-step Fourier method, and the pseudospectral method. After this work the split-step Fourier method (SSFM) became the mainstream method in nonlinear optics. Here we discuss the SSFM and how it can be used to solve the governing equation for short pulse evolution along a single-mode fibre [406,407]

$$\frac{\partial u}{\partial z} = i\sum_{k=2}^{k_{max}} \frac{i^k}{k!}\mathrm{sgn}(\beta_k)d_k\frac{\partial^k u}{\partial t^k} + \epsilon\left(1+\frac{i}{\omega_0 T_0}\frac{\partial}{\partial t}\right)\left[u\int_0^\infty R(s)\,|u(t-s)|^2 ds\right] + gu. \tag{103}$$

The kernel $R(t)$ accounts for the non-linear response of the optical fibre medium (that can be approximated from the experimental data described in [80,366,406–409]) and contains both electronic and vibrational (Raman) components

$$R(t) = (1-f_R)\,\delta(t) + f_R h_R(t), \tag{104}$$

where $\delta(t)$ is the Dirac delta function and f_R represents the fractional contribution of the delayed Raman response to nonlinear polarization. For instance, in optical fibre $f_R = 0.18$ [406–408]. In general, the Raman response function $h_R(t)$ is rather complex due to the amorphous nature of silica glass and to model it accurately a superposition of a large number of basis functions is required [409,410]. It is more practical and typical, therefore, to slightly sacrifice accuracy by approximating the Raman response by damping oscillations (associated with a single vibrational mode) leading to a Lorentzian-shaped gain spectrum [406]. Eq. (103) is general, including potentially all orders of dispersion as well as a number of nonlinear effects in the second term of the right hand side such as self-phase modulation, cross-phase modulation, modulation instability, stimulated Raman scattering, four-wave mixing, self-steepening and shock wave formation [366]. In the limit $f_R = 0$, $\omega_0 T_0 \to \infty$ (for pulses of width $T_0 > 5$ ps, $\omega_0 T_0 > 200$), and $k_{max} = 2$ we obtain the standard NLSE (2).

In the SSFM the linear operator is computed in the frequency domain, while the nonlinear operator is solved in the time domain. Specifically, consider the evolution equation

$$u_z = (\hat{L} + \hat{N})u, \tag{105}$$

where $\hat{L}$ and $\hat{N}$ are linear and nonlinear operators, respectively. The linear and nonlinear operators typically do not commute with each other as is the case in Eq. (103) where

$$\hat{L} = i\sum_{k=2}^{k_{max}} \frac{i^k}{k!}\mathrm{sign}(\beta_k)d_k\frac{\partial^k}{\partial t^k} + g \tag{106a}$$

$$\hat{N} = \epsilon\left(1+\frac{i}{\omega_0 T_0}\frac{\partial}{\partial t}\right)\left[\int_0^\infty R(s)\,|u(t-s)|^2 ds\right]. \tag{106b}$$

The key idea in the split-step method is to approximate the exact solution of Eq. (105) by solving the purely linear and purely nonlinear equations in a given sequential order, in which the solution of one subproblem is employed as an initial condition for the next subproblem. This may be implemented by using a solution operator $\psi_n(\Delta z)$ that includes an appropriate combination of products of the exponential operators $\exp[\Delta z\hat{L}]$ and $\exp[\int_z^{z+\Delta z}\hat{N}(s)ds]$ [411]. However, this produces a splitting error due to the noncommutativity of $\hat{L}$ and $\hat{N}$ that can be reduced by the Baker–Hausdorff formula [412]. According to the Baker–Hausdorff formula, the first-order solution operator is given by

$$u(z+\Delta z, t) = \psi_1(\Delta z)\times u(z,t), \quad \text{where } \psi_1(\Delta z) = \exp\left(\Delta z\hat{L}\right)\exp\left(\int_z^{z+\Delta z}\hat{N}(s)ds\right). \tag{107}$$

To obtain a second-order method, Eq. (107) is modified by letting $\psi_1(\Delta z) = \psi_2(\Delta z)$, where

$$\psi_2(\Delta z) = \exp\left(\int_z^{z+\Delta z/2}\hat{N}(s)ds\right)\exp\left(\Delta z\hat{L}\right)\exp\left(\int_{z+\Delta z/2}^{z+\Delta z}\hat{N}(s)ds\right). \tag{108}$$

Approximations of higher order can be constructed by a proper composition of the second-order symmetric approximation [413–415]. For example, a fourth-order splitting has the following form [411,413]

$$\psi_4(\Delta z) = \psi_2(\eta\Delta z)\times\psi_2([1-2\eta]\Delta z)\times\psi_2(\eta\Delta z), \tag{109}$$

where $\eta = \left(2+2^{1/3}+2^{-1/3}\right)/3$. In general, the operators $\hat{L}$ and $\hat{N}$ in Eqs. (107)–(109) may be interchanged without affecting the order of the method.

In order to use the schemes presented in Eqs. (107)–(109), we must compute the operators $\hat{L}$ and $\hat{N}$. As mentioned previously, in the SSFM the linear operator is computed in the spectral domain and the nonlinear operator is computed in the time domain. The linear operator $\hat{L}$ can be presented in the Fourier domain

$$\exp\left(\Delta z\hat{L}\right)B(z,t) = \left[\mathcal{F}^{-1}\exp\left(\Delta z\hat{L}(i\omega)\right)\mathcal{F}\right]B(z,t). \tag{110}$$

Here ω is the frequency in the Fourier domain, $\mathcal{F}$ denotes the Fourier transform operation, and $\hat{L}(i\omega)$ is obtained by replacing the differential operator $\partial/\partial t$ by $i\omega$ in Eq. (106). Thus to obtain the linear operator in each propagation step two Fourier transforms are required. The use of the Fast Fourier Transform (FFT) algorithm makes the numerical evaluation the Fourier transforms relatively fast, with $O(N\log N)$ operations needed to be performed, where N is the number of grid points in the time/frequency domain [416]. To calculate nonlinear operator, we must compute the convolution integral term in Eq. (103)

$$N(u,t)=\int_0^{\infty} R(s)\,P(t-s)ds, \tag{111}$$

where $P(t)=|u(t)|^2$ is the signal power. Since integration is performed over an asymmetric domain, the numerical implementation of this integral using the convolution theorem and the FFT is rather complicated and will typically take N^2 operations. A more efficient way to compute the integral arises when we are interested in localized pulses. Specifically, if we assume that the power $P(z,t)$ is localized from $t\in[-a,a]$ (the step size of the time variable is $\Delta t=2a/N$) so that $s\in[0,2a]$, then after discretization $\vec{R}=\{R(t_k)\}$, where $t_k=k\Delta t$, $k=[0,1,\ldots,N]$ and $\vec{P}=\{P(t_j)\}$, where $t_j=j\Delta t$, $j\in[-N/2+1,\ldots,N/2]$. The length of the resulting convolution vector is $2N$ and its first N components are the values of integral (111) at the points $t_j=j\Delta t$, $j\in[-N/2+1,\ldots,N/2]$. Thus the number of operations required for the calculation of the convolution integral $N(u,t)$ is reduced from N^2 operations to $N\log_2 N$ operations [417]. Further reductions in the operation count to compute (111) can be obtained if the function $R(s)$ has a particular functional form. Often the Raman response function $h_R(t)$ in Eq. (104) is assumed to be a damped oscillator of the form [366,406]

$$h_R(t)=\frac{\tau_1^2+\tau_2^2}{\tau_1\tau_2^2}\exp(-t/\tau_2)\sin(t/\tau_1). \tag{112}$$

Here the parameters τ_1 and τ_2 are used as fitting parameters to obtain the best fit of the measured spectrum of the Raman amplification. Commonly used values for optical fibre are $\tau_1=12.2$ fs and $\tau_2=32$ fs along with the fractional contribution in Eq. (104) $f_R=0.18$ [406–408]. Using Eq. (112) in Eq. (104), it is possible to use the so-called recursive algorithm to calculate the nonlinear integral term in Eq. (111) [406,417]. Specifically, it is necessary to compute the integral

$$\tilde{N}(u,t)=\int_0^{\infty}\exp\left(-\frac{s}{\tau_2}\right)\sin\left(\frac{s}{\tau_1}\right)P(t-s)ds. \tag{113}$$

Letting $r=t-s$ and using standard trigonometric formulae it is possible to show that

$$\tilde{N}(P,t)=\exp\Bigl(-\frac{t}{\tau_2}\Bigr)\times\left[\sin\left(\frac{t}{\tau_1}\right)\tilde{N}_1(P,t)-\cos\left(\frac{t}{\tau_1}\right)\tilde{N}_2(P,t)\right], \tag{114}$$

where

$$\tilde{N}_1(P,t)=\int_{-\infty}^{t}\exp\left(\frac{r}{\tau_2}\right)\cos\left(\frac{r}{\tau_1}\right)P(r)dr=\int_{-\infty}^{t}\tilde{n}_1(P,t,r)dr \tag{115a}$$

$$\tilde{N}_2(P,t)=\int_{-\infty}^{t}\exp\left(\frac{r}{\tau_2}\right)\sin\left(\frac{r}{\tau_1}\right)P(r)dr=\int_{-\infty}^{t}\tilde{n}_2(P,t,r)dr. \tag{115b}$$

The calculation of the integrals $\tilde{N}_1$ and $\tilde{N}_2$, and thus the calculation of Eq. (111) can be computed in $\sim N$ operations recursively using

$$\tilde{N}_i(P,t_{j+1})=\tilde{N}_i(P,t_j)+\int_{t_j}^{t_{j+1}}\tilde{n}_i(P,t_{j+1},s)ds, \tag{116}$$

where $t_j=j\Delta t, j\in[-N/2+1,\ldots,N/2]$, $t_j\in[-a,a]$. Here it is possible to use such a recursive scheme since $h_R(t)$ is the product of an exponential and a trigonometric function, and thus the variables can be separated out. For a general function $h_R(t)$, this is typically not possible and one must compute the convolution integral.

As with any numerical method, it is important to understand the accuracy and stability of the SSFM algorithm. Indeed, the step sizes in z and t must be selected carefully to maintain the required accuracy of calculation, depending on the order of the method used. Such accuracy can easily be monitored by, for instance, calculating the conserved quantities such as the system energy (in the absence of dissipative terms). Although since the SSFM is explicit and thus conditionally stable, numerical instabilities are still possible. In a recent study, a numerical instability in the background of a soliton was observed when using the SSFM to solve the NLS equation [418]. The instability was found to be very sensitive to small changes in the numerical grid and the soliton parameters, unlike the instability of most finite-difference schemes. In this example the period of oscillations of the unstable Fourier modes is much smaller than the width of the soliton, thus the principle of "frozen coefficients", in which variable coefficients are treated as locally constant for the purpose of stability analysis, is strongly violated.

Please cite this article in press as: S.K. Turitsyn, et al., Dispersion-managed solitons in fibre systems and lasers, Physics Reports (2012), doi:10.1016/j.physrep.2012.09.004

The SSFM requires two Fourier transforms (for the linear operator) and the calculation of the convolution integral (for the nonlinear operator) for a single discretization step in z. As discussed above, each operation roughly takes $O(N \log N)$ operations, making the SSFM potentially faster by up to two orders than most finite-difference schemes [371]. This quality is mainly responsible for the SSFM being widely used. Improvements in computation speed using the SSFM can be achieved by optimizing the step-size [419] and employing a logarithmic step-size [420], Fourier series analysis and the multi-level method [421,422], predictor–corrector techniques [423], and a fast spectral algorithm using an explicit (implicit) method for the nonlinear (linear operator) [424], among others.

Currently much work is being done to improve the speed of known numerical techniques through parallel computing. Indeed, parallelization is key for many systems that require intense computational efforts. For instance, WDM communications systems require propagation of a wide range of frequencies through optical fibre coupled by nonlinearity. Path-averaged GVD effects cause the optical pulses in distinct WDM channels to move with different group velocities. Consequently, modelling of WDM systems requires a long time interval with a high resolution in the frequencies, leading to a very large number of Fourier modes. Fast parallel algorithms will be the key to realize the so-called technique of nonlinear backward propagation, which will compensate nonlinear transmission impairments for on-chip device implementation in coherent transmission systems. The efficiency of using supercomputers for SSFM has been shown to be limited because parallel algorithms for the one dimensional FFT (contrary to multidimensional FFT) provides only a moderate speed up [425]. For example, one of the leading implementations [426] shows an at best four times acceleration on 16 processor cores with shared memory. Indeed, including more processors can be inefficient as this requires the use of a distributed memory approach (cluster), which has higher latency of nodes interconnection media. The experimental data shows that at harmonics up to 2^{21}, a shared memory approach is more efficient. But for higher harmonics, moderate acceleration can be achieved on a cluster, although scaling would still be far from linear [426]. The parallel implementation of the SSFM was also considered in Ref. [427], and in recent work the implementation of a parallel algorithm [428] for the simulation of dispersion-managed WDM optical fibre systems in the case of weak nonlinearity have linear scalability with the number of computer cores [425].

To take a Fourier transform it is necessary to include all Fourier modes since they are connected with each other nonlocally. Since at any point in the computational domain you need to use information from across the whole domain, using the SSFM to numerically solve systems that require a large number of Fourier modes is not optimal. In addition to SSFM, finite-difference schemes have also been implemented to solve various NLS-type equations [371–378]. In contrast to the SSFM, finite-difference methods are implemented in such a way that it is only necessary to know information about the local, or nearest points. In this way FDM offers the potential for increased computational speed when a large number of modes are present in a parallel format. Here we present an example of a compact implicit finite-difference scheme of order $O(\Delta z^2, \Delta t^4)$ for the one-dimensional NLSE [429]

$$\frac{\partial u}{\partial z} = -i\frac{d}{2}\frac{\partial^2 u}{\partial t^2} + i\gamma f, \quad f = |u|^2 u. \tag{117}$$

In constructing the finite-difference schemes for solving the NLSE, we use the classical schemes for the linear parabolic heat equation, where $d = i\tilde{d}$ and $\gamma = 0$ [430]. Let Δz and Δt be the steps of a uniform grid in z and t respectively, and u_j^n be the solution $u(z, t) = u(n\Delta z, j\Delta t)$. Various difference schemes can be used to provide both stability and accuracy. For example, consider the difference scheme for Eq. (117) with weights α $(0 \le \alpha \le 1)$

$$\frac{u^{n+1} - u^n}{\Delta z} = -i\frac{d}{2}\Lambda(\alpha u^{n+1} + (1-\alpha)u^n) + i\gamma(\alpha f^{n+1} + (1-\alpha)f^n), \quad f = |u|^2 u. \tag{118}$$

The second order differential operator in time Λ is defined such that $\Lambda u^n = (u_{j+1}^n - 2u_j^n + u_{j-1}^n)/(\Delta t^2)$. To understand the stability of a certain finite-difference scheme, it is important to compute the amplification factor to the linear equation $(\gamma = 0)$. Let $u_j^n = \exp[ikt_j]$, where k is the grid wave-number and $t_j = j\Delta t$, and define the amplification factor ρ_k by letting $u_j^{n+1} = \rho_k u_j^n$. Substituting this into the difference equation (118) we obtain

$$\rho_k = \frac{i + r(\alpha - 1)\psi_k}{i + r\alpha\psi_k}, \qquad r = \frac{2d\Delta z}{\Delta t^2}, \qquad \psi_k = \sin^2\left(\frac{k\Delta t}{2}\right). \tag{119}$$

If the square module of the amplification factor is greater than unity ($|\rho_k|^2 > 1$), the finite difference scheme is unstable. In the case of the linear heat equation ($d = i\tilde{d}$), the difference scheme (118) is unconditionally stable for $\alpha \ge 1/2$, and conditionally stable if $\alpha < 1/2$. For the linearized NLSE it is easy to see that the difference scheme is unconditionally stable when $\alpha \ge 1/2$ and absolutely unstable when $\alpha < 1/2$. Two schemes are particularly important, the purely implicit scheme with $\alpha = 1$ and the Crank–Nicolson scheme with $\alpha = 1/2$. The implicit method has the largest margin of stability as $|\rho_k|^2 < 1$, but it is only first order in z. The Crank–Nicolson method is second order in both z and t, however $|\rho_k|^2 = 1$, which means there is no strong stability. In the case of mathematical modelling of ultra-long fibre links or fibre lasers for many round-trip times this stability margin may be insufficient to obtain reliable results. It is possible, however, to overcome this shortcoming by modifying the Crank–Nicolson scheme by adding a term proportional to Δz to the weight α, so that $\alpha = 1/2 + c\Delta z$, where $c > 0$.

Please cite this article in press as: S.K. Turitsyn, et al., Dispersion-managed solitons in fibre systems and lasers, Physics Reports (2012), doi:10.1016/j.physrep.2012.09.004

Table 1
Computation results for the linear problem on a sequence of grids for the Crank–Nicolson (CN) scheme (118) and the modified scheme (120).

nt	nz	δ (CN)	K (CN)	δ (Modified)	K (Modified)
20	20	8.7144-02		1.2963-02	
40	80	2.2095-02	3.94	8.2559-04	15.69
80	320	5.4733-03	4.02	5.1446-05	16.05
160	1280	1.3645-03	4.02	3.2122-06	16.02
320	5120	3.4089-04	4.00	2.0072-07	16.05
640	10480	8.5210-05	4.00	1.2545-08	15.99

Table 2
Computation results for the nonlinear problem on a sequence of grids for the Crank–Nicolson (CN) scheme (118) and the modified scheme (120).

nt	nz	δ (CN)	K (CN)	δ (Modified)	K (Modified)
20	20	1.4643-00		7.6688-01	
40	80	7.1275-01	2.06	6.6585-02	11.52
80	320	2.2153-01	3.22	6.2449-03	10.66
160	1280	7.6367-02	2.90	5.5693-04	11.21
320	5120	2.6835-02	2.85	4.9901-05	11.16
640	10480	9.4732-03	2.83	4.3687-06	11.42

Over the years there have been many implementations of finite-difference schemes to obtain higher order accuracy at roughly the same computational cost as the Crank–Nicolson scheme discussed above. Here we outline one such scheme. Following Ref. [429], taking a specific value of the weight $\alpha = 1/2 - i/(3r)$ and a special form of a right-hand side difference scheme introduced in [430], a higher order ($O(\Delta z^2 + \Delta t^4)$) finite difference scheme of the form

$$\frac{u^{n+1}-u^n}{\Delta z} = -i\frac{d}{2}\Lambda(\alpha u^{n+1} + (1-\alpha)u^n) + i\gamma\left(\frac{f^{n+1}+f^n}{2} + \frac{\Delta t^2}{12}\Lambda f^n\right), \quad f = |u|^2 u \tag{120}$$

was obtained. For this high-order scheme, the amplification factor $\rho_k = [(1-\psi_k/3)i - r/2\psi_k]/[(1-\psi_k/3)i + r/2\psi_k]$ and its modulus, as in the Crank–Nicolson scheme, is exactly equal to 1, giving absolute, but not strong stability. Again it is possible to slightly modify the weight $\alpha = 1/2 + c\Delta z - i/(3r)$ $(c > 0)$ to obtain strong stability since $|\rho_k|^2 = 1 - [2c\Delta z r^2\psi_k^2]/[1 + r^2\alpha^2\psi_k^2] < 1$. It can be shown that the small change in the weight α is equivalent to the addition of an artificial dissipative term $c\Delta z^2 \partial u/\partial z$ in Eq. (117) [429]. Similar finite-difference schemes have been implemented, including a similar scheme in the case when $c = 0$ [431] and a $O(\Delta z^2 + \Delta t^4)$ scheme that requires three points in space and nine points in time [432]. Eq. (120) is an implicit nonlinear scheme, and must be solved iteratively. To obtain the iterations, a simple method of linearization, similar to the two-step procedure used in the predictor–corrector schemes, is done for each fixed layer n on an evolutionary variable z. Specifically, we define the sequence $v_0, v_1, \ldots, v_s$ (s is the iteration number) that will converge to the solution u^{n+1} on the $(n+1)$th layer. After an initial approximation for v_0, one can iterate the linearized equation [429]

$$(iI - \frac{d\alpha\Delta z}{2}\Lambda)\frac{v_{s+1}-u^n}{\Delta z} - \frac{d}{2}\Lambda u^n + \gamma\left(\frac{|v_s|^2 v_s + |u^n|^2 u^n}{2} + \frac{\Delta t^2}{12}\Lambda|u^n|^2u^n\right) = 0, \tag{121}$$

to obtain the series $v_0, v_1, \ldots, v_s$ until $|v_s - v_{s-1}| < \varepsilon$, where $\varepsilon \sim 10^{-8}$ is the tolerance level chosen. In the linearized equation (121), I is the identity matrix, and it is obtained by letting $u^{n+1} = v_{s+1}$ and $f^{n+1} = |v_s|^2 v_s$ in Eq. (120).

To test the order of both the Crank–Nicolson scheme (118) with $\alpha = 1/2 + c\Delta z$ and the modified scheme (120) discussed above, we calculate the numerical solution of Eq. (117) in two limits where exact solutions $u_e(z,t)$ are known. We decrease the step size by 1/2 in both t and z and calculate the global C-norm error of the numerical solution $\delta = \max|u_j^n - u_e(z_n, t_j)|$ for the schemes. This error will obviously depend on the step size $\delta = \delta(\Delta t)$, and can be used to calculate the order of the method (here we focus on the order of the method in the time variable). Specifically, by assuming a power law $\delta \sim \Delta t^p$, where p is the order of the method, we can calculate $K = \delta(\Delta t)/\delta(\Delta t/2) = 2^p$, giving us the order p. In the linear limit $(\gamma = 0)$ when $d = -1$ there is an exact solution $u_e(z,t) = P_0\exp[-t^2/(2w)]/\sqrt{w}$, where $w = P_0^2 - idz$ and $P_0 = 1.8$. Table 1 shows the numerical simulation results where the domain was $(0 \le z \le 10) \times (-5 \le t \le 5)$ and the artificial parameter $c = 0.01$. The K values confirm that the Crank–Nicolson scheme is second order ($K \sim 4$, $p = 2$) while the modified scheme (120) is fourth order accurate ($K \sim 16$, $p = 4$). To test the scheme for a nonlinear problem, we choose the parameters $d = -1$ and $\gamma = 1$ in Eq. (117), which has an exact soliton solution $u_e(z,t) = \mathrm{sech}(t)\exp[iz/2]$. For the iterative solution to the linear equation (121), iterations were carried out with a chosen tolerance $\varepsilon = 10^{-8}$ and an upper limit of 8 iterations. Table 2 shows the numerical simulation results where the domain was $(0 \le z \le 4\pi) \times (-10 \le t \le 10)$ and the artificial parameter $c = 0.01$. The K parameter again shows reasonable agreement to the theoretically calculated orders of convergence for both finite difference schemes, and certainly highlights the higher accuracy of the modified method. In addition to numerical error due to the step size of the grid in t and z, we can also expect numerical error due to the artificial

Please cite this article in press as: S.K. Turitsyn, et al., Dispersion-managed solitons in fibre systems and lasers, Physics Reports (2012), doi:10.1016/j.physrep.2012.09.004

Table 3
The calculated error for various values of artificial dissipative parameter c for two different grids using the modified scheme (120) on the nonlinear NLSE with soliton solution.

c	0.0	0.0001	0.001	0.01	0.1
grid 320 × 1280	0.0444	0.0440	0.0399	0.0021	0.4057
grid 640 × 2360	0.0105	0.0103	0.0087	0.0081	0.1763

dissipative parameter c. To quantify the error caused by this term, we solved the same nonlinear problem as that in Table 2 where the domain was $(0 \le z \le 20\pi) \times (-10 \le t \le 10)$ for two different grids and various values of the parameter c with the modified scheme. Table 3 shows that the error decreases as c is increased from zero, and reaches a minimum at some point $c < 0.1$. Indeed, it has been numerically established that in all calculations the best value of the coefficient of the artificial dissipation is in the range from $0.001 \le c \le 0.01$. The numerical simulation results shown show that indeed the finite-difference scheme is second order in z and fourth order in t in both the linear and nonlinear regimes. Indeed, the addition of a small amount of dissipation makes this scheme unconditionally stable, however the amount of error increases for large values of the artificial dissipative parameter. This method can provide a high accuracy at a reduced computational cost since it only uses a small number of local points, and can be useful in modelling physical systems that require many Fourier modes.

6.2. Numerical algorithm to solve the Gabitov–Turitsyn equations

In this section we describe the numerical algorithm that allows us to find DM soliton solutions of the path-averaged equation (61) [433]

$$i\frac{\partial\hat{\varphi}}{\partial z} = \langle d\rangle\,\omega^2\,\hat{\varphi} - \epsilon\int T_{\omega 123}\,\delta(\omega+\omega_1-\omega_2-\omega_3)\,\hat{\varphi}_1^*\,\hat{\varphi}_2\,\hat{\varphi}_3\,d\omega_1 d\omega_2 d\omega_3, \tag{122}$$

where $T_{\omega 123} = T_{\omega 123}(\Delta\Omega)$ is defined in Eq. (60c). Similar to the well-studied NLSE (T is a constant), we seek a soliton solution of in the form $\hat{\varphi}(z,\omega) = \Psi(\omega)\exp(i\lambda^2 z)$, giving

$$[\lambda^2 + \langle d\rangle\omega^2]\Psi = \epsilon\int T_{\omega 123}\delta(\omega+\omega_1-\omega_2-\omega_3)\Psi_1^*\Psi_2\Psi_3 d\omega_1 d\omega_2 d\omega_3 \equiv F(\Psi,\omega). \tag{123}$$

It was shown that if $G(z,\omega) = 1/(\lambda^2 + \langle d\rangle\omega^2)$ and

$$S_1 = \int |\Psi(\omega)|^2 d\omega \qquad S_2(z) = \left|\int \Psi^*(\omega)G(z,\omega)F(\Psi,\omega)d\omega\right|, \tag{124}$$

Eq. (123) can be solved by iteration of the form [434,435]

$$\Psi^{n+1}(\omega) = \left(\frac{S_1}{S_2^n}\right)^{\alpha} G^n(z,\omega)F(\Psi^n,\omega). \tag{125}$$

For convergence of the iterative routine the parameter $1 < \alpha < 2$ (typically $\alpha = 3/2$). This method was originally proposed by Petviashvili [434,435] for conventional soliton solutions and was applied to DM soliton systems [149,436].

In each iteration in the method proposed by Petviashvili the integral term $F(\Psi,\omega)$ must be computed. After a simple integration utilizing the delta function ($\omega_3 = \omega + \omega_1 - \omega_2$),

$$F(\Psi,\omega) = \int_{-\infty}^{+\infty}\int_{-\infty}^{+\infty} T(\Delta\Omega)\Psi^*(\omega_1)\Psi(\omega_2)\Psi(\omega+\omega_1-\omega_2)d\omega_1 d\omega_2\,. \tag{126}$$

Thus computing $F(\Psi,\omega)$ involves a double integration, generally requiring $O(N^3)$ operations, where N is a number of grid points in the time/frequency domain. We assume that the solution is localized in the interval $[-a,a]$. Then $\omega,\omega_1,\omega_2 \in [-a,a]$ and $\Delta\Omega = \omega^2+\omega_1^2-\omega_2^2-\omega_3^2 = 2(\omega_2-\omega)(\omega_1-\omega_2) \in [-2a^2, 2a^2]$. Here we apply a numerical algorithm that relies on an approximation of the matrix element $T(\Delta\Omega)$ using both polynomial and trigonometric expansions. This approximation allows us to apply a fast computation of convolutions and to reduce a number of operations to $M\,N\log_2(N)$, where M depends on the approximation of $T(\Delta\Omega)$.

First let us approximate the matrix element T by a polynomial expansion

$$T(\Delta\Omega) = \sum_{j=0}^{s} a_j(\Delta\Omega)^j \tag{127}$$

so that

$$F(\Psi,\omega)=\sum_{j=0}^{s}a_j2^j\int_{-\infty}^{+\infty}\int_{-\infty}^{+\infty}(\omega_1-\omega_2)^j(\omega_2-\omega)^j\Psi^*(\omega_1)\Psi(\omega_2)\Psi(\omega+\omega_1-\omega_2)d\omega_1d\omega_2$$
$$=\sum_{j=0}^{s}a_j2^j\int_{-\infty}^{\infty}\int_{-\infty}^{\infty}x^j(\omega_1-x-\omega)^j\Psi(x+\omega)\Psi^*(\omega_1)\Psi(\omega_1-x)d\omega_1dx$$

where $x=\omega_2-\omega$. Using the binomial theorem $(\omega_1-x-\omega)^j=\sum_{k=0}^{j}C_j^k(-\omega)^{j-k}(\omega_1-x)^k$

$$F(\Psi,\omega)=\sum_{j=0}^{s}a_j2^j\int_{-\infty}^{\infty}x^j\sum_{k=0}^{j}C_j^k(-\omega)^{j-k}\Psi(\omega+x)\left[\int_{-\infty}^{+\infty}(\omega_1-x)^k\Psi(\omega_1-x)\Psi^*(\omega_1)d\omega_1\right]dx.$$

If we let the function $f_k(x)$ be the integral within the square brackets

$$F(\Psi,\omega)=\sum_{j=0}^{s}a_j2^j\sum_{k=0}^{j}C_j^k(-\omega)^{j-k}\int_{-\infty}^{+\infty}x^jf_k(x)\Psi(\omega+x)dx. \tag{128}$$

Since we are dealing with pulse solutions, the convolution integral will take $N\log_2 N$ operations to solve. Considering this, along with the summations the total number of operations it takes to calculate $F(\Psi,\omega)$ is $(s^2N\log_2 N)/2$, which is a significant reduction from the number of operations necessary to solve the original integral (126).

In general, the matrix element of $T(\Delta\Omega)$ can have an oscillatory structure and a polynomial approximation is not appropriate. Oscillating kernels are better approximated with trigonometric functions so that

$$T(\Delta\Omega)=\sum_{n=0}^{M}T_n\exp(it_n\Delta\Omega)\,. \tag{129}$$

Using the symmetrical substitution of variables $\bar{\omega_1}=\omega_2-\omega$ and $\bar{\omega_2}=\omega_1-\omega_2$ along with (129) in Eq. (126) we obtain

$$F(\Psi,\omega)=\int_{-\infty}^{+\infty}\int_{-\infty}^{+\infty}\sum_{n=0}^{M}T_n\exp(it_n\Delta\Omega)\Psi^*(\omega+\bar{\omega}_1+\bar{\omega}_2)\Psi(\omega+\bar{\omega}_1)\Psi(\omega+\bar{\omega}_2)d\bar{\omega}_1d\bar{\omega}_2\,,$$

where $\Delta\Omega=\omega^2+(\omega+\bar{\omega}_1+\bar{\omega}_2)^2-(\omega+\bar{\omega}_1)^2-(\omega+\bar{\omega}_2)^2$. The separation of the integration variables allows us to write

$$F(\Psi,\omega)=\sum_{n=0}^{M}T_ne^{it_n\omega^2}\int_{-\infty}^{+\infty}\int_{-\infty}^{+\infty}\left[e^{-it_n(\omega+\bar{\omega}_1+\bar{\omega}_2)^2}\Psi(\omega+\bar{\omega}_1+\bar{\omega}_2)\right]^*$$
$$\times\left[e^{-it_n(\omega+\bar{\omega}_1)^2}\Psi(\omega+\bar{\omega}_1)\right]\left[e^{-it_n(\omega+\bar{\omega}_2)^2}\Psi(\omega+\bar{\omega}_2)\right]d\bar{\omega}_1d\bar{\omega}_2. \tag{130}$$

Integral (130) can be calculated by successive implementation of the correlation procedures and the sum is over the number of approximating trigonometric functions. It can be shown that to calculate $F(\Psi,\omega)$ it takes $\sim MN\log_2(N)$ operations, where M is number of approximating functions. Thus, as in the case of using a polynomial approximation for $T(\Delta\Omega)$, using trigonometric functions to approximate the kernel also reduces the computational time needed to solve the original integral (126).

6.3. Iterative methods for the construction of exact DM solitons

As discussed above, to obtain exact periodic DM pulse evolution it is necessary to start with the correct initial condition. In Ref. [437], a numerical averaging method (Nijhof's method) for the computation of exact periodic solutions was introduced. The algorithm is as follows [437]:

- Start with an arbitrary field distribution $u(t)=u_0(t)$. For example, $u_0(t)$ could be a Gaussian pulse with approximately the correct parameters.
- Propagate the pulse and calculate the peak power $|u(t)|^2$ at a fixed point in every dispersion map, e.g., in the middle of the anomalous GVD segment.
- Record the field $u_{\min}(t)$ for which the peak power has a minimum and the field $u_{\max}(t)$ where the peak power has a maximum. To know if the peak power has an extremum, it is necessary to look one map period ahead, so that one can put $u_{\min}(t)=u_{\text{last}}$ or $u_{\max}(t)=u_{\text{last}}$.
- Let $u_{\text{last}}=u(t)$ and propagate for another map period, until both $u_{\min}$ and $u_{\max}$ have been found. When both have been found, assuming that both $u_{\min}(t)$ and $u_{\max}(t)$ both have their peaks at $t=0$, create the profile

$$u'(t)=\frac{u_{\min}(0)}{|u_{\min}(0)|}u_{\min}(t)+\frac{u_{\max}(0)}{|u_{\max}(0)|}u_{\max}(t).$$

The profile $u'(t)$ is the combination of $u_{\min}(t)$ and $u_{\max}(t)$ so that their peaks are in phase, effectively leading to the greatest discrimination between the periodic pulse and the background.

- Rescale $u'(t)$ so that the new field energy has the same energy as the original field

$$u_{\text{new}}(t) = u'(t) \times \sqrt{\frac{\int |u_0(t)|^2 dt}{\int |u'(t)|^2 dt}}.$$

- Restart the procedure with $u_0(t) = u_{\text{new}}(t)$, until the solution has converged sufficiently.

In general, this procedure leads rapidly to an exactly periodic solution unless the nonlinearity is too small (in which case convergence takes longer) or too large (in which case the procedure may not converge because of instabilities). Variations of the method for finding solutions of fixed energy and fixed pulse width as well as the effects of including fibre loss were considered [437].

An alternative iterative scheme was used to obtain exact periodic DM solitons numerically in Ref. [438]. In this method the initial condition is propagated through one dispersion map period. The output pulse at the end of the dispersion map is, generally, not identical to the input pulse. However, the output pulse can be used to modify the input pulse in the next iteration. Specifically, when the input pulse $u_{\text{in}}(t)$, taken at z = 0, generates an output pulse $u_{\text{out}}(t)$ at the end of the map period, the input for the next iteration is constructed as

$$\tilde{u}_{\text{in}}(t) = C\left[(1-\alpha)\, u_{\text{in}}(t) \exp\left(-i\phi_{in}(0)\right) + \alpha u_{\text{out}}(t) \exp\left(-i\phi_{\text{out}}(0)\right)\right]. \tag{131}$$

Here the re-scaling constant C is chosen in a way to restore the initial pulse energy, $\phi(t)$ is the phase of the pulse which is subtracted from both the input and output pulses at the reference point $t = 0$, and α $(0 < \alpha < 1)$ is a relaxation parameter. Computations using this algorithm are iterated until the output pulse is within some specified numerical tolerance of the input pulse. The difference of the algorithm from the averaging method discussed above [437] is that Eq. (131) includes a simple linear combination of the input and output pulse configurations, rather than those taken at points where the pulse width takes its minimum and maximum values.

6.4. Numerical methods for periodic solutions of the TM equations

As mentioned in the previous sections, it is useful to be able to numerically solve the TM equations (50) or the extended TM equations (91), which are nonlinear ordinary differential equations with periodic boundary conditions, also known as boundary value problems. Such problems arise in all fields of science, and several well known methods have been used to find numerical solutions. These include, among others, finite difference methods [439], direct shooting method (DSM) [440,441], multiple shooting method (MSM) [440–442], collocation method (CM) [443–446], and the discrete orthogonalization method [447]. Provided it converges, the DSM is the fastest, most accurate, and easiest to implement for such problems. However, it is well known that the DSM can fail to converge for problems whose solutions are very sensitive to initial conditions. For such problems, FDM and CM can be more reliable, although such schemes are typically much harder to set up than the shooting methods [441]. The MSM was developed as a compromise between the DSM and the FDM methods, and was capable of keeping the advantages of the DSM while being able to solve a wide variety of problems [442].

Here we give an example of the numerical algorithm that can be used to implement the direct shooting method for solving for the periodic solutions of Eq. (91). This method was used to create solution curves in Fig. 9, with all dissipative terms equal to zero ($g = Q_1 = Q_2 = 0$ in Eq. (91)). In general, the shooting method reduces the boundary value problem to an initial value problem that is solved iteratively, so that

$$G_1(\tau_0, C_0, P_0) = |\tau_0 - \tau(L)| \to 0, \tag{132a}$$

$$G_2(\tau_0, C_0, P_0) = |C_0 - C(L)| \to 0, \tag{132b}$$

$$G_3(\tau_0, C_0, P_0) = |P_0 - P(L)| \to 0. \tag{132c}$$

Here $[\tau(0) = \tau_0,\ C(0) = C_0,\ P(0) = P_0]$ is the initial condition and $[\tau(L),\ C(L),\ P(L)]$ is the solution after solving Eq. (91) over one dispersion map period. The iteration procedure is implemented in the following way:

- Choose initial conditions $[\tau_0,\ C_0,\ P_0]$ and solve for G_1, G_2 and G_3. In general, these initial conditions will not satisfy the periodic boundary conditions so $G_i \neq 0$.
- Calculate the Jacobian matrix J, where row i $(i = 1, 2, 3)$ in this matrix is given by the vector $[\partial G_i/\partial\tau,\ \partial G_i/\partial C,\ \partial G_i/\partial P]$, and the partial derivatives are calculated numerically so that, for instance, $\partial G_i/\partial\tau = [G_i(\tau_0 + \delta X, C_0, P_0) - G_i(\tau_0, C_0, P_0)]/\delta X$, for some chosen $\delta X \sim 10^{-9}$.
- We wish to find perturbations $[\delta\tau,\ \delta C,\ \delta P]$ so that

$$G_1(\tau_0 + \delta\tau, C_0 + \delta C, P_0 + \delta P) = 0, \tag{133a}$$

$$G_2(\tau_0 + \delta\tau, C_0 + \delta C, P_0 + \delta P) = 0, \tag{133b}$$

$$G_3(\tau_0 + \delta\tau, C_0 + \delta C, P_0 + \delta P) = 0. \tag{133c}$$

Eq. (133) can be linearized so that the approximate perturbation can be found by solving

$$J\begin{pmatrix}\delta\tau\\ \delta C\\ \delta P\end{pmatrix} = -\begin{pmatrix}\tau_0\\ C_0\\ P_0\end{pmatrix}. \tag{134}$$

In order to minimize numerical errors when solving Eq. (134), it is useful to replace J by $J \times \delta X$, so that we are solving for the perturbed quantities divided by δX.

- Update the initial condition so that $\tau_0^{\text{new}} = \tau_0 + \delta\tau$, $C_0^{\text{new}} = C_0 + \delta C$, and $P_0^{\text{new}} = P_0 + \delta P$ and solve the initial value problem Eq. (91). If the tolerance condition

$$|\tau_0^{\text{new}} - \tau(L)| + |C_0^{\text{new}} - C(L)| + |P_0^{\text{new}} - P(L)| < \Delta \tag{135}$$

is satisfied, then stop the iterative process. The tolerance parameter Δ is typically chosen at a value between 10^{-6} and 10^{-9}.

In this way, the DSM is a relatively easy way to find periodic solutions to nonlinear ordinary differential equations as in Eq. (91). Convergence and the speed of convergence depends on a variety of factors, including, among others, the initial guess, tolerance levels, as well as sensitivity of the system to slight perturbations in both initial and system parameters. Of course, numerical solutions of boundary value problems have been studied extensively over the years, and here we are not trying to give a comprehensive analysis of all relevant numerical methods, as it is far beyond the scope of this review.

7. Conclusions and future perspectives

Mathematical nonlinear models with periodic modulation of the system parameters occur in a broad range of research problems from solid state physics and optics to biology. The nonlinearity might result into localization of distributed fields leading to appearance of stable dynamical structures that have been encountered in many areas of science and engineering. Propagation of localized nonlinear waves in periodic media with periodic management of parameters, on the one hand, creates rich opportunities for manipulation and control of such waves, but on the other hand gives possibilities for the generation of completely different objects. Periodicity introduces a new spatial or temporal scale (period) compared to similar systems without periodic management. In addition, periodicity of the system changes the interactions between nonlinearity and dispersion (or other linear mechanisms leading to spreading of waves such as diffraction). The balance between nonlinearity and dispersion in nonlinear systems with periodic management is implemented on average over one (or several) period, as opposite to a continuous balance between nonlinearity and dispersion, such as with conventional solitons. This means that stable nonlinear structures can feature natural oscillations (breathing) of the characteristics linked to the periodicity of dispersion or nonlinearity management. Such "breathing" dynamics provide more flexibility in the parameters of stable structures compared to the "rigid" evolution of solitons with a static shape. In the context of ultrashort lasers, there are many similarities between such breathing dynamics with the so-called chirped-pulse amplification (CPA) technique when the ultrashort pulse is not amplified directly, but it is first stretched, then amplified, and only after amplification is re-compressed. The CPA is one example that clearly shows the advantage of having "breathing" or pulsating dynamics of the optical pulse. DM solitons can help to reconcile two apparently conflicting requirements: to achieve high energy (or fluence) and to have minimum peak power (or intensity) to minimize the undesirable nonlinear effects. In general terms, compared to the traditional soliton with a fixed shape and pulse parameters (during evolution), the DM soliton can keep more energy while avoiding possible nonlinear problems with high local intensity.

Though we have presented an overview of dispersion-managed soliton theory focused on the fibre-optic and laser applications, the results and ideas discussed can also be relevant to many other fields of science. In general, many evolutionary nonlinear partial differential equations with periodically varying coefficients possess oscillating localized solutions. We have introduced here a general framework for the analysis of such breather-like solutions in nonlinear systems with periodic variation of parameters. However, fibre-optic contexts and applications are of special interest, both because of a variety of practical applications from signal processing to lasers and due to the fact that most fibre-optic models can be considered one dimensional and, as a consequence, more treatable. Another important property of fibre-optic is the availability of fibres with different dispersion to build various dispersion maps. Remarkable inventions have been made in the designs of the optical fibre waveguide that allow to tailor fibre characteristics—nonlinearity (from very low to very high) and dispersion. Rich opportunities are offered by photonic crystal fibres [448–451] where dispersion can be controlled by design of the fibre medium or by using gas or liquid in the holes in the fibre structure, e.g. in the fibre centre. The technology of microstructure fibres such as index-guided, photonic bandgap and hollow fibres, has reached a mature state and provides a great level of sophistication in dispersion control. The highly practical all-fibre method for dispersion management can be achieved using such new types of fibre. Indeed, recently such fibres have been used in an all-normal dispersion laser to avoid inherent limitations on the pulse bandwidth due to the gain bandwidth [353], allowing for significant compression from such a laser source. There are bright perspectives for achieving amazing control over dispersion in fibre optics with corresponding huge impact on optical transmission, all-optical signal processing and ultra-fast fibre laser technologies. We hope that our review paper will provide some guidance for some emerging applications in these fields and other areas of science dealing with nonlinear systems with periodic modulation of parameters.

Please cite this article in press as: S.K. Turitsyn, et al., Dispersion-managed solitons in fibre systems and lasers, Physics Reports (2012), doi:10.1016/j.physrep.2012.09.004

Acknowledgements

We acknowledge important contributions of our colleagues into the original papers on dispersion-managed solitons and solitons discussed in this review: I. Gabitov, V. K. Mezentsev, E. G. Shapiro, S. Medvedev, N. Doran, T. Shafer, K.H. Spatschek, T. Yang, W. Kath, J. Nijhof, J. N. Kutz, F. W. Wise, E. A. Kuznetsov, Yu. Kivshar, S. Boscolo, E. Turitsyna, O. Schwartz, O. Shtyrina, R. Herda, O. Okhotnikov, A. I. Latkin, A. A. Sysoliatin, S. Musher. Special thanks are due to O. Shtyrina, V. Mezentsev and O. Schwartz for help in preparation and providing some figures. We would also like to acknowledge the financial support of the European Research Council, the EPSRC, the Leverhulme Trust, FP7 Marie Curie project IRSES, the research grant of the Russian Federation Government N11.G34.31.0035 and the grant N11.519.11.4001 of the Ministry of Education and Science of the Russian Federation.

References

[1] N.J. Zabusky, M.D. Kruskal, Interaction of 'solitons' in a collisionless plasma and the recurrence of initial states, Phys. Rev. Lett. 15 (1965) 240–243.
[2] A. Scott, Nonlinear Science. Emergence and Dynamics of Coherent Structures, Oxford University Press, 1999.
[3] V.E. Zakharov, S. Manakov, S.P. Novikov, L.P. Pitaevskii, Theory of Solitons. The Inverse Scattering Method, Plenum, New York, 1984.
[4] A. Newell, Solitons in Mathematics and Physics, SIAM, Philadelphia, 1985.
[5] L. Mollenauer, J.P. Gordon, Solitons in Optical Fibers, Elsevier Academic Press, 2006.
[6] A. Hasegawa, Y. Kodama, Solitons in Optical Communications, Claredon Press, Oxford, 1995.
[7] E. Iannone, F. Matera, A. Mecozzi, M. Settembre, Nonlinear Optical Communication Networks, John Wiley & Sons, 1998.
[8] J.R. Taylor, Optical Solitons: Theory and Experiment, Cambridge Univ. Press, Cambridge, 1992.
[9] N. Akhmediev, A. Ankiewicz (Eds.), Dissipative Solitons, in: Lecture Notes in Physics, vol. 661, Springer, Berlin-Heidelberg, 2005.
[10] N. Akhmediev, A. Ankiewicz (Eds.), Dissipative Solitons: From optics to biology and medicine, in: Lecture Notes in Physics, vol. 751, Springer, Berlin-Heidelberg, 2008.
[11] Y.S. Kivshar, G.P. Agrawal, Optical Solitons: From Fibers to Photonic Crystals, Academic Press, 2003.
[12] M. Ablowitz, H. Segur, Solitons and the Inverse Scattering Transform, SIAM, Philadelphia, 1981.
[13] F. Calogero, A. Degasperis, Spectral Transform and Solitons I, North Holland, Amsterdam, 1982.
[14] M. Ablowitz, P. Clarkson, Solitons, Nonlinear Evolution Equations and Inverse Scattering, Cambridge University Press, 1991.
[15] K. Lonngren, A. Scott (Eds.), Solitons in Action, Academic Press, London, 1978.
[16] R. Dodd, J. Eilbeck, J. Gibbon, H. Morris, Solitons and Nonlinear Waves, Academic Press, London, 1982.
[17] S.E. Trullinger, V.E. Zakharov, V.L. Pokrovsky (Eds.), Solitons, Elsevier Science Publishers, 1986.
[18] B.S. Kerner, V.V. Osipov, Autosolitons, Kluwer Academic Publ, Dordrecht, 1994.
[19] M. Remoissenet, Waves Called Solitons: Concepts and Experiments, Springer-Verlag, Berlin, 1994.
[20] B.A. Malomed, Soliton Management in Periodic Systems, Springer, New York, 2007.
[21] E. Infeld, G. Rowlands, Nonlinear Waves, Solitons and Chaos, Cambridge Univ. Press, Cambridge, 1990.
[22] R. Rajaraman, Solitons and instantons, 1st ed., Elsevier, 1982.
[23] A.M. Kosevich, The Crystal Lattice: Phonons, Solitons, Dislocations, first ed., Wiley-VCH, 1999.
[24] N.S. Manton, P. Sutcliffe, Topological Solitons, first ed., Cambridge University Press, 2004.
[25] Y. Novokshenov, Asymptotic at $t \to \infty$ of the cauchy problem for the nonlinear Schrödinger equation, Dokl. Acad. Nauk SSSR 251 (1980) 799–802.
[26] V. Zakharov, S. Manakov, Theory of resonance interaction of wave packets in nonlinear media, Sov. Phys. JETP 42 (1976) 842–850.
[27] V. Zakharov, A. Mikhailov, Relativistically invariant two dimensional models of field theory which are integrable by means of the inverse scattering problem method, Sov. Phys. JETP 47 (1978) 1017–1027.
[28] L. Alonso, Effect of the radiation component on soliton, Phys. Rev. D 32 (1985) 1459–1466.
[29] E.A. Kuznetsov, A.V. Mikhailov, I.A. Shimokhin, Effect of the radiation component on soliton, Phys. Rev. D 87 (1995) 201–215.
[30] V.L. Ginzburg, L.D. Landau, On the theory of superconductivity, Zh. Eksp. Teor. Fiz (Sov JETP) 20 (1950) 1064–1082.
[31] A. Newell, J. Whitehead, Finite bandwidth, finite amplitude convection, J. Fluid Mech. 38 (1969) 279–303.
[32] W. Eckhaus, Studies in Nonlinear Stability Theory, Springer, Berlin, 1965.
[33] H.A. Haus, Theory of mode-locking with a fast saturable absorber, J. Appl. Phys. 46 (7) (1975) 3049–3058.
[34] A.C. Newell, Envelope equations, in: Lectures in Applied Mathematics, Nonlinear Wave Motion, vol. 15, 1974, pp. 157–194.
[35] I.S. Aranson, L. Kramer, The world of the complex Ginzburg–Landau equation, Rev. Modern Phys. 74 (2002) 99–143.
[36] N. Akhmediev, A. Ankiewicz, Dissipative solitons in the complex Ginzburg–Landau and swift Hohenberg equations, in: N. Akhmediev, A. Ankiewicz (Eds.), Dissipative Solitons, Springer, Berlin, 2005, pp. 1–17.
[37] N.N. Bogoliubov, On the theory of superfluidity, J. Phys. 11 (1) (1947) 23–32.
[38] E.P. Gross, Structure of a quantized vortex in boson systems, Nuovo Cimento 20 (3) (1961) 454–477.
[39] L.P. Pitaevskii, Vortex lines in an imperfect bose gas, Sov. Phys. JETP Lett. 13 (2) (1961) 451–454.
[40] R.Y. Chao, E. Garmire, C.H. Townes, Self-trapping of optical beams, Phys. Rev. Lett. 13 (1964) 479–481.
[41] P.L. Kelly, Self focusing of optical beams, Phys. Rev. Lett. 15 (1965) 1005–1007.
[42] V.I. Talanov, Self focusing of wave beams in nonlinear media, Sov. Phys. JETP Lett. 2 (1965) 138–140.
[43] V.E. Zakharov, Instability of the light self-focusing, Zh. Eksp. Teor. Fiz (Sov JETP) 53 (1967) 1735–1743.
[44] V. Zakharov, Stability of periodic waves of finite amplitude on the surface of deep fluid, Sov. Phys. J. Appl. Mech. Tech. Phys. 4 (1968) 190–194.
[45] A.V. Mikhailov, E.A. Kuznetsov, A.C. Newell, V.E. Zakharov, The nonlinear Schrödinger equation, Physica D 87 (1–4) (1995) 1–300.
[46] V. Zakharov, A. Shabat, Exact theory of two-dimensional self focusing and one dimensional modulation of waves in nonlinear media, Zh. Eksp. Teor. Fiz (Sov. JETP) 61 (1971) 118–134.
[47] A. Hasegawa, F. Tappert, Transmission of stationary nonlinear optical pulses in dispersive dielectric fibers. I. anomalous dispersion, Appl. Phys. Lett. 23 (1973) 142–144.
[48] L. Mollenauer, R. Stolen, J. Gordon, Experimental observation of picosecond pulse narrowing and solitons in optical fibers, Opt. Lett. 45 (1980) 1095–1097.
[49] L. Mollenauer, J.P. Gordon, M.N. Islam, Soliton propagation in long fibers with periodicaly compensated loss, IEEE J. Quantum Electron. QE-22 (1986) 157–173.
[50] L. Mollenauer, S. Evangelides, H. Haus, Long-distance soliton propagation using lumped amplifiers and dispersion-shifted fiber, IEEE J. Lightwave Tech. 9 (1991) 194–197.
[51] M. Nakazawa, K. Suzuki, E. Yamada, H. Kubota, Y. Kimura, M. Takaya, Experimental demonstration of soliton data transmission over unlimited distances with soliton control in time and frequency domains, Electron. Lett. 29 (9) (1993) 729–730.
[52] E.A. Kuznetsov, M.D. Spector, Modulation instability of soliton trains in fiber communication systems, Teoret. Mat. Fiz. 120 (2) (1977) 222–236.
[53] N. Akhiezer, Elements of the theory of elliptic functions, American Mathematical Society, Providence, 1990.
[54] E.A. Kuznetsov, A. Mikhailov, Stability of stationary waves in nonlinear weakly dispersive media, Sov. Phys. JETP 40 (5) (1975) 855–859.
[55] E.A. Kuznetsov, S.K. Turitsyn, Instability and collapse of solitons in media with a defocusing nonlinearity, Sov. Phys. JETP 67 (1988) 1583–1588.

[56] Y.S. Kivshar, Dark solitons in nonlinear optics, IEEE J. Quantum. Electron. 28 (1993) 250–265.
[57] Y.S. Kivshar, B. Luther-Davies, Optical dark solitons: physics and applications, Phys. Rep. 298 (2/3) (1998) 81–197.
[58] L. Gagnon, P. Winternitz, Lie symmetries of a generalized nonlinear Schrödinger equation. i. the symmetry group, J. Phys. A 24 (1988) 1493–1511.
[59] L. Gagnon, Exact traveling-wave solutions for optical models based on the nonlinear cubic–quintic Schrödinger equation, J. Opt. Soc. Am. A 6 (9) (1989) 1477–1483.
[60] L. Gagnon, P. Winternitz, Symmetry classes of variable coefficient nonlinear Schrödinger equations, J. Phys. A 26 (1993) 7061–7076.
[61] A.V. Mikhailov, V.V. Sokolov, A.B. Shabat, The symmetry approach to classification of integrable equations, in: V.E. Zakharov (Ed.), What is Integrability?, Springer Verlag, 1991, pp. 113–184.
[62] J. Satsuma, N. Yajima, Initial value problems of one-dimensional self-modulation of nonlinear waves in dispersive media, Suppl. Progr. Theoret. Phys. 55 (1974) 284–306.
[63] J.M. Dudley, G. Genty, S. Coen, Supercontinuum generation in photonic crystal fiber, Rev. Modern Phys. 78 (4) (2006) 122–147.
[64] S.V. Smirnov, J.D. Ania-Castanon, T.J. Ellingham, S.M. Kobtsev, S. Kukarin, S.K. Turitsyn, Optical spectral broadening and supercontinuum generation in telecom applications, Optic. Fiber Techn. 12 (2) (2006) 122–147.
[65] E.A. Kuznetsov, Solitons in a parametrically unstable plasma, Sov. Phys. - Dokl. 22 (1977) 507–508. Engl. Transl.
[66] T. Kawata, H. Inoue, Inverse scattering method for nonlinear evolution equations under non-vanishing conditions, J. Phys. Soc. Japan 44 (5) (1978) 1722–1729.
[67] Y.C. Ma, The perturbed plane-wave solutions of the cubic Schrödinger equation, Stud. Appl. Math. 60 (1979) 43–58.
[68] N. Akhmediev, V.I. Korneev, Modulation instability and periodic solutions of the nonlinear Schrödinger equation, Theoret. Math. Phys. 69 (1986) 1089–1093.
[69] N. Akhmediev, V. Eleonskii, N. Kulagin, Exact first-order solutions of the nonlinear Schrödinger equation, Theoret. Math. Phys. 72 (1987) 809–818.
[70] A.A. Belavin, A.M. Polyakov, A.S. Schwartz, Y.S. Tyupkin, Pseudoparticle solutions of the Yang–Mills equations, Phys. Lett. B 59 (1975) 85–87.
[71] S. Coleman, Uses of instantons, in: S. Coleman (Ed.), Aspects of Symmetry, Cambridge University Press, Cambridge, 1985, pp. 265–348.
[72] G. Falkovich, I. Kolokolov, V. Lebedev, A. Migdal, Instantons and intermittency, Phys. Rev. E 54 (5) (1996) 4896–4907.
[73] D.H. Peregrine, Water waves, nonlinear Schrödinger equations and their solutions, J. Aust. Math. Soc. Ser. B 25 (1983) 16–43.
[74] N.N. Akhmediev, J. Soto-Crespo, A. Ankiewicz, Extreme waves that appear from nowhere: on the nature of rogue waves, Phys. Lett. A 373 (2009) 2137–2145.
[75] V.I. Shrira, V. Geoigjaev, What makes the peregrine soliton so special as a prototype of freak waves?, J. Eng. Math. 67 (2010) 11–22.
[76] B. Kibler, J. Fatome, C. Finot, G. Millot, F. Dias, G. Genty, N. Akhmediev, J.M. Dudley, The peregrine soliton in nonlinear fibre optics, Nat. Phys. 6 (2010) 790–795.
[77] D. Anderson, M. Desaix, M. Karlsson, M. Lisak, M.L. Quiroga-Teixeiro, Wave-breaking-free pulses in nonlinear-optical fibers, J. Opt. Soc. Am. B 10 (1993) 1185–1190.
[78] E. Desurvire, Erbium-Doped Fiber Amplifiers: Principles and Applications, Wiley Interscience, New York, 1994.
[79] M.J. Connelly, Semiconductor Optical Amplifiers, Springer-Verlag, 2002.
[80] C. Headley, G.P. Agrawal, Raman Amplification in Fiber Optical Communication Systems, Academic Press, 2004.
[81] M.N. Islam (Ed.), Raman Amplifiers for Telecommunications 2: Sub-Systems and Systems, Springer-Verlag, 2004.
[82] A. Hasegawa, Y. Kodama, Guiding-center soliton in optical fibers, Opt. Lett. 15 (1990) 1443–1444.
[83] K. Blow, N. Doran, Average soliton dynamics and the operation of soliton systems with lumped amplifiers, IEEE Photon. Technol. Lett. 3 (1991) 369–379.
[84] A. Hasegawa, Y. Kodama, Guiding-center soliton, Phys. Rev. Lett. 66 (1991) 161–164.
[85] W. Forysiak, N.J. Doran, F.M. Knox, K.J. Blow, Average soliton dynamics and the operation of soliton systems with lumped amplifiers, Opt. Comm. 117 (1–2) (1995) 65–70.
[86] A. Mecozzi, J. Moores, H. Haus, Y. Lai, Soliton transmission control, Opt. Lett. 16 (1991) 1841–1843.
[87] J.N. Elgin, Inverse scattering theory with stochastic initial potentials, Phys. Lett. A 110 (1985) 441–443.
[88] J.P. Gordon, H.A. Haus, Random walk of coherently amplified solitons in optical fiber transmission, Opt. Lett. 11 (1986) 665–666.
[89] J.N. Elgin, Perturbations of optical solitons, Phys. Rev. A 47 (1993) 4331–4341.
[90] J.N. Elgin, Stochastic perturbations of optical solitons, Opt. Lett. 18 (1993) 10–12.
[91] S.M. Kelly, Characteristic sideband instability of periodically amplified average soliton, Electron. Lett. 28 (1992) 806–807.
[92] L.M. Hocking, K. Stewartson, On the nonlinear response of a marginally unstable plane parallel flow to a two-dimensional disturbance, Proc. R. Soc. London Ser. A 326 (1972) 289–313.
[93] N.R. Pereira, L. Stenflo, Nonlinear Schrödinger equation including growth and damping, Phys. Fluids 20 (1977) 1733–1735.
[94] N. Bekki, K. Nozaki, Formations of spatial patterns and holes in the generalized Ginzburg–Landau equation, Phys. Lett. A 110 (1985) 133–135.
[95] A.I. Chernykh, S.K. Turitsyn, Soliton and collapse regimes of pulse generation in passively mode-locking laser systems, Opt. Lett. 20 (4) (1995) 398–400.
[96] L. Kramer, E.A. Kuznetsov, S. Popp, S.K. Turitsyn, Optical pulse collapse in defocusing active medium, JETP Lett. 61 (11) (1995) 904–910.
[97] W.H. Renninger, A. Chong, F.W. Wise, Dissipative solitons in normal dispersion fiber lasers, Phys. Rev. A 77 (2008) 023814.
[98] E. Podivilov, V.L. Kalashnikov, Heavily-chirped solitary pulses in the normal dispersion region: new solutions of the cubic–quintic complex Ginzburg–Landau equation, JETP Lett. 82 (2005) 524–528.
[99] V.L. Kalashnikov, E. Podivilov, A. Chernykh, A. Apolonski, Chirped-pulse oscillators: theory and experiment, Appl. Phys. B 83 (2006) 503–510.
[100] V.L. Kalashnikov, Chirped dissipative solitons of the complex cubic–quintic Ginzburg–Landau equation, Phys. Rev. E 80 (2009) 046606.
[101] V.L. Kalashnikov, A. Apolonski, Chirped-pulse oscillators: a unified standpoint, Phys. Rev. A 79 (2009) 043829.
[102] D.S. Kharenko, O.V. Shtyrina, I.A. Yarutkina, E. Podivilov, M.P. Fedoruk, S.A. Babin, Highly chirped dissipative solitons as a one-parameter family of stable solutions of the cubic–quintic Ginzburg–Landau equation, J. Opt. Soc. Am. B 28 (2011) 2314–2320.
[103] J.M. Soto-Crespo, N.N. Akhmediev, V.V. Afanasjev, Stability of the pulselike solutions of the quintic complex Ginzburg–Landau equation, J. Opt. Soc. Am. B 13 (1996) 1439–1449.
[104] J.M. Soto-Crespo, N.N. Akhmediev, V.V. Afanasjev, S. Wabnitz, Pulse solutions of the cubic–quintic complex Ginzburg–Landau equation in the case of normal dispersion, Phys. Rev. E 55 (1997) 4783–4796.
[105] N. Akhmediev, J.M. Soto-Crespo, M. Grapinet, P. Grelu, Dissipative soliton interactions inside a fiber laser cavity, Opt. Fib. Tech. 11 (2005) 209–228.
[106] W. van Saarloos, P.C. Hohenberg, Fronts, pulses, sources and sinks in generalized complex Ginzburg–Landau equations, Physica D 56 (1992) 303–367.
[107] C. Lin, H. Kogelnik, L. Cohen, Optical-pulse equalization of low-dispersion transmission in single-mode fibers in the 1.3–1.7 μm spectral region, Opt. Lett. 5 (1980) 476–478.
[108] T. Georges, Soliton interaction in dispersion-managed links, JOSA B 15 (1998) 1553–1562.
[109] A. Tonello, A.D. Capobianco, S. Wabnitz, O. Leclerc, B. Dany, E. Pincemin, Stability and optimization of dispersion-managed soliton control, Opt. Lett. 25 (2000) 1496–1498.
[110] S. Wabnitz, F. Neddam, Pulse interactions and collisions in asymmetric higher-order dispersion managed fiber link, Opt. Comm. 183 (2000) 395–405.
[111] L.D. Mouza, E. Seve, H. Mardoyan, S. Wabnitz, S. Sillard, P. Nouchi, High-order dispersion-managed solitons for dense wavelength-division multiplexed transmissions, Opt. Lett. 26 (2001) 1128–1130.
[112] E. Pincemin, D. Hamoir, O. Audouin, S. Wabnitz, Distributed-raman-amplification effect on pulse interactions and collisions in long-haul dispersion-managed soliton transmissions, J. Opt. Soc. Am. B 19 (2002) 973–980.
[113] S. Wabnitz, F. Neddam, Role of intra and inter-channel cross-phase modulation in higher-order fiber dispersion management, Photon. Techn. Lett. 12 (2000) 798–800.

Please cite this article in press as: S.K. Turitsyn, et al., Dispersion-managed solitons in fibre systems and lasers, Physics Reports (2012), doi:10.1016/j.physrep.2012.09.004

[114] F. Knox, W. Forysiak, N. Doran, 10 gbit/s soliton communication systems over standard fibre at 1.55 μm and the use of dispersion compensation, IEEE J. Lightwave Technol. 13 (1994) 1955–1960.
[115] M. Suzuki, I. Morita, N. Edagawa, S. Yamamoto, H. Taga, S. Akiba, Reduction of gordon-haus timing jitter by periodic dispersion compensation in soliton transmission, Electron. Lett. 31 (1995) 2027–2030.
[116] L.F. Mollenauer, J.P. Gordon, P.V. Mamyshev, Solitons in high-bit-rate, long distance transmission, in: I.P. Kaminow, T.L. Koch (Eds.), Optical Fiber Telecommunications, Vol. III A, Academic Press, 1997, pp. (chapter 12, Sec. V–F).
[117] D.L. Guen, F. Favre, M. Moulinard, M. Henry, F. Devaux, T. Georges, 320 gbit/s soliton wdm transmission over 1100 km with 100 km dispersion-compensated spans of standard fibre, ECOC'97, Edinburgh, Post Deadline paper V.5, 1997, 25–30.
[118] T. Hirooka, S. Wabnitz, Stabilization of dispersion managed solitons by nonlinear gain, Electron. Lett. 35 (1999) 665–667.
[119] T. Hirooka, S. Wabnitz, Nonlinear gain control of dispersion-managed soliton amplitude and collisions, Optical Fiber Technol. 6 (2000) 109–121.
[120] S. Vergeles, S. Turitsyn, Optical rogue waves in telecommunication data streams, Phys. Rev. A 83 (2011) 061801(R).
[121] L. Mollenauer, R.H. Stolen, The soliton laser, Opt. Lett. 9 (1984) 13–15.
[122] K. Tamura, E.P. Ippen, H.A. Haus, L.E. Nelson, 77-fs pulse generation from a stretched-pulse mode-locked all-fiber ring laser, Opt. Lett. 18 (1993) 1080–1082.
[123] L.E. Nelson, D.J. Jones, K. Tamura, H.A. Haus, E.P. Ippen, Ultrashort-pulse fiber ring lasers, Appl. Phys. B 65 (1997) 277–294.
[124] J.D. Ania-Castanon, I.O. Nasieva, N. Kurukitkoson, S.K. Turitsyn, C. Borsier, E. Pincemin, Nonlinearity management in fibre transmission systems with hybrid amplification, Opt. Commun. 233 (2004) 353–357.
[125] M. Struwe, Variational Methods, 3rd ed., Springer, 1990.
[126] D. Anderson, Variational approach to nonlinear pulse propagation in optical fibers, Phys. Rev. A 27 (1983) 3135–3145.
[127] B.A. Malomed, Applications of solitons, in: E. Wolf (Ed.), Variational Methods in Nonlinear Fiber Optics and Related Fields, Progress in Optics 43, North Holland, Amsterdam, 2001, pp. 69–191.
[128] S. Turitsyn, E. Shapiro, Variational approach to the design of optical communication systems with dispersion management, Opt. Fiber Technol. 4 (1998) 151–160.
[129] I. Gabitov, S. Turitsyn, Breathing solitons in optical fiber links, JETP Lett. 63 (1996) 863–868.
[130] S. Turitsyn, V. Mezentsev, Dynamics of self-similar dispersion-managed soliton presented in the basis of chirped gauss-hermite functions, JETP Lett. 67 (1998) 640–643.
[131] S.N. Vlasov, V.A. Petrishchev, V.I. Talanov, Averaged description of wave beams in linear media and nonlinear media (the method of moments), Radiophys. Quantum Electron. 14 (1971) 1062–1070.
[132] F.H. Berkshire, J.D. Gibbon, Collapse in the n-dimensional non-linear schrodinger equation — a parallel with Sundman results in the n-body problem, Stud. Appl. Math. 69 (1983) 229–262.
[133] D. Marcuse, Rms width of pulses in nonlinear dispersive fibers, IEEE J. Lightwave Technol. 10 (1992) 17–21.
[134] P. Belanger, N. Belanger, Rms characteristics of pulses in nonlinear dispersive lossy fibers, Opt. Commun. 117 (1995) 56–60.
[135] J.N. Kutz, P. Holmes, S.G. Evangelides, J.P. Gordon, Hamiltonian dynamics of dispersion managed breathers, JOSA B 15 (1998) 87–93.
[136] H. Haus, K. Tamura, L. Nelson, E. Ippen, Stretched-pulse additive pulse mode-locking in fiber ring lasers: theory and experiment, IEEE J. Quantum Electron. 31 (1995) 591–595.
[137] I. Gabitov, S. Turitsyn, Averaged pulse dynamics in a cascaded transmission system with passive dispersion compensation, Opt. Lett. 21 (1996) 327–329.
[138] N. Smith, F. Knox, N. Doran, K. Blow, I. Bennion, Enhanced power solitons in optical fiber transmission line, Electron. Lett. 32 (1996) 54–56.
[139] P. Lushnikov, Oscillating tails of a dispersion-managed soliton, J. Opt. Soc. Am. B 26 (2004) 1535–1537.
[140] T. Georges, B. Charbonnier, Reduction of the dispersive wave in periodically amplified links with initially chirped solitons, IEEE Photon. Techn. Lett. 9 (1997) 127–131.
[141] N. Smith, N. Doran, F. Knox, W. Forysiak, Energy scaling characteristics of solitons in strongly dispersion-managed fibers, Opt. Lett. 21 (1997) 1981–1983.
[142] S. Turitsyn, E. Shapiro, V. Mezentsev, Dispersion-managed solitons and optimization of the dispersion management, Opt. Fiber Techn. 4 (1998) 384–402.
[143] T. Yang, W.L. Kath, S.K. Turitsyn, Optimal dispersion maps for wavelength-division-multiplexed soliton transmission, Opt. Lett. 23 (1998) 597–599.
[144] J. Nijhof, N. Doran, W. Forysiak, F. Knox, Stable soliton-like propagation in dispersion managed systems with net anomalous, zero and normal dispersion, Electron. Lett. 33 (1997) 1726–1728.
[145] M. Wald, I.M. Uzunov, F. Lederer, S. Wabnitz, Optimization of soliton transmissions in dispersion-managed fiber links, Opt. Comm. 145 (1997) 48–52.
[146] J.P. Gordon, L.F. Mollenauer, Scheme for the characterisation of dispersion-managed solitons, Opt. Lett. 24 (1999) 323–325.
[147] G. Bento, F. Neddam, S. Wabnitz, Role of adjacent-pulse overlap in the interaction between dispersion-managed solitons, Opt. Lett. 25 (2000) 144–146.
[148] A. Hasegawa, Y. Kodama, A. Maruta, Recent progress in dispersion-managed soliton transmission technologies, Opt. Fiber Techn. 3 (1997) 197–200.
[149] M. Ablowitz, G. Biondini, Multiscale pulse dynamics in communication systems with strong dispersion management, Opt. Lett. 23 (1998) 384–386.
[150] S. Turitsyn, T. Shafer, K. Spatschek, V. Mezentsev, Path-average theory of chirped dispersion-managed soliton, Opt. Commun. 163 (1999) 122–158.
[151] H.A. Haus, Y. Chen, Dispersion-managed solitons as nonlinear bloch waves, J. Opt. Soc. Am. B 16 (1999) 889–894.
[152] I. Gabitov, E. Shapiro, S. Turitsyn, Optical pulse dynamics in fiber links with dispersion compensation, Opt. Commun. 134 (1996) 317–325.
[153] I. Gabitov, E. Shapiro, S. Turitsyn, Asymptotic breathing pulse in optical transmission systems with dispersion compensation, Phys. Rev. E 55 (1997) 3624–3630.
[154] S. Turitsyn, V. Mezentsev, On the theory of chirped optical soliton in fiber lines with varying dispersion, JETP Lett. 68 (11) (1998) 830–836.
[155] S. Turitsyn, T. Schäfer, V. Mezentsev, Self-similar core and oscillatory tails of a path-averaged chirped dispersion-managed optical pulse, Opt. Lett. 23 (1998) 1351–1353.
[156] S. Wabnitz, I. Uzunov, F. Lederer, Soliton transmission with periodic dispersion compensation: effects of radiation, IEEE Photon. Techn. Letters 8 (1996) 1091–1093.
[157] S.K. Turitsyn, J.H.B. Nijhof, V.K. Mezentsev, N.J. Doran, Symmetries, chirp-free points, and bistability in dispersion-managed fiber lines, Opt. Lett. 24 (1999) 1871–1873.
[158] S.K. Turitsyn, M.P. Fedoruk, T.S. Yang, W.L. Kath, Magic dispersion maps for multi-channel soliton transmission, IEEE J. Quantum Electron. 36 (3) (2000) 290–299.
[159] T. Yang, W.L. Kath, S.K. Turitsyn, The multiple-scale averaging and dynamics of dispersion-managed optical solitons, J. Eng. Math. 36 (1–2) (1999) 163–184.
[160] A. Hasegawa, Y. Kodama, Guiding-center soliton in fibers with periodically varying dispersion, Opt. Lett. 23 (1998) 1385–1387.
[161] J. Kevorkian, J.D. Cole, Perturbation Methods in Applied Mathematics, Springer, New York, 1981.
[162] J.C. Bronski, J.N. Kutz, Guiding-center pulse dynamics in nonreturn-to-zero (return-to-zero) communications systems with mean-zero dispersion, J. Opt. Soc. Am. B 14 (4) (1997) 903–911.
[163] T. Yang, W. Kath, Analysis of enhanced-power solitons in dispersion-managed optical fibers, Opt. Lett. 22 (1997) 985–987.
[164] M. Wald, I. Uzunov, F. Lederer, S. Wabnitz, Optimization of periodically dispersion compensated breathing soliton transmissions, IEEE Photon. Techn. Lett. 9 (1997) 1670–1672.
[165] E. Shapiro, S.K. Turitsyn, Enhanced power breathing soliton in communication systems dispersion management, Phys. Rev. E 56 (1997) R4951–R4955.
[166] E. Shapiro, S.K. Turitsyn, Theory of guiding-center breathing soliton propagation in optical communication systems with strong dispersion management, Opt. Lett. 22 (1997) 1544–1546.

Please cite this article in press as: S.K. Turitsyn, et al., Dispersion-managed solitons in fibre systems and lasers, Physics Reports (2012), doi:10.1016/j.physrep.2012.09.004

[167] S. Turitsyn, T. Schäfer, V.K. Mezentsev, Generalized momentum method to describe high-frequency solitary wave propagation in systems with varying dispersion, Phys. Rev. E 58 (5) (1998) R5264–R5267.
[168] S. Turitsyn, Self-similar dynamics and oscillatory tails of a breathing soliton in systems with varying dispersion, Phys. Rev. E 58 (1998) R1256–R1261.
[169] A. Berntson, N. Doran, W. Forysiak, J. Nijhof, Power dependence of dispersion-managed solitons for anomalous, zero and normal path-average dispersion, Opt. Lett. 23 (1998) 900–902.
[170] J.N. Kutz, S.G. Evangelides, Dispersion managed breathers with average normal dispersion, Opt. Lett. 23 (1998) 685–687.
[171] V.S. Grigoryan, C.R. Menyuk, Dispersion-managed soliton at normal average dispersion, Opt. Lett. 23 (1998) 609–611.
[172] S. Turitsyn, E. Shapiro, Dispersion-managed soliton in optical amplifier transmission systems with zero average dispersion, Opt. Lett. 23 (1996) 682–684.
[173] T. Georges, F. Favre, Transmission systems based on dispersion-managed solitons: Theory and experiment, in: Proc. of II International Symposium on Physics and Applications of Optical Solitons in Fibers, Kyoto, 1997, pp. 2–A–2.
[174] S.K. Turitsyn, E.G. Shapiro, S.B. Medvedev, M.P. Fedoruk, V.K. Mezentsev, Physics and mathematics of dispersion-managed optical solitons, Comptes Rendus Physique, Académie des sciences/Éditions scientifiques et médicales 4 (2003) 145–161.
[175] S. Turitsyn, A. Aceves, C. Jones, V. Zharnitsky, V.K. Mezentsev, Hamiltonian averaging in soliton-bearing systems with periodically varying dispersion, Phys. Rev. E 59 (1999) R3843–R3846.
[176] O.Y. Schwartz, S. Turitsyn, Multiple-period dispersion-managed solitons, Phys. Rev. A 76 (2007) 043819.
[177] T. Lakoba, J. Yang, D.J. Kaup, B.A. Malomed, Conditions for stationary pulse propagation in the string disperison management regime, Opt. Comm. 146 (1998) 366–372.
[178] S. Medvedev, S. Turitsyn, Hamiltonian averaging and integrability in nonlinear systems with periodically varying dispersion, JETP Lett. 69 (7) (1999) 499–506.
[179] V. Zakharov, S. Manakov, On propagation of short pulses in strong dispersion managed optical lines, JETP Lett. 70 (9) (1999) 573–578.
[180] V.E. Zakharov, Propagation of optical pulses in nonlinear systems with varying dispersion, in: V.E. Zakharov, S. Wabnitz (Eds.), Optical Solitons. Theoretical Challenges and Industrial Perspectives, Springer, 1999, pp. 74–89.
[181] S.K. Turitsyn, M. Fedoruk, A. Gornakova, Reduced power optical soliton in fiber lines with short-scale dispersion management, Opt. Lett. 24 (1999) 869–871.
[182] A.F. Evans, Novel fibers for soliton communications, in: Optical Fiber Communication Conference Vol. 2, in: 1998 OSA Technical Digest Series, OSA, Washington, D.C., 1998, p. 22.
[183] I. Gabitov, T. Schäfer, S. Turitsyn, Lie-transform averaging in nonlinear optical transmission systems with strong and rapid periodic variations, Phys. Lett. A 265 (2000) 274–281.
[184] T. Lakoba, D.J. Kaup, Hermite-gaussian expansion for pulse propagation in strongly dispersion managed fibers, Phys. Rev. E 58 (1998) 6728–6732.
[185] A.H. Liang, H. Toda, A. Hasegawa, High-speed soliton transmission in dense periodic fibers, Opt. Lett. 24 (1999) 799–801.
[186] T. Hirooka, T. Nakada, A. Hasegawa, Feasibility of densely dispersion managed soliton transmission at 160 gb/s, IEEE Photon. Tech. Lett. 12 (1999) 633–635.
[187] A.B. Moubissi, K. Nakkeeran, P.T. Dinda, S. Wabnitz, Average dispersion decreasing densely dispersion-managed fiber transmission systems, Photon. Techn. Lett. 14 (2002) 1279–1281.
[188] J. Fatome, S. Pitois, P.T. Dinda, G. Millot, Experimental demonstration of 160-ghz densely dispersion-managed soliton transmission in a single channel over 896 km of commercial fibres, Opt. Express 11 (2003) 1553–1558.
[189] L. Yin, Q. Lin, G.P. Agrawal, Dispersion tailoring and soliton propagation in silicon waveguides, Opt. Lett. 31 (2006) 1295–1297.
[190] S.P. Stark, A. Podlipensky, P.S.J. Russell, Soliton blue-shift in tapered photonic crystal fibers, Phys. Rev. Lett. 106 (2011) 083903.
[191] J.C. Travers, J.M. Stone, A.B. Rulkov, B.A. Cumberland, A.K. George, S.V. Popov, J.C. Knight, J.R. Taylor, Optical pulse compression in dispersion decreasing photonic crystal fiber, Opt. Express 15 (2007) 13203–13211.
[192] A. Kudlinski, A.K. George, J.C. Knight, J.C. Travers, A.B. Rulkov, S.V. Popov, J.R. Taylor, Zero-dispersion wavelength decreasing photonic crystal fibers for ultraviolet-extended supercontinuum generation, Opt. Express 14 (2006) 5715–5722.
[193] J.C. Travers, J.R. Taylor, Soliton trapping of dispersive waves in tapered optical fibers, Opt. Lett. 34 (2009) 115–117.
[194] M.E. Fermann, V.I. Kruglov, B.C. Thomsen, J.M. Dudley, J.D. Harvey, Self-similar propagation and amplification of parabolic pulses in optical fibers, Phys. Rev. Lett. 84 (2000) 6010–6015.
[195] S.K. Turitsyn, S. Boscolo, Dissipative nonlinear structures in fiber optics, in: N. Akhmediev, A. Ankiewicz (Eds.), Dissipative Solitons: From Optics to Biology and Medicine, in: Series: Lecture Notes in Physics, vol. 751, Springer-Verlag, Berlin, Heidelberg, 2008, pp. 195–220.
[196] J.M. Dudley, C. Finot, G. Millot, D.J. Richardson, Self-similarity and scaling phenomena in nonlinear ultrafast optics, Nat. Phys. 3 (2007) 597–603.
[197] T. Hirooka, M. Nakazawa, Parabolic pulse generation by use of a dispersion-decreasing fiber with normal group-velocity dispersion, Opt. Lett. 29 (2004) 498–500.
[198] A.I. Latkin, S.K. Turitsyn, A.A. Sysoliatin, Theory of parabolic pulse generation in tapered fiber, Opt. Lett. 32 (2004) 3313–3315.
[199] P. Emplit, J.P. Hamaide, F. Reynaud, A. Barthelemy, Picosecond steps and dark pulses through nonlinear single mode fibers, Opt. Commun. 62 (1987) 374–381.
[200] D.N. Christodoulides, R.I. Joseph, Vector solitons in birefringent nonlinear dispersive media, Opt. Lett. 13 (1) (1988) 53–55.
[201] Y.S. Kivshar, S.K. Turitsyn, Vector dark solitons, Opt. Lett. 18 (1993) 337–339.
[202] G. Millot, E. Seve, S. Wabnitz, M. Haelterman, Dark-soliton-like pulse train generation from induced modulational polarization instability in a birefringent fiber, Opt. Lett. 23 (1998) 511–513.
[203] Y.J. Chen, J. Atai, Average dark soliton dynamics in periodically dispersion compensated fiber transmission systems, IEEE Photon. Techn. Lett. 10 (9) (1998) 1280–1282.
[204] Y.J. Chen, Dark solitons in dispersion compensated fiber transmission systems, Opt. Commun. 161 (1999) 267–274.
[205] M.J. Ablowitz, Z.H. Musslimani, Dark and gray strong dispersion managed solitons, Phys. Rev. E 67 (2003) R 025601.
[206] M. Stratmann, F. Mitschke, Chains of temporal dark solitons in dispersion-managed fiber, Phys. Rev. E 72 (2005) 066616.
[207] H. Zhang, D.Y. Tang, L.M. Zhao, X. Wu, Dark pulse emission of a fiber laser, Phys. Rev. A 80 (2009) 045803.
[208] C. Finot, Dispersion managed self-similar parabolic pulses, J. Optics A 10 (2008) 085101.
[209] X. Feng, F. Poletti, A. Camerlingo, F. Parmigiani, P. Horak, P. Petropoulos, W.H. Loh, D.J. Richardson, Dispersion-shifted all-solid high index-contrast microstructured optical fiber for nonlinear applications at 1.55 μm, Opt. Express 17 (22) (2009) 20249.
[210] F. Poletti, X. Feng, G.M. Ponzo, M.N. Petrovich, W.H. Loh, D.J. Richardson, All-solid highly nonlinear singlemode fibers with a tailored dispersion profile, Opt. Express 19 (1) (2011) 66–80.
[211] F. Poletti, A. Camerlingo, P. Petropoulos, D.J. Richardson, Dispersion management in highly nonlinear carbon disulfide filled holey fibers, IEEE Photon. Tech. Lett. 20 (17) (2008) 1449–1451.
[212] F. Poletti, K. Furusawa, Z. Yusoff, N.G.R. Broderick, D.J. Richardson, Nonlinear tapered holey fibers with high SBS threshold and controlled dispersion, J. Opt. Soc. Am. B 24 (9) (2007) 2185–2194.
[213] S.P. Stark, F. Biancalana, A. Podlipensky, P.S.J. Russell, Nonlinear wavelength conversion in photonic crystal fibers with three zero dispersion points, Phys. Rev. A 83 (2011) 023808.
[214] A. Sysoliatin, A.K. Senatorov, A.I. Konyukhov, L.A. Melnikov, V.A. Stasyuk, Soliton fission management by dispersion oscillating fiber, Opt. Express 15 (2007) 16302–16307.
[215] M. Adamova, I.O. Zolotovskii, R. Herda, O.G. Okhotnikov, A.S. Sysoliatin, Pulse compression in a longitudinally inhomogeneous fiber, Laser Phys. 18 (11) (2008) 1279–1289.

Please cite this article in press as: S.K. Turitsyn, et al., Dispersion-managed solitons in fibre systems and lasers, Physics Reports (2012), doi:10.1016/j.physrep.2012.09.004

[216] M. Adamova, I.O. Zolotovskii, D.I. Sementsov, Pulse compression dynamics in a nonlinear longitudinally inhomogeneous optical fiber, J. Comp. Tech. and Electron. 53 (6) (2008) 695–699.
[217] B.A. Malomed, A. Bernston, Propagation of an optical pulse in a fiber link with random dispersion management, J. Opt. Soc. Am. B 18 (2001) 1243–1250.
[218] M. Chertkov, I. Gabitov, P. Lushnikov, J. Moeser, Z. Toroczkai, Pinning method of pulse confinement in optical fiber with random dispersion, JOSA B 19 (11) (2002) 2538–2550.
[219] T. Schafer, R.O. Moore, C. Jones, Pulse propagation in media with deterministic and random dispersion variations, Opt. Comm. 214 (1–6) (2002) 353–362.
[220] F.K. Abdullaev, J. Garnier, Optical solitons in random media, in: E. Wolf (Ed.), in: Progress in Optics, vol. 48, North Holland, 2005, pp. 35–106.
[221] E. Poutrina, G.P. Agrawal, Impact of dispersion fluctuations on 40-gb/s dispersion-managed lightwave systems, J. Lightwave Tech. 23 (2003) 990–996.
[222] M. Böhm, F. Mitschke, Soliton propagation in a dispersion map with deviation from periodicity, Appl. Phys. B 81 (2005) 983–987.
[223] V. Zharnitsky, E. Grenier, C. Jones, S. Turitsyn, Stabilizing effects of dispersion management, Physica D 152–153 (2001) 794–817.
[224] M. Kunze, On a variational problem with lack of compactness related to the Strichartz inequality, Calc. Var. Partial Differential Equations 19 (3) (2004) 307–336.
[225] M. Kunze, J. Moeser, V. Zharnitsky, Ground states for the higher order dispersion managed nls equation in the absence of average dispersion, J. Differential Equations 209 (2005) 77–100.
[226] M. Stanislavova, Regularity of ground state solutions of dmnls, J. Differential Equations 210 (2005) 87–105.
[227] D. Hundertmark, V. Zharnitsky, On sharp Strichartz inequalities for low dimensions, Int. Math. Res. Not. 2006 (2006) 34080.
[228] D. Hundertmark, Y.R. Lee, Decay estimates and smoothness for solutions of the dispersion managed non-linear Schrödinger equation, Comm. Math. Phys. 286 (3) (2009) 851–873.
[229] D.E. Pelinovsky, V. Zharnitsky, Averaging of dispersion-managed solitons: existence and stability, SIAM J. Appl. Math. 63 (3) (2003) 745–776.
[230] B.M. Erdogan, D. Hundertmark, Y.-R. Lee, Exponential decay of dispersion managed solitons for vanishing average dispersion, Math. Research. Lett. 18 (1) (2011) 11–24.
[231] S. Boscolo, J. Nijhof, S. Turitsyn, A perturbative analysis of dispersion-managed solitons, Phys. Scr. 62 (6) (2003) 479–485.
[232] E.V. Doktorov, Dynamics of subpicosecond dispersion-managed soliton in a fibre: a perturbative analysis, J. Mod. Opt. 53 (18) (2006) 2701–2723.
[233] T. Lakoba, Non-integrability of equations governing pulse propagation in dispersion-managed optical fibers, Phys. Lett. A 260 (1–2) (1999) 68–77.
[234] D.E. Pelinovsky, On the dispersion managed soliton, Chaos 10 (3) (2000) 515–528.
[235] M. Wald, B.A. Malomed, F. Lederer, Gordon haus effect in dispersion-managed soliton systems, Opt. Lett. 22 (1997) 1870–1872.
[236] M. Wald, B.A. Malomed, F. Lederer, Interactions of dispersion-managed solitons in wavelength-division-multiplexed optical transmission lines, Opt. Lett. 26 (2001) 965–967.
[237] S. Kumar, J. Mauro, S. Raghavan, D. Chowdhury, Intra-channel four wave mixing in dispersion managed transmission systems, IEEE Sel. Top. J. Quant. Electron. 8 (3) (2001) 626–631.
[238] S. Kumar, Noise suppression using dispersion decreasing fibers for rz transmission systems, IEEE Photon. Techn. Lett. 16 (2004) 810–812.
[239] K. Porsezian, R. Ganapathy, A. Hasegawa, V.N. Serkin, Nonautonomous soliton dispersion management, IEEE J. Quan. Elect. 45 (12) (2010) 1577–1583.
[240] S. Kumar, M. Wald, F. Lederer, A. Hasegawa, Soliton interaction in strongly dispersion-managed optical fibers, Opt. Lett. 23 (13) (1998) 1019–1021.
[241] A. Mikhailov, V. Novokshenov, The Riemann–Hilbert problem for analytic description of the dm solitons, Theor. Math. Phys. 137 (3) (2002) 1723–1732.
[242] M. Ablowitz, T. Hirooka, Nonlinear effects in quasi-linear dispersion managed pulse transmission, IEEE Photon. Techn. Lett. 13 (2001) 1082–1084.
[243] M. Ablowitz, T. Hirooka, Managing nonlinearity in strongly dispersion-managed optical pulse transmission, J. Opt. Soc. Am. B 19 (2002) 425–439.
[244] P.T. Dinda, A.B. Moubissi, K. Nakkeeran, A collective variable approach for dispersion-managed solitons, J. Phys. A 34 (10) (2001) L103–L110.
[245] M. Ablowitz, B. Ilan, S. Cundiff, Carrier-envelope phase slip of ultra-short dispersion managed solitons, Opt. Lett. 29 (2004) 1808–1820.
[246] Q. Quraishi, S. Cundiff, B. Ilan, M. Ablowitz, Dynamics of nonlinear and dispersion managed soltions, Phys. Rev. Lett. 94 (2005) 243904.
[247] D.E. Pelinovsky, P. Kevrekidis, D.J. Frantzeskakis, Averaging for solitons with nonlinearity management, Phys. Rev. Lett. 91 (24) (2003) 240201.
[248] A. Biswas, Higher order Gabitov–Turitsyn equation for dispersion-managed solitons in birefringent fibers, Int. J. Theor. Phys. 46 (12) (2007) 3339–3354.
[249] A. Biswas, Higher-order Gabitov–Turtsyn equation for solitons in optical fibers, Optik 118 (3) (2007) 120–133.
[250] A. Biswas, E. Zerrad, Higher order Gabitov–Turitsyn equation for dispersion-managed vector solitons, Dyn. of Cont. Disc. and Impul. Sys. Series A-Math Aanalysis 13 (6) (2006) 687–711.
[251] A. Bononi, P. Serena, M. Bertolini, Unified analysis of weakly-nonlinear dispersion-managed optical transmission systems using a perturbative approach, Comptes Rendus Phys. 9 (2008) 947–962.
[252] M. Ablowitz, T. Horikis, B. Ilan, Solitons in dispersion-managed mode-locked lasers, Phys. Rev. A 77 (2008) 033814.
[253] D.E. Pelinovsky, Instabilities of dispersion-managed solitons in the normal dispersion regime, Phys. Rev. E. 62 (3) (2003) 4283–4293.
[254] B.A. Malomed, Soliton Management in Periodic Systems, Springer, 2010.
[255] V.S. Grigoryan, C.R. Menyuk, R.M. Mu, Calculation of timing and amplitude jitter in dispersion-managed optical fiber communications using linearization, J. Lightwave Technol. 17 (1999) 1347–1356.
[256] C.J. Mckinstrie, Effects of filtering on gordon-haus timing jitter in dispersion-managed systems, J. Opt. Soc. Am. B 19 (2002) 1275–1285.
[257] C.J. Mckinstrie, C. Xie, T.I. Lakoba, Efficient modeling of phase jitter in dispersion-managed soliton systems, Opt. Lett. 27 (2002) 1887–1889.
[258] C.J. Mckinstrie, J. Santhanam, G.P. Agrawal, Gordon–Haus timing jitter in dispersion-managed systems with lumped amplification: analytical approach, J. Opt. Soc. Am. B 19 (2002) 640–649.
[259] E. Poutrina, G.P. Agrawal, Timing jitter in dispersion-managed soliton systems with distributed, lumped, and hybrid amplification, J. Lightwave Technol. 20 (2002) 790–797.
[260] J. Santhanam, G.P. Agrawal, Raman-induced timing jitter in dispersion-managed optical communications systems, IEEE J. Sel. Topics Quant. Electron. 8 (2002) 632–639.
[261] J. Santhanam, G.P. Agrawal, Reduced timing jitter in dispersion-managed light-wave systems through parametric amplification, J. Opt. Soc. Am. B. 20 (2003) 284–291.
[262] J. Garnier, Stabilization of dispersion-managed solitons in random optical fibers by strong dispersion management, Opt. Commun. 206 (2002) 411–438.
[263] A.D. Capobianco, G. Nalesso, A. Tonello, F. Consolandi, C.D. Angelis, F. Gringoli, Noise evolution and soliton internal modes in dispersion-managed fiber systems, Opt. Lett. 28 (2003) 1754–1756.
[264] E. Spiller, G. Biondini, Importance sampling for dispersion-managed solitons, SIAM J. Appl. Dyn. Sys. 9 (2) (2010) 432–461.
[265] E. Spiller, G. Biondini, Phase noise of dispersion-managed solitons, Phys. Rev. A. 80 (1) (2009) 011805–011809.
[266] F.K. Abdullaev, J. Garnier, Solitons in media with random dispersive perturbations, Physica D 134 (1999) 303–315.
[267] H.A. Haus, J.G. Fujimoto, E.P. Ippen, Structures for additive pulse mode-locking, J. Opt. Soc. Am. B 8 (1991) 2068–2076.
[268] H.A. Haus, J.G. Fujimoto, E.P. Ippen, Analytic theory of additive pulse mode-locking, IEEE J. Quantum Electron. 28 (1992) 2086–2096.
[269] H.A. Haus, Mode-locking of lasers, IEEE J. Sel. Top. Quantum Electron. 6 (2000) 1173–1185.
[270] J.N. Kutz, Mode-locked soliton lasers, SIAM Rev. 48 (2006) 629–678.
[271] J. Lega, J.V. Moloney, A.C. Newell, Swift-hohenberg equation for lasers, Phys. Rev. Lett. 73 (1994) 2978–2981.
[272] K.P. Komarov, Theory of stationary ultrafast pulses in solid-state lasers with passive mode-locking, Opt. Spectrosc. 60 (1986) 231–234.
[273] K.P. Komarov, A.S. Kuchyanov, V.D. Ugozhayev, Generation of stationary ultra-short pulses by a passive mode-locking solid-state laser, Opt. Comm. 57 (1986) 279–284.

Please cite this article in press as: S.K. Turitsyn, et al., Dispersion-managed solitons in fibre systems and lasers, Physics Reports (2012), doi:10.1016/j.physrep.2012.09.004

[274] P. Lazaridis, G. Debarge, P. Gallion, Time-bandwidth product of chirped sech^2 pulses: application to phase-amplitude-coupling factor measurement, Opt. Lett. 20 (1995) 1160–1162.
[275] B. Proctor, E. Westwig, F. Wise, Characterization of a kerr-lens mode-locked ti:sapphire laser with positive group-velocity dispersion, Opt. Lett. 18 (1993) 1654–1656.
[276] T. Kapitula, Stability of bright solitary-wave solutions to perturbed nonlinear Schrödinger equations, Physica D 124 (1998) 58–103.
[277] T. Kapitula, J.N. Kutz, B. Sandstede, Stability of pulses in the master-modelocking equation, J. Opt. Soc. Am. B 19 (2002) 740–746.
[278] G. Biondini, The dispersion-managed ginzburg-landau equation and its application to femtosecond lasers, Nonlinearity 21 (12) (2008) 2849–2870.
[279] A. Fuerbach, A. Fernandez, A. Apolonski, F. Krausz, Chirped-pulse oscillators for the generation of high-energy femtosecond laser pulses, Laser and Part. Beams 23 (2005) 113–116.
[280] A. Chong, J. Buckley, W.H. Renninger, F. Wise, All normal-dispersion femtosecond fiber laser, Opt. Express 14 (2006) 10095–10100.
[281] B.G. Bale, J.N. Kutz, W.H. Renninger, A. Chong, F.W. Wise, Spectral filtering for high-energy mode-locking in normal dispersion fiber lasers, J. Opt. Soc. Am. B 25 (2008) 1763–1770.
[282] W.H. Renninger, A. Chong, F.W. Wise, Area theorem and energy quantization for dissipative optical solitons, J. Opt. Soc. Am. B 27 (2010) 1978–1982.
[283] E. Golovchenko, J. Jacob, A. Pilipetskii, C. Menyuk, G. Carter, Dispersion-managed solitons in a fiber loop with in-line filtering, Opt. Lett. 22 (1997) 289–291.
[284] S.K. Turitsyn, E.G. Turitsyna, Dispersion-managed soliton in fiber links with in-line filtering presented in the basis of chirped gauss-hermite functions, J. Opt. Soc. Am. B 16 (1999) 1321–1331.
[285] A. Tonello, A.D. Capobianco, S. Wabnitz, S.K. Turitsyn, Tuning of in-line filter position for dispersion-managed soliton transmission, Opt. Comm. 175 (2000) 103–108.
[286] B.G. Bale, S. Boscolo, J.N. Kutz, S.K. Turitsyn, Intracavity dynamics in high-power mode-locked fiber lasers, Phys. Rev. A 81 (2010) 033828.
[287] B.G. Bale, S. Wabnitz, Strong spectral filtering for a similariton mode-locked fiber laser, Opt. Lett. 35 (2010) 2466–2468.
[288] D. Strickland, G. Mourou, Compression of amplified chirped optical pulses, Opt. Commun. 56 (1985) 219–221.
[289] T.F. Carruthers, I.N.D. Iii, M. Horowitz, C.R. Menyuk, Dispersion management in a harmonically mode-locked fiber soliton laser, Opt. Lett. 25 (2000) 153–155.
[290] H. Lim, F.W. Wise, Control of dispersion in a femtosecond ytterbium laser with hollow-core bandgap fiber, Opt. Express 12 (2004) 2231.
[291] G. Imeshev, I. Hartl, M. Fermann, An optimized er gain band all-fiber chirped pulse amplification system, Opt. Express 12 (26) (2004) 6508–6514.
[292] G. Imeshev, M. Fermann, 230-kw peak power femtosecond pulses from a high power tunable source based on amplification in tm-doped fiber, Opt. Express 13 (2005) 7424–7431.
[293] M. Rusu, S. Karirinne, M. Guina, A.B. Grudinin, O.G. Okhotnikov, Femtosecond neodymium-doped fiber laser operating in the 894–909-nm spectral range, IEEE Photon. Technol. Lett. 16 (2004) 1029–1031.
[294] V. Pervak, F. Krausz, A. Apolonski, Dispersion-control over the ultraviolet–visible-near-infrared spectral range with hfo2/sio2-chirped dielectric multilayers, Opt. Lett. 32 (2007) 1183–1185.
[295] B. Orta, M. Plötner, T. Schreiber, J. Limpert, A. Tünnermann, Experimental and numerical study of pulse dynamics in positive net-cavity dispersion modelocked yb-doped fiber lasers, Opt. Express 15 (2007) 15595–15602.
[296] M. Schultz, O. Prochnow, A. Ruehl, D. Wandt, D. Kracht, S. Ramachandran, S. Ghalmi, Sub-60-fs ytterbium-doped fiber laser with a fiber-based dispersion compensation, Opt. Lett. 32 (2007) 2372–2374.
[297] F. Tavella, Y. Nomura, L. Veisz, V. Pervak, A. Marcinkevicius, F. Krausz, Dispersion management for a sub-10-fs, 10 tw, Opt. Lett. 32 (2007) 2227.
[298] F. Tavella, Y. Nomura, L. Veisz, V. Pervak, A. Marcinkevicius, F. Krausz, Dispersion management for a sub-10-fs 10 tw optical parametric chirped-pulse amplifier, Opt. Lett. 32 (2007) 2227–2229.
[299] S. Zhou, F.W. Wise, D.G. Ouzounov, Divided-pulse amplification of ultrashort pulses, Opt. Lett. 32 (2007) 871–873.
[300] A. Chong, W.H. Renninger, F.W. Wise, Observation of antisymmetric dispersion-managed solitons in a mode-locked laser, Opt. Lett. 33 (2008) 1717–1719.
[301] E.E. Serebryannikov, A.M. Zheltikov, K.H. Liao, A. Galvanauskas, A. Baltuöka, Dispersion and nonlinear phase-shift compensation in high-peak-power short-pulse fiber laser sources using photonic-crystal fibers, Laser Physics 18 (12) (2008) 1389–1399.
[302] V. Pervak, I. Ahmad, S.A. Trushin, Z. Major, A. Apolonski, S. Karsch, F. Krausz, Chirped-pulse amplification of laser pulses with dispersive mirrors, Opt. Express 17 (2009) 19204–19212.
[303] P. Dombi, P. Racz, M. Lenner, V. Pervak, F. Krausz, Dispersion management in an actively modelocked fiber laser with kerr nonlinearly, Opt. Express 17 (2009) 20598–20604.
[304] A. Tünnermann, T. Schreiber, J. Limpert, Fiber lasers and amplifiers: an ultrafast performance evolution, Appl. Opt. 49 (2010) F71–F78.
[305] M.Y. Sander, E.P. Ippen, F.X. Ärtner, Carrier-envelope phase dynamics of octave-spanning dispersion-managed Ti:sapphire lasers, Opt. Express 18 (2010) 4948–4960.
[306] Z. Sun, T. Hasan, F. Wang, A.G. Rozhin, I. White, A.C. Ferrari, Ultrafast stretched-pulse fiber laser mode-locked by carbon nanotubes, Nano. Research 3 (6) (2010) 404–411.
[307] D.E. Spence, P.N. Kean, W. Sibbett, 60-fsec pulse generation from a self-mode-locked Ti:sapphire laser, Opt. Lett. 16 (1991) 42–44.
[308] I.N. Duling, M.L. Dennis, Modelocking of all-fiber lasers, in: I.N. Duling (Ed.), Compact Sources of Ultrashort Pulses, Cambridge University Press, 1995, pp. 140–178.
[309] U. Keller, Recent developments in compact ultrafast lasers, Nature 424 (2003) 831–838.
[310] U. Keller, Short and ultrashort pulse generation, in: G. Herziger, H. Weber, R. Proprawe (Eds.), Landolt-Börnstein, Group VIII/1B1, Laser Physics and Applications. Subvolume B: Laser Systems. Part I, Springer Verlag, 2007, pp. 33–167.
[311] V. Pervak, S. Naumov, F. Krausz, A. Apolonski, Chirped mirrors with low dispersion ripple, Opt. Express 15 (2007) 13768.
[312] K. Tamura, H.A. Haus, E.P. Ippen, Self-starting additive pulse mode-locked erbium fibre ring laser, Electron. Lett. 28 (1992) 2226–2228.
[313] M.E. Fermann, K. Sugden, I. Bennion, Environmentally stable high-power soliton fiber lasers that use chirped fiber Bragg gratings, Opt. Lett. 20 (1995) 1625–1627.
[314] M.E. Fermann, K. Sugden, I. Bennion, High-power soliton fiber laser based on pulse width control with chirped fiber Bragg gratings, Opt. Lett. 20 (1995) 172–174.
[315] R. Gumenyuk, C. Thür, S. Kivistö, O.G. Okhotnikov, Tapered fiber Bragg gratings for dispersion compensation in mode-locked yb-doped fiber laser, IEEE J. Quantum Electron. 46 (5) (2010) 769–773.
[316] W. Reeves, J. Knight, P. Russell, P. Roberts, Demonstration of ultra-flattened dispersion in photonic crystal fibers, Opt. Express 10 (2002) 609–613.
[317] A. Isomki, O.G. Okhotnikov, All-fiber ytterbium soliton mode-locked laser with dispersion control by solid-core photonic bandgap fiber, Opt. Express 14 (2006) 4368–4373.
[318] R. Herda, S. Kivistö, O.G. Okhotnikov, A.F. Kosolapov, A.E. Levchenko, S.L. Semjonov, E.M. Dianov, Environmentally stable mode-locked fiber laser with dispersion compensation by index-guided photonic crystal fiber, IEEE Photonics Technol. Lett. 20 (3) (2008) 217–219.
[319] K. Furusawa, T.M. Monro, P. Petropoulos, D.J. Richardson, Mode-locked laser based on ytterbium doped holey fibre, Elecron. Lett. 37 (2001) 560–561.
[320] J. Limpert, T. Schreiber, S. Nolte, H. Zellmer, A. Tünnermann, R. Iliew, F. Lederer, J. Broeng, G. Vienne, A. Petersson, C. Jakobsen, High-power air-clad large-mode-area photonic crystal fiber laser, Opt. Express 11 (2003) 818–823.
[321] R.H. Stolen, J. Botineau, A. Ashkin, Intensity discrimination of optical pulses with birefringent fibers, Opt. Letters 7 (1982) 512–514.
[322] V.J. Matsas, T.P. Newson, D.J. Richardson, D.N. Payne, Self-starting passively mode-locked fibre ring soliton laser exploiting non-linear polarisation rotation, Electron. Letters 28 (1992) 1391–1393.
[323] D.U. Noske, N. Pandit, J.R. Taylor, Subpicosecond soliton pulse formation from self-mode-locked erbium fibre laser using intensity dependent polarisation rotation, Electron. Lett. 28 (1992) 2185–2186.

[324] M. Hofer, M.H. Ober, F. Haberl, M.E. Fermann, Characterization of ultrashort pulse formation in passively mode-locked fiber lasers, IEEE J. Quantum Electron. 28 (1992) 720–728.
[325] M.E. Fermann, M.J. Andrejco, Y. Silberberg, A.M. Weiner, Generation of pulses shorter than 200 fs from a passively mode-locked er fiber laser, Opt. Lett. 18 (1993) 48–50.
[326] D.J. Richardson, R.I. Laming, D.N. Payne, V. Matsas, M.W. Phillips, Self-starting, passively mode-locked erbium fibre ring laser based on the amplifying sagnac switch, Electron. Lett. 27 (1982) 542–544.
[327] I.N. Duling, Subpicosecond all-fibre erbium laser, Electron. Lett. 27 (1991) 544–545.
[328] M.L. Dennis, I.N. Duling, High repetition rate figure eight laser with extracavity feedback, Electron. Lett. 28 (1992) 1894–1896.
[329] F.Ö. Ilday, F.W. Wise, T. Sosnowski, High-energy femtosecond stretched-pulse fiber laser with a nonlinear optical loop mirror, Opt. Lett. 27 (2002) 1531–1533.
[330] U. Keller, K.J. Weingarten, F.X. Kärtner, D. Kopf, B. Braun, I.D. Jung, R. Fluck, C. Hönninger, N. Matuschek, J.A. der Au, Semiconductor saturable absorber mirrors (sesams) for femtosecond to nanosecond pulse generation in solid-state lasers, IEEE J. Select. Topics Quantum Electron. 2 (1996) 435–453.
[331] R. Herda, O.G. Okhotnikov, Dispersion compensation-free fiber laser mode-locked and stabilized by high-contrast saturable absorber mirror, IEEE J. Quant. Electron. 40 (2004) 893–899.
[332] A.G. Rozhin, S. Youichi, N. Shu, T. Madoka, Sub-200-fs pulsed erbium-doped fibre laser using a carbon nanotube-polyvinylalchohol mode locker, Appl. Phys. Lett. 88 (2006) 051118.
[333] T. Hasan, Z. Sun, F. Wang, F. Bonaccorso, P.H. Tan, A.G. Rozhin, A.C. Ferrari, Nanotube-polymer composites for ultrafast photonics, Adv. Mater. 21 (2009) 3874–3899.
[334] K. Tamura, C.R. Doerr, L.E. Nelson, H.A. Haus, E.P. Ippen, Technique for obtaining high-energy ultrashort pulses from an additive-pulse mode-locked erbium-doped fiber ring laser, Opt. Lett. 19 (1994) 46–48.
[335] K. Tamura, M. Nakazawa, Optimizing power extraction in stretched-pulse fiber ring lasers, Appl. Phys. Lett. 67 (1995) 3691–3693.
[336] G. Lenz, K. Tamura, H.A. Haus, E.P. Ippen, All-solid-state femtosecond source at 1.55 μm, Opt. Lett. 20 (1995) 1289–1291.
[337] S. Namiki, H.A. Haus, Noise of the stretched pulse filter laser i: theory, IEEE J. Quantum Electron. 33 (1997) 649–659.
[338] S. Namiki, E.P. Ippen, H.A. Haus, C.X. Yu, Energy rate equations for mode-locked lasers, J. Opt. Soc. Am. B 14 (1997) 2099–2111.
[339] B.G. Bale, S. Boscolo, S.K. Turitsyn, Dissipative dispersion-managed solitons in mode-locked lasers, Opt. Lett. 34 (2009) 3286–3288.
[340] C. Antonelli, J. Chen, F.X. Kärtner, Intracavity pulse dynamics and stability for passively mode-locked lasers, Opt. Express 15 (2007) 5919–5924.
[341] J. Goodberlet, J. Wang, J.G. Fugimoto, P.A. Schulz, Fast quantum-dot saturable absorber for passive mode-locking of solid-state lasers, Opt. Lett. 14 (1989) 1125–1127.
[342] S.H. Cho, F.X. Kärtner, U. Morgner, E.P. Ippen, J.G. Fujimoto, J.E. Cunningham, W.H. Knox, Generation of 90-nJ pulses with a 4-mhz repetition-rate kerr-lens mode-locked $Ti:Al_2O_3$ laser operating with net positive and negative intracavity dispersion, Opt. Lett. 26 (2001) 560–562.
[343] A. Fernandez, T. Fuji, A. Poppe, A. Fürbach, F. Krausz, A. Apolonski, Chirped-pulse oscillators: a route to high-power femtosecond pulses without external amplification, Opt. Lett. 29 (2004) 1366–1368.
[344] F.Ö. Ilday, J.R. Buckley, W.G. Clark, F.W. Wise, Self-similar evolution of parabolic pulses in a laser, Phys. Rev. Lett. 92 (2004) 213902.
[345] J.R. Buckley, F.W. Wise, F.Ö. Ilday, T. Sosnowski, Femtosecond fiber lasers with pulse energies above 10 nJ, Opt. Lett. 30 (2005) 1888–1890.
[346] A. Ruehl, O. Prochnow, D. Wandt, D. Kracht, B. Burgoyne, N. Godbout, S. Lacroix, Dynamics of parabolic pulses in an ultrafast fiber laser, Opt. Lett. 31 (2006) 2734–2736.
[347] L.M. Zhao, D.Y. Tang, J. Wu, Gain-guided soliton in a positive group-dispersion fiber laser, Opt. Lett. 31 (2006) 1788–1790.
[348] A. Chong, W.H. Renninger, F.W. Wise, All-normal-dispersion femtosecond fiber laser with pulse energy above 20 nJ, Opt. Lett. 32 (2007) 2408–2410.
[349] B. Oktem, C. Ülgüdür, F.Ö. Ilday, Soliton-similariton fibre laser, Nat. Photon. 4 (2010) 307–311.
[350] W.H. Renninger, A. Chong, F.W. Wise, Self-similar pulse evolution in an all-normal-dispersion laser, Phys. Rev. A 82 (2010) 021805(R).
[351] B. Ortac, M. Baumgartl, J. Limpert, A. Tünnermann, Approaching microjoule-level pulse energy with mode-locked femtosecond fiber lasers, Opt. Lett. 34 (2009) 1585–1587.
[352] F.W. Wise, A. Chong, W.H. Renninger, High-energy femtosecond fiber lasers based on pulse propagation at normal dispersion, Laser Phot. Rev. 2 (2008) 58–73.
[353] A. Chong, H. Liu, B. Nie, B.G. Bale, S. Wabnitz, W.H. Renninger, M. Dantus, F.W. Wise, Pulse generation without gain-bandwidth limitation in a laser with self-similar evolution, Opt. Express. 20 (2012) 14213–14220.
[354] B.G. Bale, J.N. Kutz, A. Chong, W.H. Renninger, F.W. Wise, Spectral filtering for mode locking in the normal dispersive regime, Opt. Lett. 33 (2008) 941–943.
[355] U. Keller, D.A.B. Miller, G.D. Boyd, T.H. Chiu, J.F. Ferguson, M.T. Asom, Solid-state low-loss intracavity saturable absorber for nd:ylf lases: an antiresonant semi-conductor fabry-perot saturable absorber, Opt. Lett. 17 (1992) 505–507.
[356] D. Kopf, G. Zhang, R. Fluck, M. Moser, U. Keller, All-in-one dispersion-compensating saturable absorber mirror for compact femtosecond laser sources, Opt. Lett. 21 (1996) 486–488.
[357] R. Paschotta, G.J. Spühler, D.H. Sutter, N. Matuschek, U. Keller, M. Moser, R. Hövel, V. Scheuer, G. Angelow, T. Tschudi, Double-chirped semiconductor mirror for dispersion compensation in femtosecond lasers, Appl. Phys. Lett. 75 (1999) 2166–2168.
[358] U. Keller, Semiconductor nonlinearities for solid-state laser mode-locking and q-switching, in: E. Garmire, A. Kost (Eds.), Nonlinear Optics in Semiconductors, vol. 59, Academic Press Inc., 1999, pp. 211–286.
[359] R. Pashotta, U. Keller, Ultrafast solid-state lasers, in: M.E. Fermann, A. Galvanauskas, G. Sucha (Eds.), Ultrafast lasers: Technology and Applications, Marcel Dekker Inc., 2003, pp. 1–60.
[360] E.P. Ippen, H.A. Haus, L.Y. Liu, Additive pulse modelocking, J. Opt. Soc. Am. B 6 (1989) 1736–1745.
[361] T. Brabec, C. Spielmann, P.F. Curley, F. Krausz, Kerr lens mode locking, Opt. Lett. 17 (1992) 1292–1294.
[362] M. Guina, N. Xiang, A. Vainionpää, O.G. Okhotnikov, T. Sajavaara, J. Keinonen, Self-starting stretched-pulse fiber laser mode locked and stabilized with slow and fast semiconductor saturable absorbers, Opt. Lett. 26 (2001) 1809–1811.
[363] O.G. Okhotnikov, L. Gomes, N. Xiang, T. Jouhti, A. Grudinin, Mode-locked ytterbium fiber laser tunable in the 980–1070-nm spectral range, Opt. Lett. 28 (2003) 1522–1524.
[364] F.X. Kärtner, J.A.d. Au, U. Keller, Mode-locking with slow and fast saturable absorbers—whats the difference?, Sel. Top. Quantum Electron. 4 (1998) 159–168.
[365] O. Shtyrina, M. Fedoruk, S. Turitsyn, R. Herda, O. Okhotnikov, Evolution and stability of pulse regimes in sesam-mode-locked femtosecond fiber lasers, J. Opt. Soc. Am. B 26 (2) (2009) 346–352.
[366] G.P. Agrawal, Nonlinear Fiber Optics, 3rd ed., Academic Press, 2001.
[367] R. Gumenyuk, I. Vartiainen, H. Tuovinen, O.G. Okhotnikov, Dissipative dispersion-managed soliton 2μm thulium/holmium fiber laser, Opt. Lett. 36 (2011) 609–611.
[368] S. Turitsyn, M. Fedoruk, E. Shapiro, V. Mezentsev, E. Turitsyna, Novel approaches to numerical modelling of periodic dispersion-managed fiber, IEEE J. Select. Topics Quantum Electron. 6 (2000) 263–275.
[369] R.H. Hardin, F.D. Tappert, Applications of the split-step fourier method to the numerical solution of non-linear and variable-coefficient wave equations, SIAM Rev. Chronicle 15 (1973) 423.
[370] B.M. Lake, H. Yuen, H. Rungaldier, W.E. Ferguson, Nonlinear deep-water waves; theory and experiment. part 2. evolution of a continuous wave train, J. Fluid Mech. 83 (1977) 49–74.
[371] T.R. Taha, M.J. Ablowitz, Analytical and numerical aspects of certain nonlinear evolution equations. ii. numerical, nonlinear Schrödinger equation, J. Comput. Phys. 55 (1984) 203–230.
[372] Q. Chang, E. Jia, W. Suny, Difference schemes for solving the generalized nonlinear Schrödinger equation, J. Comput. Phys. 148 (1999) 397–415.

Please cite this article in press as: S.K. Turitsyn, et al., Dispersion-managed solitons in fibre systems and lasers, Physics Reports (2012), doi:10.1016/j.physrep.2012.09.004

[373] M. Delfour, M. Fortin, G. Payre, Finite difference solution of a nonlinear nonlinear Schrödinger equation, J. Comput. Phys. 44 (1981) 277–288.
[374] J. Sanz-Serna, Methods for the numerical solution of the nonlinear Schrödinger equation, Math. Comp. 43 (1984) 21–27.
[375] E. Twizell, A. Bratsos, J. Newby, A finite-difference method for solving the cubic Schrödinger equation, Math. Comput. Simul. 43 (1997) 67–75.
[376] L. Wu, Dufortfrankel-type methods for linear and nonlinear Schrödinger equations, Math. Comput. Simul. 33 (1996) 1526–1533.
[377] F. Zhang, V. Perez-Grarciz, L. Vazquez, Numerical simulation of nonlinear Schrödinger systems: a new conservative scheme, Appl. Math. Comput. 71 (1995) 165–177.
[378] L. Zhang, A high accurate and conservative finite difference scheme for nonlinear Schrödinger equation, Acta Math. Appl. Sin. 28 (2005) 178–186.
[379] L. Gardner, G. Gardner, S. Zaki, Z.E. Sahrawi, B-spline finite element studies of the non-linear Schrödinger equation, Comput. Methods Appl. Mech. Eng. 108 (1993) 303–318.
[380] B. Herbst, J. Morris, A. Mitchell, Numerical experience with the nonlinear Schrödinger equation, J. Comput. Phys. 60 (1985) 282–305.
[381] Y. Tourigny, J. Morris, An investigation into the effect of product approximation in the numerical solution of the cubic nonlinear Schrödinger equation, J. Comput. Phys. 76 (1988) 103–130.
[382] O. Karakashian, C. Makridakis, A space–time finite element method for the nonlinear Schrödinger equation: the discontinuous Galerkin method, Math. Comp. 67 (1998) 479–499.
[383] Y. Xu, C.W. Shu, Local discontinuous Galerkin methods for nonlinear Schrödinger equations, J. Comput. Phys. 205 (2005) 72–97.
[384] M.P. Robinson, G. Fairweather, B.M. Herbst, On the numerical solution of the cubic Schrödinger equation in one space variable, J. Comput. Phys. 104 (1993) 277–284.
[385] M.P. Robinson, The solution of nonlinear Schrödinger equations using orthogonal spline collocation, Comput. Math. Appl. 33 (1997) 39–57.
[386] J. Weideman, B. Herbst, Split-step methods for the solution of the nonlinear Schrödinger equation, SIAM J. Numer. Anal. 23 (3) (1986) 485–507.
[387] H. Wang, Numerical studies on the split step finite difference method for the nonlinear Schrödinger equations, Appl. Math. Comput. 170 (2005) 17–35.
[388] Y.F. Tang, L. Vázquez, F. Zhang, V. Pétez-García, Simplectic methods for the nonlinear Schrödinger equation, Comput. Math. Appl. 32 (5) (1996) 73–83.
[389] J.B. Chen, M.Z. Qin, Y.F. Tang, Symplectic and multi-symplectic methods for the nonlinear Schrödinger equation, Comput. Math. Appl. 43 (2002) 1095–1106.
[390] A. Islas, C. Schober, Multi-symplectic methods for generalized Schrödinger equations, Future Gener. Comput. Syst. 19 (2003) 403–413.
[391] C. Heitzinger, C. Ringhofer, A note on the symplectic integration of the nonlinear Schrödinger equation, J. Comput. Electron. 3 (2004) 33–44.
[392] A. Aricò, C.V. der Mee, S. Seatzu, Structured matrix numerical solution of the nonlinear Schrödinger equation by the inverse scattering transform, Electron. J. Diff. Equations 2009 (15) (2009) 1–21.
[393] A. Shapeev, Unconditionally stable explicit high-order scheme for the nonlinear Schrödinger equation (in Russian), in: Y. Shokin (Ed.), Proceedings of the Youth Scientific Conference dedicated to the 10th anniversary of Institute of Computational Technologies SB RAS, Institute of Computational Technologies SB RAS, Novosibirsk, 2001, pp. 175–179.
[394] M. Ismail, C. Alamri, Highly accurate finite difference method for coupled nonlinear Schrödinger equation, Int. J. Comput. Math. 81 (2004) 333–351.
[395] F. Ivanauska, M. Radziunas, On convergence and stability of the explicit difference method for for solution of nonlinear Schrödinger equation, SIAM J. Numer. Anal. 36 (1999) 1466–1481.
[396] J. Sun, X. Gu, Z. Ma, Numerical study of the soliton waves of the coupled nonlinear Schrödinger system, Physica D 196 (2004) 311–328.
[397] M. Ismail, Numerical solution of coupled nonlinear Schrödinger equation by Galerkin method, Math. Comput. Simul. 78 (2008) 532–547.
[398] R. Thaib, Parrallel split step fourier method for the coupled nonlinear Schrödinger type equation, J. Supercomputer 32 (2005) 5–23.
[399] Y. Emmanuel, Generalized hyperbolic functions to find soliton-like solutions for a system of coupled nonlinear Schrödinger equation, Phys. Lett. A. 372 (2008) 1612–1618.
[400] M. Ismail, R. Thaib, A linearly implicit conservative scheme for the coupled nonlinear Schrödinger equation, Math. Comput. Simul. 74 (2007) 302–311.
[401] J. Sun, M. Qin, Multi-symplectic methods for the coupled 1d nonlinear Schrödinger system, Comput. Phys. Commun. 155 (2003) 221–235.
[402] A. Aydin, B. Karasozen, Symplectic and multisymplectic methods for the coupled nonlinear Schrödinger equations with periodic solutions, Comput. Phys. Commun. 177 (2007) 566–583.
[403] A. Rashid, A. Ismail, A chebyshev spectral collocation method for the coupled nonlinear Schrödinger equations, Appl. Comput. Math. 9 (2010) 104–115.
[404] Q. Xu, Q. Chang, New numerical methods for the coupled nonlinear Schrödinger equations, Acta Math. Appl. Sinica, English series 26 (2010) 205–218.
[405] M. Ablowitz, J. Ladik, On the solution of a class of nonlinear partial differential equations, Stud. Appl. Math. 57 (1977) 1–12.
[406] K.J. Blow, D. Wood, Theoretical description of transient stimulated raman scattering in optical fibers, IEEE J. Quantum Electron. 25 (1989) 2665–2673.
[407] P.V. Mamyshev, S.V. Chernikov, Ultrashort-pulse propagation in optical fibers, Opt. Lett. 15 (1990) 1076–1078.
[408] R.H. Stolen, J.P. Gordon, W.J. Tomlinson, H.A. Haus, Raman response function of silicacore fibers, J. Opt. Soc. Amer. B 6 (1989) 1159–1166.
[409] Q. Lin, G.P. Agrawal, Raman response function for silica fibers, Opt. Lett. 31 (2006) 3086–3088.
[410] D. Hollenbeck, C.D. Cantrell, Multiple-vibrational-mode model for fiber-optic raman gain spectrum and response function, J. Opt. Soc. Am. B 19 (2002) 2886–2892.
[411] G. Muslu, H. Erbay, Higher-order split-step fourier schemes for generalized nonlinear Schrödinger equation, Math. Comput. Simul. 67 (2005) 581–595.
[412] G. Weiss, A. Maradudin, The baker-hausdorff formula and a problem in crystal physics, J. Math. Phys. 3 (1962) 771–777.
[413] R. Mclachlan, Symplectic integration of hamiltonian wave equations, Numer. Math. 66 (1994) 465–492.
[414] M. Suzuki, General theory of higher-order decomposition of exponential operators and symplectic operators, Phys. Lett. A 165 (1992) 387–395.
[415] H. Yoshida, Construction of higher order symplectic integrators, Phys. Lett. A 150 (1990) 262–268.
[416] J. Cooley, J.W. Tukey, An algorithm for the machine calculation of complex fourier series, Math. Comp. 19 (1965) 297–301.
[417] Y. Shokin, O. Shtyrina, M. Fedoruk, Mathematical modelling of nonlinear effects in optical fiber, Russ. J. Numer. Anal. Math. Modelling 25 (2010) 93–104.
[418] T.I. Lakoba, Stability analysis of the split-step fourier method on the background of a soliton of the nonlinear Schrödinger equation (2010) 1–28. arXiv:1008.4974v1.
[419] O.V. Sinkin, R. Holzlohner, J. Zweck, C.R. Menyuk, Optimization of the split-step fourier method in modeling optical-fiber communications systems, J. Lightwave Technol. 21 (2003) 61–68.
[420] G. Bosco, A. Carena, V. Curri, R. Gaudino, P. Poggiolini, S. Benedetto, Suppression of spurious tones induced by the split-step method in fiber systems simulation, IEEE Photon. Technol. Lett. 12 (2000) 489–491.
[421] H.G. Shiraz, P. Shum, M. Nagata, A novel method for analysis of solition propagation in optical fibers, IEEE J. Quantum Electron. 31 (1995) 190–200.
[422] G. Mocbs, A multilevel method for the resolution of a stochastic weakly damped nonlinear Schrödinger equation, Appl. Numerical Math. 26 (1998) 353–375.
[423] X. Liu, B. Lee, A fast method for nonlinear Schrödinger equation, IEEE Photon. Technol. Lett. 15 (2003) 1549–1551.
[424] B. Fornberg, T.A. Driscoll, A fast spectral algorithm for nonlinear wave equations with linear dispersion, J. Comput. Phys. 155 (1999) 456–467.
[425] A.O. Korotkevich, P.M. Lushnikov, Proof-of-concept implementation of the massively parallel algorithm for simulation of dispersion-managed wdm optical fiber systems, Opt. Lett. 36 (2011) 1851–1853.
[426] Intel http://software.intel.com/en.us/articles/mkl.fft.performance.using.local.and.distributed.implementation/, Accessed: 01/09/2010.
[427] S. Zoldi, V. Ruban, A. Zenchuk, S. Burtsev, Parallel implementation of the split-step fourier method for solving nonlinear Schrödinger systems, SIAM News 32 (1999) 1–5.
[428] P.M. Lushnikov, Fully parallel algorithm for simulating dispersion managed wavelength-division-multiplexed optical fiber systems, Opt. Lett. 27 (2002) 939–941.

Please cite this article in press as: S.K. Turitsyn, et al., Dispersion-managed solitons in fibre systems and lasers, Physics Reports (2012), doi:10.1016/j.physrep.2012.09.004

[429] V. Paasonen, M. Fedoruk, Dissipative compact scheme for nonlinear Schrödinger equation, J. Comput. Technol. 16 (6) (2011) 397–415 (in Russian).
[430] S.E. Mikeladze, On the numerical integration of elliptic and parabolic type equations, Izv. AN SSSR 5 (1941) 57–74 (in Russian).
[431] Z. Wang, X. Xuang, A high order accurate numerical scheme for a class of Schrödinger equation, in: Proceedings of the 2009 International Workshop on Information Security and Application, IWISA 2009, Academy Publisher, 2009, pp. 342–344.
[432] S. Xie, G. Li, S. Yi, Compact finite difference schemes with high accuracy for one-dimensional nonlinear Schrödinger equation, Comput. Methods Appl. Mech. Eng. 198 (2009) 1052–1060.
[433] S. Medvedev, O. Shtyrina, S. Musher, M. Fedoruk, Path-averaged optical soliton in double-periodic dispersion-managed systems, Phys. Rev. E 66 (2002) 066607.
[434] V.I. Petviashvili, Equation of an extraordinary soliton, Sov. J. Plasma Phys. 2 (1976) 257–258.
[435] V.I. Petviashvili, O.A. Pokhotelov, Solitary waves in plasmas and in the atmosphere, Gordon & Breach, 1992.
[436] P. Lushnikov, Dispersion-managed soliton in a strong dispersion map limit, Opt. Lett. 11 (2001) 1913–1918.
[437] J. Nijhof, W. Forisiak, N. Doran, The averaging method for finding exactly periodic dispersion-managed solitons, IEEE J. Select. Topics Quant. Electron 6 (2000) 330–336.
[438] P.Y.P. Chen, P.L. Chu, B.A. Malomed, An iterative numerical method for dispersion-managed solitons, Opt. Comm. 245 (2005) 425–435.
[439] J. Holt, Numerical solution of nonlinear two-point boundary problems by finite difference methods, Commun. ACM 2 (1964) 366–373.
[440] H. Keller, Numerical methods for two-point boundary value problem, Blaisdell Publishing Co., 1968.
[441] S. Roberts, S.J.S., Two-point Boundary Value Problems: Shooting Methods, Elsevier, 1972.
[442] D. Morrison, J. Riley, J. Zancanaro, Multiple shooting method for two-point boundary value problems, Commun. ACM 2 (1962) 613–614.
[443] J. Villadsen, W. Stewart, Solution of boundary-value problems by orthogonal collocation, Chem. Eng. Sci. 22 (1967) 1483–1501.
[444] U. Ascher, J. Christiansen, R.D. Russel, A collocation solver for mixed order systems of boundary value problems, Math. Comp. 33 (1979) 659–679.
[445] U. Ascher, J. Christiansen, R.D. Russel, Collocation software for boundary value odes, ACM. Trans. Math. Software 7 (1981) 209–222.
[446] U. Ascher, Collocation for two-point boundary value problem revisited, SIAM J. Num. Anal. 23 (1986) 596–609.
[447] S.K. Godunov, Numerical solution of boundary-value problems for systems of linear ordinary differential equations, Uspekhi Mat. Nauk 16 (3) (1961) 171–174 (in Russian).
[448] J.C. Knight, J. Broeng, T.A. Birks, P.S.J. Russell, Photonic band gap guidance in optical fibers, Science 282 (1998) 1476–1478.
[449] J.C. Knight, Photonic crystal fibres, Nature 424 (2003) 847–851.
[450] P.S.J. Russell, Photonic crystal fibers, Science 299 (2003) 358–362.
[451] P.S.J. Russell, Photonic crystal fibers, J. Lightwave. Technol. 24 (12) (2006) 4729–4749.

Please cite this article in press as: S.K. Turitsyn, et al., Dispersion-managed solitons in fibre systems and lasers, Physics Reports (2012), doi:10.1016/j.physrep.2012.09.004